Effect of proteinase-activated receptor 2 activating peptide, 2-furoyl-LIGRLO-amide, on murine mesenteric endothelial cell Ca^{2+}-events.

By

© John C. Hennessey

A thesis submitted to the School of Graduate Studies

in partial fulfillment of the

requirements for the degree

Master of Science (Medicine)

Cardiovascular and Renal Sciences

Division of BioMedical Sciences

Faculty of Medicine

Memorial University

May 2015

St. John's Newfoundland and Labrador

Abstract

Proteinase-activated receptor 2 (PAR2)-mediated elevations of cytosolic Ca^{2+}, induced by PAR2 agonist 2-furoyl-LIGRLO-amide (2fly), have been demonstrated in cell culture experiments. The properties of individual PAR2-mediated Ca^{2+}-events in endothelial cells (EC) have yet to be described, and the role that these Ca^{2+}-events play in the preservation of PAR2-mediated vascular reactivity in endothelial dysfunction is not understood. Male C57BL/6J (PAR2-WT) and PAR2 knockout (PAR2-KO) mice were implanted with sub-cutaneous micro-osmotic pumps containing either saline (control) or angiotensin II (endothelial dysfunction). Doses of angiotensin II were 1.5 mg/kg/day, control pumps were filled with 100 µl of saline. Imaged under spinning disk confocal microscopy, Fluo-4 loaded Ang II-treated ECs exhibited 21% and 23% attenuation in the density of ACh-evoked muscarinic (M_3)-mediated, Ca^{2+}-events in PAR2-WT and PAR2-KO, respectively. 2fly-mediated Ca^{2+}-events were unaffected by Ang II treatment. The density of Ca^{2+}-release sites were reduced by IP3R inhibition using xestospongin-C and TRPV channel inhibition using ruthenium red. This study identified two populations of non-propagating Ca^{2+}-events in murine mesenteric ECs: small peripheral and large-repeating transients. The study concluded that PAR2 Ca^{2+}-signaling is preserved in the presence of endothelial dysfunction. Immunocytochemistry experiments of fixed and permeabilized ECs, on a line-scan confocal microscope, revealed that the distribution of eNOS was significantly attenuated with Ang II treatment. This reduction of eNOS in Ang II-treated ECs may contribute to the attenuation of resistance vessel relaxation in endothelial dysfunction.

Acknowledgements

I would like to thank Drs. John McGuire and Bruno Stuyvers for their guidance, material and moral support, sharing of technical expertise and the editing of this thesis. Dr. Bruce Van Vliet was very helpful for his advice and for the review of the thesis. I also would like to thank Elizabeth Chia for her wisdom and practical advice on experimental protocol. Amarnath Mukhopadhyay has been instrumental in the implementation of this work through the preparation of reagents, genotyping, and assistance in surgical procedures. The animal care staff at Memorial University is appreciated for their help in the management of the mouse colony used in this work. I acknowledge the faculty and staff of the Division of BioMedical Sciences, Faculty of Medicine at Memorial University for their support on various matters experimental and otherwise. This research was funded by grants awarded to Dr. McGuire and Dr. Stuyvers by the Canadian Institutes of Health Research, the Research and Development Corporation of Newfoundland and Labrador, and the Canada Foundation for Innovation.

Table of Contents

List of Tables

List of Figures

Appendices

List of Abbreviations

2-APB – 2-aminoethoxydiphenyl borate

2fly – 2-furoyl-LIGRLO-amide

Ab – Antibody

ACh – Acetylcholine

Ang II – Angiotensin II

ANP – Atrial natriuretic peptide

ATP – Adenosine-5’-triphosphate

BK_{Ca} – Large conductance calcium-activated potassium channel

BNP – Brain natriuretic peptide

BSA – Bovine serum albumin

cAMP – 3'-5'-cyclic adenosine monophosphate

CBS – Cystathionine β-synthase

CCD – Charge-coupled device

CCh - Carbachol

cGMP – 3’, 5’-cyclic guanosine monophosphate

ChTX – Charybdotoxin

CICR – Calcium-induced calcium-release

CNP – C-type natriuretic peptide

COX-*n* – Cyclooxygenase (*n*): enzyme subtype

CRC – Concentration response curve

CRU – Calcium release unit

CSE – Cystathionine γ-lyase

CSE-/- – Cystathionine γ-lyase knockout mouse

CVC – Cutaneous vascular conductance

CWW – Cell wide Ca^{2+}-wave

Cx – Connexin

CYP – Cytochrome P450

DAG – Diacylglycerol

DDT – Dithiothreitol

DHET – Dihydroxyeicosatrienoic acid

DHP – Dihydropyridine

EC – Endothelial cell

ECL*n* – Extracellular loop (*n*): loop number

EDCF – Endothelium-derived contracting factor

EDH – Endothelium-derived hyperpolarization

EDHF – Endothelium-derived hyperpolarizing factor

EDRF – Endothelium-derived relaxing factor

EDV – Endothelium-dependent vasodilation

EET – Epoxyeicosatrienoic acid

EGTA – Ethylene glycol tetraacetic acid

eNOS – Endothelial nitric oxide synthase

eNOS-/- – Endothelial nitric oxide synthase knockout mouse

ER – Endoplasmic reticulum

ERK – Extracellular-signal-regulated kinases

FPS – Frames per second

FWHM – Full width at half maximum amplitude

GDP – Guanosine-5'-diphosphate

GPCR – G-protein coupled receptor

GTP – Guanosine-5'-triphosphate

HEK – Human embryonic kidney cell

HEPES – 4-(2-hydroxyethyl)-1-piperazineethanesulfonic acid

HETE – hydroxyeicosatrienoic acid

HT – Colon carcinoma cell

HT29 – Human colon adenocarcinoma grade II

HUVEC – Human umbilical vein endothelial cell

IbTX – Iberiotoxin

ICC - Immunocytochemistry

ICL*n* – Intracellular loop (*n*): loop number

IEL – Internal elastic lamina

IK_{ca} – Intermediate conductance calcium-activated potassium channel

IP1 – Prostacyclin receptor

IP_3 – Inositol triphosphate

IP3R – Inositol triphosphate receptor

IUPHAR – International Union of Pharmacology

K_{Ca} – Calcium activated potassium channel

K_{ir} – Inward-rectifier potassium channel

KLK – Kallikrein-related peptidase

KNRK – Kirsten murine sarcoma virus transformed rat kidney epithelial cell

K_V – Voltage-dependent potassium channel

L-NAME – N_ω-nitro-L-arginine-methyl ester hydrochloride

LPA – Lysophosphatidic acid

M_3 – Muscarinic receptor type 3

MAPK – Mitogen-activated protein kinase

MCA – Middle cerebral artery

MEGJ – Myoendothelial gap junction

MLCK – Myosin light chain kinase

NADPH – Nicotinamide adenine dinucleotide phostphate

NO – Nitric oxide

NOx – Nitrite and nitrate forms of NO

ODQ – 1H-[1, 2, 4] oxadiazolo [4, 3-α] quinoxalin-1-one

PAR*n* – Proteinase-activated receptor

PAR*n*-AP – Proteinase-activated receptor activating peptide (*n*): PAR subtype

PAR2-KO – B6.Cg-*F2rl1*^{tm1mslb}/J *par*2 knockout mice

PAR2-WT – C57BL/6J *par*2 wild-type mice

PAR2-HET – C57BL/6J x B6.Cg-*F2rl1*^{tm1mslb}/J *par*2 heterozygous mice

PBS – Phosphate buffered saline

PECAM-1 – Platelet endothelial cell adhesion molecule

PGI_2 – Prostacyclin

PGE_2 – Prostaglandin E_2

PGH_2 – Prostaglandin H_2

PGX – Prostaglandin X

PIP_2 – Phosphatidylinositol-4,5-bisphosphate

PKA – Protein kinase A

PLC – Phospholipase C

PVAT – Perivascular adipose tissue

ROS – Reactive oxygen species

RR – Ruthenium red

RyR – Ryanodine receptor

s.c. – Sub cutaneous

SERCA – Sarco-endoplasmic reticulum Ca^{2+}-ATPase

sGC – Soluble guanylyl cyclase

SHR – Spontaneously hypertensive rat

SK_{ca} – Small conductance calcium-activated potassium channel

SNP – Sodium nitroprusside

SOD – Superoxide dismutase

t_{rise} – Time-to-maximum amplitude

$t_{1/2}$ – Half-life

TEA – Tetraethylammonium

TRAM-34 – 1-[(2-chlorophenyl) diphenylmethyl]-1H-pyrazole

TRP – Transient-receptor potential channel

TRPV – Transient-receptor potential vanilloid channel

VDCC – Voltage-dependent calcium channel

VSMC – Vascular smooth muscle cell

XeC – Xestospongin C

Chapter 1: Introduction

1.1 Research problem, hypotheses and objectives

1.1.1 Research problem

Proteinase-activated receptor 2 (PAR2) mediated vasodilation has been demonstrated across many species, even in the presence of endothelial dysfunction where other mechanisms of vascular relaxation are impaired (McGuire et al., 2008). In experimental models of endothelial dysfunction the potent and selective PAR2 activating peptide (PAR2-AP) 2-furoyl-LIGRLO-amide (2fly) induces sustained relaxation of arteries in Ang II-treated mice where other agonists bradykinin and acetylcholine (ACh) for example, show attenuated vasodilation (Chia et al., 2011; McGuire et al., 2008). 2fly has become the most commonly used synthetic agonist for PAR2 with 10 to 300 times the *in vitro* potency for vascular relaxation and hyperpolarization as compared to legacy PAR2-AP, SLIGRL-NH_2 (McGuire et al., 2004b). Chia *et al.*, (2011) utilized myograph isometric tension experiments to demonstrate that ACh-induced relaxations of mesenteric arteries in angiotensin-II (Ang II) infused C57BL/6J *par*2 wild-type (PAR2-WT) mice and B6.Cg-*F2rl*1^{tm1mslb}/J *par*2 knockout mice (PAR2-KO) were attenuated by 12% and 14% respectively compared to saline-treated controls. Despite endothelial dysfunction reducing the muscarinic type 3 (M_3)-mediated relaxations, PAR2-mediated relaxations were sustained in PAR2-WT. It is worthwhile to note that ACh is not selective for M_3 receptors but stimulate all classes of cholinergic receptors. The vascular endothelium only expresses the M_3 subtype of cholinergic receptors. The literature suggests that mechanisms other than nitric oxide (NO) and prostacyclin (PGI_2) may account for preserved resistance vessel PAR2 vasodilation in endothelial dysfunction (Chia et al., 2011; Ramachandran et al., 2012b).

In resistance vasculature, endothelium-derived hyperpolarizing factors (EDHF) are believed to mediate the majority of vasodilator response (Garland et al., 2011; Taylor et al., 1988). Unique Ca^{2+}-events in endothelium may be the signal transduction initiators for EDHF (Ledoux et al., 2008; Tran et al., 2012). Ca^{2+}-events stimulate calcium-activated potassium channels which initiate vascular hyperpolarization (Dora et al., 2008; Ledoux et al., 2008). Aside from triggering Ca^{2+}-transients, PAR2 activation is also associated with the sensitization of transient-receptor potential vanilloid (TRPV) channel subtype 1 and 4 (Chen et al., 2011) which further enhances Ca^{2+}-influx into the endothelium (Poole et al., 2013). The Ca^{2+}-events initiated by ACh and carbachol (CCh) in vascular endothelium *in situ* have been studied in murine (Ledoux et al., 2008; Marie et al., 2002; Ohata et al., 2003), rat (Dora et al., 2008; Mumtaz et al., 2011; Oishi et al., 2001; Tang et al., 2007; Yip et al., 1996), hamster (Tran et al., 2012; Uhrenholt et al., 2007), porcine (Budel et al., 2001) and cultured endothelial cells (EC) (Mutoh et al., 2008). The PAR2 activation cascade and the resultant rise in endothelial cytosolic $[Ca^{2+}]_i$ is similar to M_3-mediated signal transduction (Browning, 2010; Macfarlane et al., 2001; Ramachandran et al., 2011).

There has been no detailed work on the Ca^{2+}-events associated with PAR2 activation in ECs. It is possible that preserved Ca^{2+}-signaling is the mechanism of persistent PAR2-mediated vascular relaxation in endothelial dysfunction. The majority of work on endothelial Ca^{2+}-events has been conducted in cultured cells or *in situ*. These studies raise the issue of dealing with the abnormal physiology of cultured cells (Dawson et al., 2012), or the interference from other cell types. Studying PAR2-mediated Ca^{2+}-signaling in freshly isolated ECs allows for the elementary components (dynamics and kinetics) of transients to be identified.

1.1.2 Hypothesis and objectives

The overall objective is to characterize the PAR2-mediated Ca^{2+}-signaling activity in isolated mesenteric endothelial cells from a murine model of endothelial cell dysfunction. To address the objective within the ECs I intend to examine 2fly-induced Ca^{2+}-events, the effects of Ca^{2+}-channel inhibitors on Ca^{2+}-signaling and expression of Ca^{2+}-signaling related proteins.

Hypothesis 1 is that Ca^{2+}-events evoked by PAR2-AP 2-furoyl-LIGRLO-amide will not diminish in a mouse model of endothelial dysfunction where Ca^{2+}-events induced by M_3-agonist ACh will be attenuated. To test hypothesis 1 2fly and ACh concentration response curves (CRC) measuring Ca^{2+}-events were obtained in freshly isolated murine mesenteric EC. Ca^{2+}-events were obtained through Nipkow spinning disk confocal microscopy. The model of endothelial dysfunction was created by surgically implanting sub-cutaneous (s.c.) micro-osmotic pumps into mice with a 14 day release of Ang II (1.5 mg/kg/day) modified from previous work (Chia et al., 2011; McGuire et al., 2008). The experimental model was compared to mice with the implantation of saline pumps over the same time course. **Objective 1:** To determine baseline Ca^{2+}-events, freshly isolated murine mesenteric ECs were examined under a Nipkow spinning disk confocal microscope with FITC (488 nm) laser excitation modified from techniques used extensively in the past (Haq et al., 2013; Ledoux et al., 2008haq; Tran et al., 2012). **Objective 2:** To characterize the effects of PAR2 and M_3 activation on the EC Ca^{2+}-events, 2fly (0.1 nM to 3 μM) and ACh (1 nM to 30 μM) concentration response curves (CRC) were constructed.

Hypothesis 2 is that inositol triphosphate receptors (IP3R) and TRPV channels contribute to the calcium activity seen in our animal models. I expect that inhibiting IP3R and TRPV channels will reduce intracellular Ca^{2+}-events in both experimental (endothelial dysfunction) and control (saline) animals. To test hypothesis 2 the same Ca^{2+} imaging techniques were employed as in hypothesis 1. **Objective 1:** Characterize the IP3R inhibition (xestospongin

C (XeC), 2 µM) in isolated ECs while PAR2 is activated (2fly; 30 nM). **Objective 2:** Characterize the effects of TRPV inhibition (ruthenium red (RR), 75 µM) in isolated ECs while PAR2 is activated (30 nM 2fly). We compared 2fly-induced Ca^{2+}-events to those elicited by ACh.

Hypothesis 3 is that the expression of PAR2 and intermediate conductance potassium channel (IK_{Ca}) will be increased in Ang II treated PAR2-WT compared to controls, and that eNOS distribution will be reduced in Ang II treated animals. PAR2 and IK_{Ca} are essential mediators of the preserved PAR2 NO/PGI_2-independent resistance vessel relaxations (Chia et al., 2011). It is expected that these proteins will be up regulated in endothelial dysfunction as a compensatory mechanism. A possible explanation for the loss of relaxation activity in vessels with endothelial dysfunction is the reduction in activity or expression of eNOS. To test hypothesis 3 immunocytochemistry experiments will be carried out and individual cells imaged by a CCD camera on a line-scan confocal microscope. **Objective 1**: Determine the expression of PAR2 and IK_{Ca}, freshly isolated ECs were incubated with protein specific 1° antibody (Ab) and FITC 2° Ab and imaged via line-scan confocal microscopy, modified from previous studies (Dora et al., 2008; Stuyvers et al., 2005). The expression of eNOS, IP3R and SK_{ca} were evaluated, to shed light on the extent of endothelial dysfunction. Finally all cells will be co-probed with 1° Ab for platelet endothelial cell adhesion molecule (PECAM-1) and Texas Red 2° Ab to positively identify cells in the preparation as ECs.

This study is expected to inform on the potential role of Ca^{2+}- signaling in the preservation of PAR2 activity during endothelial dysfunction. In particular, I anticipate an explanation at the Ca^{2+}-signal transduction level for the attenuation in M_3-mediated vascular relaxation observed in other studies on Ang II treated mice.

1.2 Literature Review

1.2.1 Hypertension, angiotensin II and endothelial dysfunction

Heart disease, atherosclerosis, myocardial infarction, stroke and ischemia related diseases accounted for 29% of deaths in Canada in 2009 (Statistics Canada, 2009). Hypertension is still on the rise, while the trend in cardiovascular related deaths has been declining (Statistics Canada, 2013). From 2005 the number of adults living with high blood pressure (greater than 140 mm Hg systolic / 90 mm Hg diastolic pressure measured in a physician's office) increased by 2.6% to 18% total in 2011 (Statistics Canada, 2013).

Endothelial dysfunction is a vascular pathology that can be defined by impaired vasodilation, increased inflammation and a greater tendency for thrombosis (Endemann et al., 2004). Generally speaking, endothelial dysfunction causes increased blood pressure when endothelium-derived contracting factors (EDCF) are increased disproportionately to endothelium-derived relaxing factors (EDRF) such as nitric oxide (NO) or prostacyclin (PGI_2) (Ayajiki et al., 2000). Possible etiologies and resultant symptoms of endothelial dysfunction are broad. Heritable conditions, hypertension, toxic substances and other cardiovascular risk factors activate endothelial cells (Deanfield et al., 2007). Prolonged exposure to cardiovascular risk factors can exhaust endothelial cells' anti-inflammatory and vasodilatory machinery (Deanfield et al., 2007; Higashi et al., 2012). Some of the endothelial proteins affected by cardiovascular risk factors include NADPH oxidase, xanthine oxidase and cyclooxygenases which may produce reactive oxygen species (Hamilton et al., 2002; Silva et al., 2012). A proposed mechanism for eNOS includes a functional shift during the prolonged risk factor period. Studies suggest that the enzyme changes to a reactive oxygen species-mediated silencing (Deanfield et al., 2007; Rhee, 2006). These reactive molecules may further perturb eNOS by uncoupling the enzyme (Yang et

al., 2009) and decreasing tetrahydrobiopterin bioavailability (Bevers et al., 2006). Some of the biological mediators which precipitate endothelial dysfunction are messengers of the renin angiotensin aldosterone system (Aroor et al., 2013; Patel et al., 2012).

Ang II infusion is used in laboratory animals to create models of endothelial dysfunction (Avendano et al., 2013; Wang et al., 2013). Ang II is converted from angiotensin I by angiotensin converting enzyme (Carey, 2013). Angiotensin I is converted from angiotensinogen through the enzyme renin, produced in juxtaglomerular cells (Herichova et al., 2013). Ang II acts to promote aldosterone release from the adrenal cortex (Ansurudeen et al., 2010) and to constrict the glomerular efferent arterioles enhancing glomerular filtration (Schiessl et al., 2013). These physiological responses are a mechanism to conserve extracellular fluid and blood volume or to prevent sodium losses (Spitzer, 1982). Ang II is a potent systemic vasoconstrictor when continually administered through infusion (Parisi et al., 1985). Ang II binds the $G_{q/11}$-protein coupled AT1 receptor on vascular smooth muscle cells (Lassegue et al., 1995). This binding activates phospholipase C which cleaves phosphatidylinositol-4,5-bisphosphate (PIP_2) into IP_3 and diacylglycerol (DAG). The increase of cytosolic $[IP_3]_i$ ultimately raises smooth muscle $[Ca^{2+}]_i$, causing constriction (Chen et al., 2013). Saturation studies of AT1 on rodent thoracic aortic rings demonstrate that Ang II causes concentration-dependent spikes in smooth muscle $[Ca^{2+}]_i$ (Arun et al., 2005). The chronic effects of Ang II on vascular smooth muscle, including consistently elevated cytosolic calcium, leads to vascular remodeling and dysfunction (Gao et al., 2013; Wakui et al., 2013).

Endothelial cells possess Ang II receptors AT1 and AT2, where exposure to Ang II increases cytosolic $[Ca^{2+}]_i$ and stimulates NO production (Pueyo et al., 1998; Rajagopalan et al., 1996). Cultured rodent microcoronary artery endothelial cells exposed to Ang II exhibit Ca^{2+}-

sparks with a measured sustained rise in cytosolic $[Ca^{2+}]_i$ (Nistri et al., 2012). Subcutaneous infusion of Ang II has been used to generate an effective model of endothelial dysfunction. Ang II infusion was used in Nox4 knockout mice by Schröder and colleagues. Ang II infusion in the absence of NO production caused vascular bed inflammation, media hypertrophy and endothelial dysfunction determined by increased oxidative stress (Schroder et al., 2012). Ang II infusion has been used in rodents to elevate NADPH-mediated vascular superoxide production (Mollnau et al., 2002). Analysis of the rodent vessels revealed Ang II treatment induced eNOS uncoupling and enhanced oxidative stress within the endothelium (Mollnau et al., 2002). Previous studies show attenuated relaxation of murine mesenteric arteries to ACh following subcutaneous Ang II infusion (Chia et al., 2011; Marchesi et al., 2013). Here we utilize the same approach using a murine model of Ang II-induced endothelial dysfunction in mesenteric arteries.

1.2.2 Proteinase-activated receptors (PARs) and their activation

Proteinase-activated receptors (PARs) are a family of four G-protein coupled 7-transmembrane domain receptors (GPCRs) (Ramachandran et al., 2012b). PAR subfamily nomenclature comes from the order of discovery, first PAR1 also known as thrombin receptor (Hollenberg, 2003). PAR2 was identified through molecular cloning and functional expression experiments that identified trypsin, but not thrombin, as an enzyme activator (Nystedt et al., 1995; Nystedt et al., 1994). PARs can be found in the tissues and isolated cells of many species (Adams et al., 2011; Thorsen et al., 2008). All PARs are found on EC plasma membranes (D'Andrea et al., 1998; Hamilton et al., 2001). PAR2 is found in generic fibroblasts (D'Andrea et al., 1998), PAR1, PAR3 and PAR4 are found on platelets (Kahn et al., 1998; Vu et al., 1991) and PAR1 in smooth muscle cells (D'Andrea et al., 1998; Hamilton et al., 2001). PARs share a

unique mechanism of activation by serine proteinases. Cleavage involves a cryptic tethered ligand binding to the second extracellular loops on the PARs (Ramachandran et al., 2012b).

The cryptic tethered ligands contain a coded residue motif (Table 1) that is revealed upon selective cleavage by trypsin-like serine proteases (Macfarlane et al., 2001). The binding of the tethered ligand to the PAR extracellular loops induces a conformational change that activates G-protein coupled pathways (Ramachandran et al., 2012b). Trypsin-like serine proteases that activate PARs demonstrate substrate specificity for the cleavage sites that produce the tethered ligands. For example, thrombin activates PAR1, PAR3 and PAR4 (Macfarlane et al., 2001) whereas trypsin activates PAR2 at low, and PAR4 at high, concentrations (Carr et al., 2000). PARs can also be activated by PAR-APs, small peptides that bind directly to an extracellular loop (ECL) of the PAR (Ramachandran et al., 2012b). In the case of PAR1 and PAR2, this loop is ECL-2 (Ramachandran et al., 2012b). PAR activation by PAR-APs is unique because it does not require exposure of the tethered ligand to induce the conformational change (Hollenberg et al., 1997). PAR-APs have become very useful tools for PAR research over the past two decades, due to their higher potency and specificity than proteases (Lee et al., 2012a).

Receptor Designation (IUPHAR)	Tethered Ligand Sequence
PAR1	Human: SFLLRN...
	Mouse: SFFLRN…
PAR2	Human: SLIGKV…
	Mouse: SLIGRL...
PAR3	Human: TFRGAP…
	Mouse: SFNGGP...
PAR4	Human: GYPGQV...
	Mouse: GYPGKF...

IUPHAR = International Union of Pharmacology
(Hollenberg et al., 2002)

Table 1. Amino terminus tethered ligand residue sequence of human and murine PARs following cleavage by trypsin-like serine proteases. Modified from (Hansen et al., 2008)

1.2.3 PAR2 activation by trypsin-like serine proteases

The proposed mediators of PAR2 activation *in vivo* are trypsin-like serine proteases (Ramachandran et al., 2012b). For PAR2, these enzymes include: pancreatic trypsin (Nystedt et al., 1995), extrapancreatic trypsin IV (Cottrell et al., 2004), mast cell tryptase (Brass et al., 1997), membrane-tethered serine-protease 1 (Takeuchi et al., 2000) and kallikreins (Ramachandran et al., 2012a). Each of these proteases has been demonstrated to activate PAR2 by endolytic cleavage of the extracellular amino terminus arm, revealing the tethered ligand motif *in vitro*. Rodent and murine PAR2 have nearly identical homology, receptor confirmation and the same tethered ligand motif "SLIGRL…" (Hansen et al., 2008). Several residues offer themselves as candidates for trypsin-like proteolysis along the amino terminus of rodent PAR2: R^{36}, R^{41}, K^{51} and K^{72} (Al-Ani et al., 2003). *In vitro* bioassays utilizing mutant rats have uncovered that only R^{36} is preferentially cleaved exposing the NH_2-S^{37}LIGRL… motif (Al-Ani et al., 2003). After cleavage of R^{36}/S^{37}, increasing $[trypsin]_o$ does not lead to further cleavage of the amino terminus. This suggests that after cleavage of this preferential locus the remaining three potential sites for cleavage are inaccessible to the enzyme (Al-Ani et al., 2003). Indeed the significance of R^{36} is

highlighted upon mutation to alanine, where no PAR2 effects could be measured *in vitro* upon the addition of trypsin (Al-Ani et al., 2003). This persistent and irreversible activation of PAR2 leads to: desensitization of the tissue to PAR2 activators (Defea et al., 2000; Ricks et al., 2009), endocytosis of the receptor (Dery et al., 1999) and reduces its vesicular trafficking (Ramachandran et al., 2012b; Roosterman et al., 2003).

1.2.4 PAR2 activation at ECL2: tethered ligand motif, PAR2-APs and small molecules

The first PAR-APs were mimetic of the tethered ligand motifs for the receptors: TFLLR-NH_2 for PAR1 (Hollenberg et al., 1997), SLIGRL for PAR2 (Hollenberg et al., 1996), TFRGAP for PAR3 (Kawao et al., 2003) and AYPGKF-NH_2 for PAR4 (Bretschneider et al., 2003). 2fly has 10- to 300-times the *in vitro* potency of SLIGRL-NH_2, depending on the in-vitro assay (McGuire et al., 2004b). 2-furoyl substitutes for the S in SLIGRL, provides a functional hydroxyl group and demonstrates some protection from aminopeptidases (Kawabata et al., 2004a). Interestingly the terminal ornithine leads to an increased potency (McGuire et al., 2004b).

The first reports of small non-peptide molecules that activated PAR2 came in 2008 by Gardell and colleagues. This cohort synthesized molecules that have anionic bonds with peptide characteristics and contain aromatic phenyl derivatives. The first small molecule activators had potencies comparable to 2fly, this was determined by assaying phosphatidylinositol hydrolysis in cell culture (Gardell et al., 2008). The non-peptidic molecules induced the same rat paw edema inflammatory response seen in other PAR2-AP studies (Gardell et al., 2008; Tae et al., 2003). Another PAR2 agonist, GB110, was shown to have potency comparable to 2fly demonstrated by Ca^{2+}-response assays in HT29 carcinoma cells (Barry et al., 2010).

PAR2-APs are still capable of activating PAR2 that has been cleaved by enzymes, such as elastase (Hansen et al., 2008). Elastase cleaves PAR2 by cleaving the carboxyl side of the

tethered ligand motif (Hansen et al., 2008). During vascular dysfunction such as blood thrombus development, neutrophil elastase leaks into the blood plasma where it is free to interact with the surface of the endothelium (Wachtfogel et al., 1983). Elastase activation of PAR2 (i.e. disarming) stimulates mitogen-activated protein kinase (MAPK) pathways which modulate gene transcription (Ramachandran et al., 2011).

1.2.5 PAR2 inhibitors and the cessation of PAR2 signaling

In vivo PAR2 silencing is thought to be mediated by phosphorylation and receptor internalization. The natural termination of PAR2 signaling follows its activation and the phosphorylation of several serine and threonine residues on the internal carboxyl terminus (Bohm et al., 1996; Ricks et al., 2009). The phosphorylation, mediated by G-protein coupled receptor kinases, is a crucial step in recruiting β-arrestin 1 and 2 which are essential to desensitize the receptor (Dery et al., 1999; Ricks et al., 2009; Seatter et al., 2004). This phosphorylated C-terminus and β-arrestin complex then docks to an AP2 adapter protein that mediates clathrin-coated pit formation around PAR2 (Wolfe et al., 2007). The C-terminus of the receptor, adapter and scaffolding protein complex is subsequently ubiquitinated and targeted for internalization and trafficking to RAB5A-positive early endosomes (Hasdemir et al., 2009).

PAR2 silencing is achieved experimentally through the use of synthetic inhibitors. The first PAR2 antagonist discovered to inhibit both the tethered ligand and PAR2-AP activation was GB83 (Barry et al., 2010). GB83 is a complex pyrroloquinazoline derivative that causes surmountable competitive inhibition against SLIGRL-NH_2 induced $[Ca^{2+}]_i$ elevation in HT29 carcinoma cells (Barry et al., 2010). Peptide-mimetic competitive inhibitors of PAR2 were synthesized by Kanke *et al.,* (2009); K-12940 and K-14585 (Kanke et al., 2009). These inhibitors

eliminated SLIGKV-induced $[Ca^{2+}]_i$ elevations in PAR2-transfected human keratinocytes and displaced radiolabelled [^{3}H]-2-furoyl-LIGRL-NH_2 from PAR2 (Kanke et al., 2009).

Antibodies against PAR2 that are specific for the amino terminus residues, have been used for immunostaining receptor expression and inhibiting proteolytic activation (Ramachandran et al., 2012b). The rabbit anti-PAR2 polyclonal antibody (Ab) B5 recognizes K^{51} and K^{72} of the amino terminus (Al-Ani et al., 2003). Anti-PAR2 Ab SAM-11 recognizes S^{37}LIGKVDGTSHVTG^{50} of the amino terminus in human PAR2, with murine and rodent cross reactivity (Kelso et al., 2006). Murine studies have demonstrated that intra-articular carrageenan/kaolin mediated joint inflammation is attenuated by B5 and SAM-11 *in vivo* (Kelso et al., 2006; Ramachandran et al., 2012b). Additionally, cell penetrating pepducins have been designed for inhibiting PAR1, 2 and 4 (Ramachandran et al., 2012b). For example, PAR2-binding lipopeptide pepducin P2pal-18S inhibited mast cell tryptase-induced paw inflammation in mice *in vivo* (Sevigny et al., 2011). The PAR2 activation and inhibitory mechanisms are shown in Figure 1. It is also important to discuss another tool for receptor investigation, the PAR2-deficient (PAR2-KO) mouse.

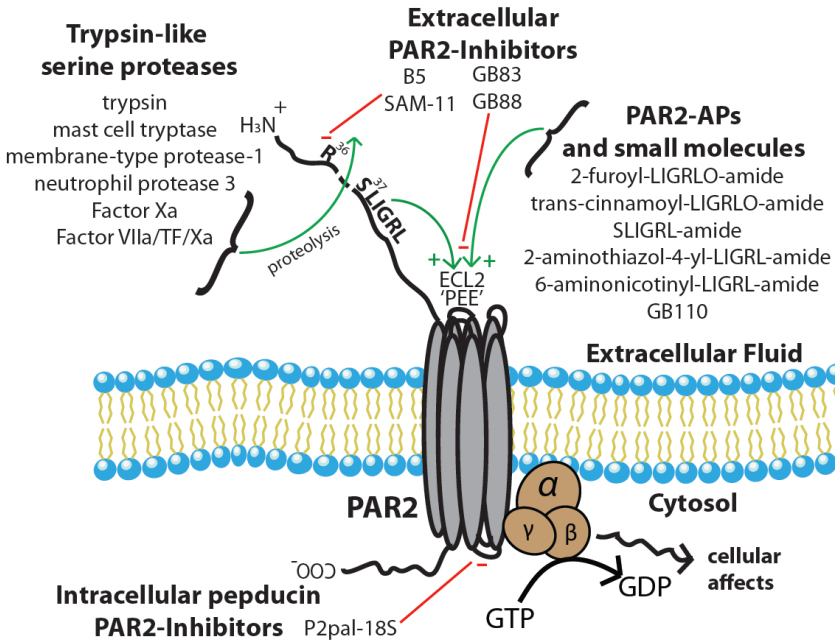

Figure 1. Mechanisms of PAR2 activation and inhibition. PAR2 activation via trypsin-like serine proteases, PAR2-APs and small molecules (green arrows). PAR2 inhibition by peptidic and non-peptidic molecules, anti-PAR2 antibodies and pepducins (red lines). See references: (Barry et al., 2010; Boitano et al., 2011; Ferrell et al., 2003; McGuire et al., 2004b; Ramachandran et al., 2012b; Sevigny et al., 2011).

1.2.6 The PAR2-KO mouse

Transgenic PAR2-KO mice are used to research the *in vivo* effects of *par*2 gene deletion and to investigate the specificity of the *in vitro* effects of PAR2 agonists. The use of whole animal *par*2 deletion is not without criticism. For example, compensatory resistance vessel relaxation pathways may be up regulated in PAR2-KO. Since the first development of a PAR2-KO mouse strain by Damiano *et al.*, (1999) some differences in the physiology of the transgenic model have been discovered. Data acquired by radiotelemetery showed that systolic blood pressure in PAR2-KO were ~5 mm Hg higher than PAR2-WT (McGuire et al., 2008). Models of inflammation appear to be decreased in PAR2-KO, which is expected considering that PAR2 activation is associated with enhanced inflammation *in vivo.*

PAR2-KO, used in experiments reported in this thesis, are progeny from crosses of *par*2 deficient mice generated by Jackson Laboratory (Bar Harbor, ME). This PAR2-KO model was first created by Lindner *et al.,* (2000). Researchers screened a 129/SvJ mouse genomic library for the *par*2 gene, located on chromosome 13, and generated a pNTK targeting vector with a neomycin phosphotransferase expression cassette. The recombinant pNTK vectors replaced the *par*2 gene and were electroporated into embryonic 129/SvJ stem cells. Selection then took place for male PAR2 heterozygous (PAR2-HET) chimeras. Male PAR2-HETs were mated with female wild-type C57BL/6J mice. B6.Cg-*F2rl*1^{tm1mslb}/J PAR2 knockout mice were generated by breeding the male and female PAR2-HETs.

1.2.7 PAR2 and animal models of human disease

The motivation for developing specific PAR-APs and antagonists lies in exploring the role of PARs in disease states (Ramachandran et al., 2012b). PAR2 may act in a beneficial or deleterious manner depending on the disease model (McGuire, 2004). In models of colitis (Lohman et al., 2012), arthritis (Kelso et al., 2006) and asthma (Gu et al., 2009) PAR2 activation has been associated with increased macrophage infiltration while PAR2-KOs showed an improved disposition (Lee et al., 2012b). Yet chronic *in vivo* activation of PAR2 lowers systolic blood pressures in mice (Hughes et al., 2013) but PAR2-KOs have modestly increased systolic blood pressures (McGuire et al., 2008). Chronic infusion of PAR2-AP 2fly also caused vascular dysfunction in mice, which may have limited its blood pressure lowering activity (Hughes et al., 2013). This PAR2-AP induced dysfunction caused attenuated NO-mediated relaxation in murine aortas (Hughes et al., 2013). PAR2 activation may benefit organ perfusion; resistance vessels relax to PAR2 agonists in the presence of endothelial dysfunction despite impairment of other vasodilation mechanisms (Chia et al., 2011; Smeda et al., 2010). Naturally the specific pathology

would dictate whether inhibition or activation of PAR2 would be of greatest therapeutic benefit (McGuire, 2004).With a foundation of PAR2 molecular biology and physiology, the endothelial signaling pathways of the receptor will now be presented.

1.2.8 NO/ PGI_2-mediated vascular smooth muscle relaxation

In 1980 classical experiments by Furchgott and Zawadzki demonstrated that isolated rabbit aortas precontracted with α_1 adrenergic receptor agonist could relax to ACh (Furchgott et al., 1980). A series of experiments by Furchgott and Zawadzki determined that the source of this relaxation was the endothelium; in endothelium denuded aortas ACh induced contraction (Furchgott et al., 1980). This contraction is not surprising, now that we know VSM cells (VSMC) have M_3 receptors (Karashima et al., 1981). Ignarro *et al.* (1987) examined perfused bovine intrapulmonary artery and vein for the relaxation properties of EDRF and compared these to NO. In the same year another consortium led by Ferid Murad recognized soluble guanylyl cyclase (sGC) and 3', 5'-cyclic guanosine monophosphate (cGMP) as secondary messengers in endothelium-dependent NO-mediated VSM relaxation (Murad et al., 1987). The collective efforts of Furchgott, Ignarro and Murad to characterize the NO-mediated vascular relaxation led to their co-award of The Nobel Prize in Physiology or Medicine in 1998 (The Nobel Foundation, 1998).

ACh binds M_3, a 7-transmembrane GPCR located on the plasma membrane of vascular ECs (Berstein et al., 1992; Dauphin et al., 1990). When M_3 is activated it initiates a signaling pathway like that shown in Figure 2. PAR2 activation follows a similar messaging cascade as that laid out below. This signal transduction pathway and its effects on VSMC $[Ca^{2+}]_i$, as they pertain to PAR2 activation, are highlighted in Figure 3.

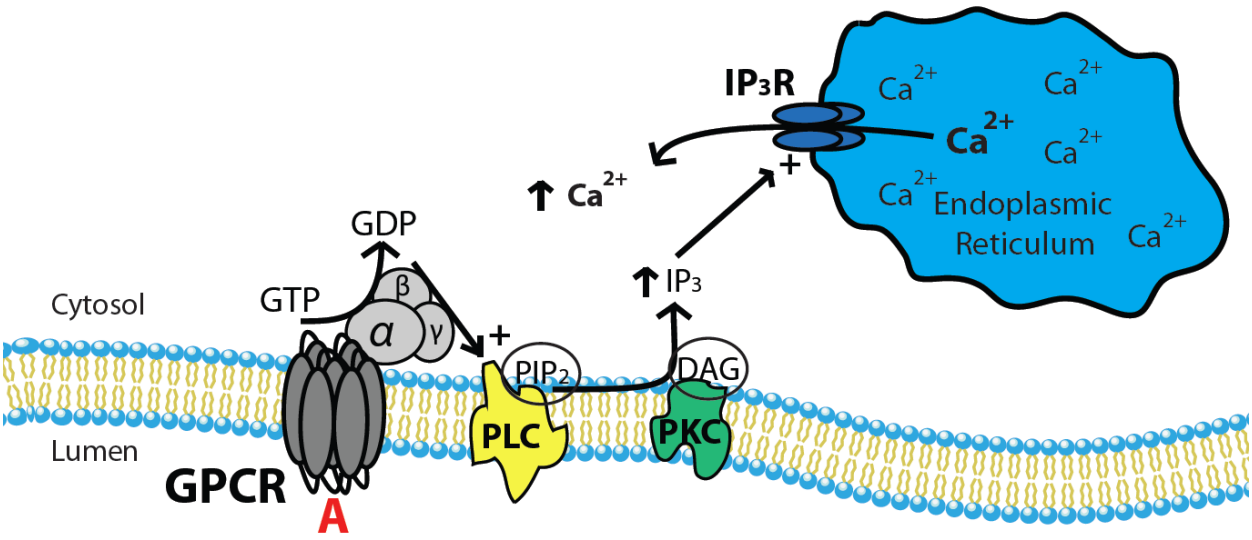

Figure 2. 7-transmembrane G-protein coupled receptor messaging cascade. This GPCR signaling pathway occurs in vascular endothelium and leads to the efflux of Ca^{2+} ions from the endoplasmic reticulum into the cytosol.

A = ligand, i.e. acetylcholine; GPCR = 7-transmembrane G-protein (αβγ) coupled receptor, i.e. M_3; DAG = diacylglycerol; PIP_2 = phosphatidylinositol-4,5-bisphosphate; PLC = phospholipase C; PKC = protein kinase C; IP_3(R) = inositol triphosphate (receptor).

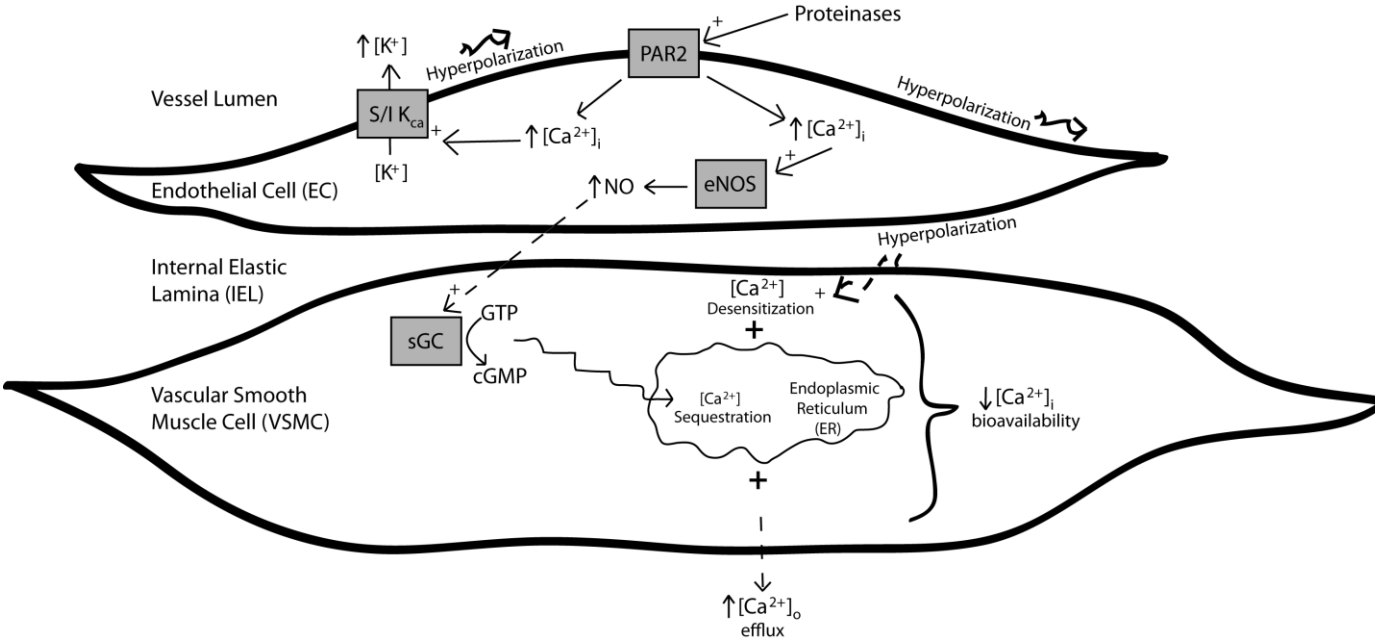

Figure 3. PAR2 Endothelial-dependent NO and K_{ca}-mediated vascular smooth muscle relaxation. Activation of PAR2 by proteinases leads to NO production and K_{ca} activation in vascular endothelium. The NO diffuses across the sarcolemma to activate soluble guanylyl cyclase. K_{ca} produces hyperpolarizing membrane potential. The result is a decrease in Ca^{2+} bioavailability in the vascular smooth muscle tissue.

PAR2 = proteinase-activated receptor 2; eNOS = endothelial nitric oxide synthase; sGC = soluble guanylyl cyclase; NO = nitric oxide; GTP = Guanosine-5'-triphosphate; cGMP =3', 5'-cyclic guanosine monophosphate; S/I K_{ca} = small/intermediate calcium-activated potassium channels.

NO-mediated vasodilation has been extensively documented following PAR2 activation. We have shown that PAR2 activation by 2fly relaxes aortas in PAR2-WT and PAR2 heterozygotes (Hennessey et al., 2013). Isometric tension experiments with NOS inhibitor, N_{ω}-nitro-L-arginine-methyl ester hydrochloride (L-NAME), obliterate PAR2-mediated relaxations in PAR2-WT and PAR2 heterozygous murine aortas (Hennessey et al., 2013). In addition many conduit arteries other than the aorta rely to varying degrees on NO or PGI_2. Vascular relaxation mechanisms are different in vessels of smaller diameter which are responsible for perfusion of the tissues (Shimokawa et al., 1996) .

In resistance vessels there is decreasing reliance on NO and PGI_2 for relaxation. In murine mesenteric arteries, trypsin and SLIGRL-NH_2 induced vasodilation is only slightly inhibited by L-NAME (McGuire et al., 2002). Rodent mesenteric artery diameter is inversely proportional to reliance on NO for vasodilation (Shimokawa et al., 1996). In murine mesenteric arteries incubated with L-NAME, indomethacin and sGC inhibitor 1H-[1, 2, 4] oxadiazolo [4, 3-α] quinoxalin-1-one (ODQ), there are still robust relaxations to 2fly (Chia et al., 2011).

1.2.9 NO/PGI_2-independent vascular smooth muscle relaxation

The first observation of vascular hyperpolarization and relaxation occurring in tandem was in guinea pig anterior mesenteric arteries after muscarinic receptor activation by CCh (Bolton et al., 1984). Without modern inhibitors, researchers of the time used methylene blue to inhibit sGC and hemoglobin to scavenge NO. Through the use of these compounds, and indomethacin to inhibit COX, investigators distinguished EDHF as a separate entity from NO and PGI_2 (Chen et al., 1988). An excellent review by Waldron and Garland in 1994 speculated that vascular hyperpolarization closed voltage-dependent calcium channels (VDCC) and attenuated smooth muscle contractility. The authors also considered that resistance arteries rely

more heavily on extracellular Ca^{2+} during contraction than intracellular stores, setting the stage for EDHF research in resistance vessels.

The NO and PGI_2 relaxation pathways are independent from endothelium-derived hyperpolarization (EDH). Still, NO has been suggested as an essential mediator in the EDHF response (Takaki et al., 2008). Acute inhibition of rodent eNOS *in vivo* with L-NAME attenuated intermediate (IK_{Ca}) and small (SK_{Ca}) conductance Ca^{2+}-activated potassium channel-sensitive EDHF-mediated vasodilatation (EDV) (Desai et al., 2006). Hyperpolarization of VSM correlates with the opening of large conductance (BK_{Ca}) Ca^{2+}-activated potassium channels (Chen et al., 2012). VSM BK_{Ca} activation increases NO release from endothelium in rat superior mesenteric artery, which may be responsible for some of the EDHF response (Climent et al., 2012). NO causes endothelium and vascular smooth muscle hyperpolarization in a variety of tissue, species and gender specific manners (Csanyi et al., 2006; Feletou et al., 2006; Feletou et al., 2012). The PGI_2 pathway is not considered to be directly involved in EDHF-mediated EDV, though it causes hyperpolarization in select studies (Giles et al., 2012; Triggle et al., 2012). Molecular candidates for EDHF include: hydrogen sulfide (H_2S) (Yang et al., 2008), hydrogen peroxide (H_2O_2) (Gao et al., 2007), arachidonic acid metabolites (Brunt et al., 2012), and c-type natriuretic peptide (Khambata et al., 2011). It is accepted that potassium channels are essential in all forms of EDH and the potassium ion itself is proposed as an EDHF.

1.2.10 K^+ channels and the K^+ ion as EDHF

Garland and colleagues disputed the contribution of K_{ATP} to the hyperpolarizing phenomenon, the EDHF-response was unaffected by glibenclamide in rat mesenteric artery and rabbit basilar artery (Adeagbo et al., 1993; Garland et al., 1992; Plane et al., 1993). Dendrotoxin studies on rat mesenteric arterial bed proved that EDHF-mediated hyperpolarization would shut

K_V, ruling out this channel as a contributor (Adeagbo et al., 1993). K_{ATP}-sensitive EDH is only observed where classical apamin/ChTX-sensitive EDHF responses are limited (Ohashi et al., 2005; Skovgaard et al., 2011).The importance of BK_{Ca} in EDHF has been challenged by studies proving the inability of IbTX to inhibit hyperpolarization (Gluais et al., 2005; White et al., 1997; Yamauchi et al., 2012). Chen *et al.*, (2012) have shown that SK_{Ca} inhibitors apamin, d-tubocurarine (dose-dependent) (Teshima et al., 2003) and scyllatoxin (Ayajiki et al., 2000) attenuate ACh-mediated relaxations of murine mesenteric arteries. Yet these relaxations and hyperpolarizations are also sensitive to IbTX (Chen et al., 2012). Determining which K^+-channels are most tightly coupled to hyperpolarization and relaxation is not so straightforward. *In vivo* all subtypes of S/I/BK_{Ca} may be active during EDH, though not all mediate the EDHF response. BK_{Ca}-sensitive relaxations with classical S/IK_{Ca}-inhibitor sensitive EDHF have been observed in: rodent femoral (Leung et al., 2006), rodent ocular ciliary (Dong et al., 2010) and bovine coronary arteries (Yi et al., 2007).

Studies have described attenuation or outright ablation of EDHF-mediated effects by SK_{Ca} inhibitor apamin (Craig et al., 2012; Edwards et al., 1998) and IK_{Ca} blockers 1-[(2-chlorophenyl) diphenylmethyl]-1H-pyrazole (TRAM-34) or ChTX but not BK_{Ca} blocker IbTX (Craig et al., 2012; Stankevicius et al., 2011). Stankevicius and colleagues (2011) examined NS309-mediated (S/IK_{Ca} activator) relaxation in rat small mesenteric arteries. They found that apamin slightly attenuated relaxation and hyperpolarization, while TRAM-34 had similar effects (Stankevicius et al., 2011). The authors found that the combination of both apamin and TRAM-34 abolished EDHF-mediated relaxation while IbTX had little effect. Table 2 provides a synopsis of recent work on K^+-channels, as they have been implicated in EDHF-mediated responses.

The "K^+-cloud" is a phenomenon described in the literature and suggested to be a contributor to EDHF. K^+-clouds are associated with a local rise in internal elastic lamina $[K^+]_o$ which is not high enough to induce VSM depolarization, yet sufficient enough to potentiate hyperpolarization and relaxation of the vasculature (Edwards et al., 2004). The precise origin and functional role of this transient and moderate rise in extracellular $[K^+]_o$ is a matter of contention. ECs release of K^+ ions from SK_{Ca} and IK_{Ca} that hyperpolarizes VSMCs by activating K_{ir} and Na^+/K^+-ATPases (Edwards et al., 2004; Weston et al., 2008). These increases in $[K^+]_o$ are typically in the range of 6-16 mM (Edwards et al., 1988; Knot et al., 1996) and are sensitive to Ba^{2+} + ouabain (Edwards et al., 1998). I can surmise the modern school of thought by stating: K^+ -channels are the quintessential generators of EDH and that several factors (EDHFs) can lead to the activation of some combination of these K^+-channels. EDH originates in the endothelium by opening SK_{Ca} and IK_{Ca} and the current traverses across myoendothelial gap junctions (MEGJs) onto VSM sarcolemma (Kerr et al., 2012; Mather et al., 2005). A more detailed discussion on MEGJs and the propagation of vascular hyperpolarizing current will be presented later. We now consider the role PAR2 has played in the dynamic field of EDHF.

Model[Reference]	Proposed EDHF	Sensitive to inhibition of K^+-channel	K^+-channel inhibitor used - channel inhibited
Murine corpus cavernosum smooth muscle strips (Joshi et al., 2012)	HNO	BK_{Ca}	IbTX - BK_{Ca}
Murine small mesenteric arteries (Chen et al., 2012)	NO	BK_{Ca}	IbTX - BK_{Ca}
Rat third-order mesenteric arteries (Favaloro et al., 2009)	NO	K_v	4-aminopyridine - K_v
Rat coronary arteries (Cheang et al., 2010)	H_2S	K_v	4-aminopyridine - K_v
Murine small mesenteric arteries (Mustafa et al., 2011)	H_2S	K_{ATP}, (some SK_{Ca} and IK_{Ca})	Glibenclamide - K_{ATP}; apamin - SK_{Ca}; ChTX - B/IK_{Ca}
Rabbit carotid arteries (Ohashi et al., 2005)	ONOO-	K_{ATP}	Glibenclamide - K_{ATP}
Rat superior mesenteric arteries (Gao et al., 2003)	H_2O_2	K_v, IK_{Ca}, BK_{Ca}	TEA - K_v; ChTX - B/IK_{Ca}; IbTX - BK_{Ca}
Human coronary arterioles (Liu et al., 2011)	H_2O_2	BK_{Ca}	IbTX - BK_{Ca}
Human forearm skin arterioles (Brunt et al., 2012)	CYP2C9-derrived EETs	K_v	TEA - K_v
Isolated porcine coronary endothelial and vascular smooth muscle cells (Weston et al., 2005)	14,15 and 11,12-EET	SK_{Ca} and IK_{Ca} (some BK_{Ca})	Apamin - SK_{Ca}; TRAM-39 - IK_{Ca}; IbTX - BK_{Ca}
Rat aortas (Lopez-Miranda et al., 2010)	Anandamide	BK_{Ca}	IbTX - BK_{Ca}
Rat small mesenteric arteries (White et al., 1997)	Anandamide	K_v	TEA - K_v
Rabbit aortas (Li et al., 2010)	CNP	K_{ATP}, K_{ir}	Glibenclamide - K_{ATP}; 60 mM [KCl] - K_{ir}
Rat pulmonary arteries (Vang et al., 2010)	CNP	BK_{Ca}	IbTX - BK_{Ca}
Rat renal arteries (Zhang et al., 2010)	Anemoside-A3 transduction product	SK_{Ca}, IK_{Ca}, K_v	Apamin - SK_{Ca}; ChTX - B/IK_{Ca}; TEA - K_v
Rat femoral arteries (Leung et al., 2006)	Acetylcholine transduction product (H_2O_2 and/or K^+)	SK_{Ca}, IK_{Ca} (some BK_{Ca} and Na^+/K^+-ATPase)	Apamin - SK_{Ca}; ChTX - B/IK_{Ca}; IbTX - BK_{Ca}; ouabain - Na^+/K^+-ATPase
Rat small mesenteric arteries (Stankevicius et al., 2011)	K^+	SK_{Ca} and IK_{Ca}	Apamin - SK_{Ca}; TRAM-34 - IK_{Ca}
Rat small mesenteric arteries (Weston et al., 2002)	K^+-derived from "K^+ cloud"	BK_{Ca} and Na^+/K^+-ATPase	IbTX - BK_{Ca}; ouabain - Na^+/K^+-ATPase

Table 2. Overview of select K^+-channels involved in EDHF-mediated vasodilation. SK_{Ca} - small conductance calcium-activated potassium channel; IK_{Ca} - intermediate conductance calcium-activated potassium channel; BK_{Ca} - large conductance calcium-activated potassium channel; ChTX - charybdotoxin; IbTX - iberiotoxin; TEA - tetraethylammonium; EET - epoxyeicosatrienoic acid; CNP - C-type natriuretic peptide.

1.2.11 PAR2 and EDHF

The presentation of EDHF is heterogeneous across tissues and experimental models. This can be illustrated with different experiments on PAR2 in resistance vasculature. K_{Ca}-sensitive, EDHF-like, PAR2-mediated relaxation was found in murine mesenteric arteries (McGuire et al., 2002). These tissues relaxed to SLIGRL-NH_2 after the NO/PGI_2 pathways were inhibited by L-NAME, indomethacin and ODQ. Relaxation of these arteries was completely inhibited by adding apamin and ChTX (McGuire et al., 2002). Independently, apamin or ChTX shifted the CRCs of SLIGRL-NH_2-mediated relaxations to the right (McGuire et al., 2002). When substituting ChTX for IbTX, the relaxations were similar to apamin. This suggests that SK_{Ca} and IK_{Ca}, but not BK_{Ca}, play the major role in this PAR2 mechanism (McGuire et al., 2002). McGuire *et al.*, (2004) directly observed VSM hyperpolarization upon activation of PAR2 with SLIGRL-NH_2. NO/PGI_2-relaxation pathways and sGC were not required to mediate the hyperpolarization (McGuire et al., 2004a). Na^+/K^+-ATPase and K_{ir} were, albeit to a much lesser extent, also implicated in the vascular hyperpolarization response (McGuire et al., 2004a). This was the first time that hyperpolarization and isometric tension data were collected concurrently upon activation of PAR2. This group went on to demonstrate that 2fly induced the EDHF response in murine small caliber blood vessels (McGuire et al., 2004b).

Simultaneous *in situ* $[Ca^{2+}]_i$ and isometric tension data were collected from PAR2-mediated relaxations in porcine coronary arteries (Nakayama et al., 2001). Using the NOS inhibitor nitroarginne and COX inhibitor indomethacin, researchers demonstrated that PAR2-mediated NO/PGI_2-independent relaxation occurred in tandem with decreases in VSM $[Ca^{2+}]_i$ (Nakayama et al., 2001). The use of apamin and ChTX completely inhibited trypsin-mediated relaxations and decreases in VSMC $[Ca^{2+}]_i$ in coronary arteries (Nakayama et al., 2001). An *in*

vivo study by Kawabata *et al.*, (2004) demonstrated that gastric mucosal blood flow was increased in rodents upon PAR2-activation by trypsin or SLIGRL-NH_2. The authors determined that PAR2-mediated increases in gastric mucosal blood flow in anesthetized rats were sensitive to apamin and ChTX but resistant to L-NAME and indomethacin (Kawabata et al., 2004b).

A SLIGRL-induced, NO/PGI_2-independent and IK_{Ca}-dependent PAR2-mediated relaxation was observed in rodent middle cerebral arteries (MCA) (McNeish et al., 2005). Modest (15 mM) increases in extracellular $[K^+]_o$ was found to hyperpolarize and relax MCA. This K^+-cloud emulation was inhibited by ouabain and Ba^{2+}, suggesting a role for VSM K^+ influx through Na^+/K^+-ATPase and K^+-channels (McNeish et al., 2005). A likely candidate for the PAR2-mediated EDHF is potassium because inhibition of K^+-channels attenuates the SLIGRL-induced hyperpolarization and relaxation effects. These data suggest that IK_{Ca} causes PAR2-mediated EDH (McNeish et al., 2005). Smeda *et al.*, (2010) observed PAR2-mediated relaxation in rodent MCA. Stroke-prone spontaneously hypertensive rats (SHR) were observed to have vascular injury, edema and inflammation which led to endothelial dysfunction and the loss of bradykinin-mediated relaxations (Smeda et al., 2010). Despite this, 2fly-induced PAR2-mediated relaxation was preserved. Significant NO/PGI_2-indepdnent relaxation was noted in SHR MCA. PAR2-mediated relaxations were sensitive to IK_{Ca} blockade by TRAM-34 and SK_{Ca} inhibition by apamin (Smeda et al., 2010). By eliminating the contribution of NO, COX, CYP metabolites, other K^+-channels and Na^+/K^+-ATPase, the authors conclude that endothelial hyperpolarizing current generated by IK_{Ca} and SK_{Ca} propagates through MEGJs to lower VSM $[Ca^{2+}]_i$ causing vasodilation (Smeda et al., 2010).

Chia *et al.*, (2011) observed similar trends in murine mesenteric arteries from mice infused with Ang II. Our group has determined that in murine models of hypertension and

endothelial dysfunction (Ang II infusion), ACh-induced relaxations are attenuated while 2fly-induced vasodilation is preserved (Chia et al., 2011). Utilizing TRAM-34, Chia *et al.,* (2011) demonstrated IK_{Ca} reliance during NO/PGI_2-indepdnent PAR2-mediated relaxation. The heterogeneous EDHF mechanisms all rely on K_{Ca}, but how are the channels activated? It is more than a rise in intracellular $[Ca^{2+}]_i$, but a complex and discrete network of Ca^{2+}-signaling events.

1.2.12 Vascular endothelium Ca^{2+}-events

The majority of work on vascular EC Ca^{2+}-transients is performed on cell culture and *in situ* arterial preparations. Few studies are available with data on freshly isolated vascular ECs. Advantages of examining isolated cells include removing cell-cell communication that could alter individual Ca^{2+}-transient dynamics and removing background-noise which can limit the sensitivity for local Ca^{2+}-transients (Cheng et al., 2008). It is difficult to distinguish cell-cell Ca^{2+}-communication across gap junctions from bona-fide local Ca^{2+}-transients and initiation sites for cell wide Ca^{2+}-waves (CWW). When comparing the available literature it is evident that Ca^{2+}-events *in situ* are more consistent and realistic than in cultured EC. The majority of studies utilize fluorescent indicator dyes, like the Fluo-4 AM dye used in this thesis. A drawback to the use of fluorescent indicators includes difficulty in standardizing baseline measurements (Takahashi et al., 1999). Fluorescent molecules have incomplete affinities for $[Ca^{2+}]_i$. Mathematical modeling allows for the changes in fluorescence to be correlated to actual ion concentrations (Takahashi et al., 1999). Hüser and Blatter (1997) examined cultured calf pulmonary artery endothelial cells (CPAE) for their local Ca^{2+} response to adenosine-5'-triphosphate (ATP). CPAE incubated with fluo-3 (cytosolic Ca^{2+}-indicating dye) showed small discrete Ca^{2+}-transients and initiation points for Ca^{2+}-induced Ca^{2+}-release (CICR) generating CWW in peripheral pseudo-phillapodia (Huser et al., 1997). These events labeled "Ca^{2+}-waves"

took 24 s to spread across the entire cultured EC, far longer than anything seen *in situ* (Cheng et al., 2008; Huser et al., 1997). It is well documented that cultured cells have different cytoskeletal, Ca^{2+} signal transduction and surface receptor properties from freshly isolated and *in situ* preparations (Dawson et al., 2012; Gauthier et al., 2002).

Ca^{2+}-puffs are transients that can propagate across the vascular endothelial layer (Cheng et al., 2008; Mumtaz et al., 2011; Tran et al., 2012). *In situ* these types of events are thought to activate SK_{Ca} and cause CICR because IP3R are located continuously throughout the ER of the endothelium and are concentrated near the plasma membrane and nucleus (Grayson et al., 2004; Ledoux et al., 2008). Ca^{2+}-events originating in the ER that activate K_{Ca} are IP3R dependent, considering that XeC and 2-aminoethoxydiphenyl borate (2-APB), a non-selective IP3R inhibitor, abolish the Ca^{2+}-events (Bintig et al., 2012; Kameritsch et al., 2012). Ca^{2+}-puffs may be initiated by smaller Ca^{2+}-events in very close proximity to the plasma membrane (Cheng et al., 2008; Isshiki et al., 2004; Mumtaz et al., 2011). Subplasmalemmal Ca^{2+}-wavelets have been recorded at < 0.2 μm from the plasma membrane in cultured endothelial cells (Isshiki et al., 2004). TRPV1 and TRPV4 are non-selective extracellular cation channels which allow extracellular Ca^{2+} into ECs upon excitation (Kassmann et al., 2013). This excitation is induced by shear stress *in vivo* and elicited by ACh (in EC) and PAR2 (demonstrated only in non-EC) *in vitro* (Amadesi et al., 2006; Chen et al., 2011; Kassmann et al., 2013; Zhang et al., 2009). The implication is that Ca^{2+}-puffs may be more than ER Ca^{2+}-store release, but an extracellular Ca^{2+}-dependent influx mediated by TRPV (Sonkusare et al., 2012; Sullivan et al., 2012). Large TRPV4-mediated Ca^{2+}-events are caused by cooperative recruitment of other TRPV4 channels during the excitation period, and are known as "Ca^{2+}-sparklets" (Sonkusare et al., 2012). These

Ca^{2+}-sparklets were ~ 11 μm^2 in diameter and had a low but sustained amplitude (study standardized $F/F_o \approx 0.19\text{-}0.29$) relative to Ca^{2+}-puffs (Sonkusare et al., 2012).

Low intraluminal pressure activates TRPV4 receptors in murine cremaster and mesenteric artery endothelium (Bagher et al., 2012). Resistance artery preparations were mounted on pressure myographs and loaded with Ca^{2+}-indicator 488 BAPTA-1 AM. The influx of Ca^{2+} from the extracellular space into the ECs was measured on spinning-disk confocal microscopy (Bagher et al., 2012). TRPV4 antagonist RN1734 was utilized to separate TRPV4 Ca^{2+}-events from other channel transients. It was concluded that the TRPV4-mediated mechanism of vasodilation at low intraluminal pressures is a counterbalance to peripheral vasculature autoregulation during hypotension (Bagher et al., 2012). Of further interest is that TRAM-34, but not apamin, has similar effects as RN1734 on pressure induced vasodilation. This additional K_{Ca} data suggests that EC signaling microdomains play a role in the counterbalance of autoregulation (Bagher et al., 2012). Our study utilized ruthenium red (RR) to inhibit TRP channels. It is important to note that this compound has other effects on cellular Ca^{2+} transport including inhibition of mitochondrial Ca^{2+}-shuttling (Yoon et al., 2014). Researchers described Ca^{2+}-event frequency and amplitude correlations to ACh in freshly isolated EC tubes from the intima of murine mesenteric arteries (Socha et al., 2012). ACh-induced observations included Ca^{2+}-event frequency of 10/min (1 µM ACh); amplitude $F/F_o \approx 3.10$ and frequency of 5/min (100 nM ACh) (Socha et al., 2012). At higher agonist concentrations the ECs displayed an even distribution of Ca^{2+}-waves and Ca^{2+}-transients while at lower ACh concentrations the events were transient in nature. These data suggest an IP3R threshold mechanism for EC-EC Ca^{2+}-communication (Socha et al., 2012). The calcium events described so far are different from those localized around the EC IEL projections.

Ledoux *et al.*, (2008) report unique Ca^{2+}-events in the endothelial IEL projections from 3rd order murine mesenteric arteries. This group utilized fast-capture, 30 frames per second (fps), Nipkow spinning disk confocal microscopy and found Ca^{2+}-events occurring in IEL projections. Large, oscillatory ACh-induced Ca^{2+}-releases were observed and named "Ca^{2+}-pulsars" (Ledoux et al., 2008). The quantitative characteristics of *in situ* Ca^{2+}-pulsars are: larger in size than puffs (14-16 μm^2), have rapid decay ($t_{1/2} \approx$ 140-170 ms) and are larger in amplitude ($F/F_o > 1.70$) with a measureable frequency (Dora et al., 2008; Ledoux et al., 2008). In XeC treated tissues, Ca^{2+}-pulsar frequency was reduced to half and vascular depolarization of ~ 8 mV was recorded. In ChTX treated tissues there was no effect on Ca^{2+}-pulsars but 8 mV depolarization still occurred (Ledoux et al., 2008). These data show the same potentiating effects occur with inhibition of Ca^{2+}-pulsars as with IK_{Ca}-inhibition. The findings are supported with observations made by Dora *et al.*, (2008), who examined Ca^{2+}-pulsars in the IEL projections of rat mesenteric artery. A summary of the vascular Ca^{2+}-event characteristics are shown in Table 3.

One possibility is that the Ca^{2+}-puffs and Ca^{2+}-pulsars activate endothelial K_{Ca}, which generate a K^+-cloud within the IEL whilst hyperpolarizing the vasculature. Studies suggest that IP_3, Ca^{2+} and other small molecules can travel between EC and VSM along MEGJs. These MEGJ are also the proposed route for the transfer of hyperpolarization from the endothelial to the smooth muscle layer (Triggle et al., 2012). It is clear that little is known about PAR2 Ca^{2+} signaling. A brief summary of the available literature is presented.

Ca^{2+}-event	Model[Reference]	$[Ca^{2+}]_o$ (mM)	Agonist	Max amplitude (F/F_o) or max local $[Ca^{2+}]_i$ (nM)	Area (μm^2) or linear spread (μm)	Velocity ($\mu m/s$)	$t_{1/2}$ (ms)	Frequency (Hz)
Puffs / endothelial sparks	*in situ* mouse mesenteric endothelial tubes[Socha et al., 2012]	2.0	[acetylcholine] = 1 µM	$F/F_o \approx 3.11 \pm 0.20$	N/A	N/A	N/A	N/A
	cultured calf-pulmonary artery cells EC (CPAE)[Huser et al., 1997]	2.0	[ATP] = 250 nM	$F/F_o \approx 1.6$ to 2.0 (~ 23 nM)	~ 30 µm	N/A	< 100	N/A
	cultured calf-pulmonary artery EC (CPAE)[Aromolaran et al., 2007]	2.0	[2-deoxy-D-glucose] =10 mM	$F/F_o \approx 1.43$	~ 12 µm	N/A	< 700	N/A
	cultured rat microcoronary EC[Nistri et al., 2012]	2.0	[angiotensin II] = 1 µM	$F/F_o \approx 2.5$	N/A	N/A	N/A	N/A
Pulsars	*in situ* mouse third order mesenteric artery EC[Ledoux et al., 2008]	2.0	[acetylcholine] = 10 µM	$F/F_o \approx 1.77$	~ 16 μm^2	N/A	~ 146	0.06 to 0.10
	in situ mouse third order mesenteric artery EC[Nausch et al., 2012]	2.0	Electric field stimulation of sympathetic neurons	$F/F_o \approx 1.37$	~ 14 μm^2	N/A	~ 153	~ 0.07
Subplasmalemmal	cultured bovine aortic EC (BAEC)[Isshiki et al., 2004]	1.2	Ca^{2+}-free medium switched to $[Ca^{2+}]$ = 1.2 mM medium	$[Ca^{2+}] \approx$ 45 to 350 nM	≤ 0.2 µm	56 ± 26	N/A	N/A
Propagating wave	*in situ* rat tail artery EC[Mumtaz et al., 2011]	2.0	[carbachol] = 1 µM	$F/F_o \approx 3.0$	~ 50 µm	14 to 44	N/A	0.08 to 0.33*
	in situ hamster feed artery EC[Uhrenholt et al., 2007]	2.0	[acetylcholine] = unknown	$F/F_o \approx 2.5$	> 750 µm	111	N/A	N/A
	cultured calf-pulmonary artery EC (CPAE) [Huser et al., 1997]	2.0	[ATP] = 250 nM	$[Ca^{2+}] \approx 50$ to 100 nM	~ 60 µm	7 to 61	< 1000	~ 0.02*
	in situ rat ureter artery EC[Burdyga et al., 2003]	2.5	Baseline	$F/F_o \approx 4.0$	40 to 80 µm	18 to 30	~ 500	0.15 to 0.4*
VSMC Sparks	freshly isolated porcine cerebral arteriole VSMC[Liang et al., 2012]	2.0	$[Na_2S]$ = 10 µM (S^{2-} donor for H_2S)	$F/F_o \approx 1.4$ (187 ± 12 nM)	> 20 µm	N/A	N/A	~ 4.0*
	freshly isolated rat cerebral artery VSMC[Perez et al., 1999]	1.6	Baseline	$F/Fo \approx 2.0$	13.6 μm^2	N/A	55.9	N/A

Table 3. Sample of Ca^{2+}-events found in isolated and *in situ* vascular endothelial cells. Vascular smooth muscle cell (VSMC) sparks are presented for comparison. Amplitude data have been standardized by individual research groups and cannot be compared unless direct translation to $[Ca^{2+}]_i$ has been made, shown where applicable. N/A indicated that the corresponding study did not report these data. * indicates where non-repeating events have Ca^{2+}-oscillations superimposed on them. The only events reported to have their own inherent frequency are Ca^{2+}-pulsars.

1.2.13 PAR2 and EC $[Ca^{2+}]_i$

It has been well documented that PAR2 activation results in elevation of cytosolic $[Ca^{2+}]_i$ (Ramachandran et al., 2012b). Most studies only examined PAR2-mediated rises in global $[Ca^{2+}]_i$ and have not commented on the discrete Ca^{2+}-transients themselves. Ca^{2+}-fluctuations have been used as an indicator of the magnitude and sensitivity of PAR2 modulation (Al-Ani et al., 1999b; Kanke et al., 2009). Al-Ani *et al.,* 1999 showed that PAR2 activation with trypsin, SLIGRL-NH_2 or SFLLR-NH_2 elevates $[Ca^{2+}]_i$ in fluo-3 loaded KNRK cells. McGuire *et al.,* 2004 demonstrated 2fly concentration-dependent increase of $[Ca^{2+}]_i$ in KNRK and HEK293 cells. Similar PAR2-mediated $[Ca^{2+}]_i$ fluctuations are reported in human umbilical vein endothelial cells (HUVEC) (Cleator et al., 2006), human epidermal keratinocytes (Kanke et al., 2009) and human colon adenocarcinoma grade II (HT29) cells (Barry et al., 2010).

PAR2-mediated $[Ca^{2+}]_i$ fluctuations were observed in rodent cerebral and testicular arterioles *in situ* via spinning-disk confocal microscopy (Misaki et al., 2006). Both trypsin (1000 U/ml) and SLIGLV-NH_2 (100 µM) elicited a time dependent rise in endothelial $[Ca^{2+}]_i$ ($F/F_o \approx$ 2.5 at 800 sec) from Ca^{2+}-indicator indo-1 AM loaded arterioles (Misaki et al., 2006). Trypsin and SLIGLV-NH_2 reversibly decreased VSM $[Ca^{2+}]_i$ and total arteriole $[Ca^{2+}]_i$ (Misaki et al., 2006). Unfortunately, Misaki *et al.,* (2006) did not describe spatial or temporal characteristics of PAR2-mediated increases in EC $[Ca^{2+}]_i$. This leaves a gap in PAR2 Ca^{2+}-event literature. If PAR2 Ca^{2+}-events are similar to ACh-induced Ca^{2+}-pulsars described by Ledoux *et al* (2008), this would explain a portion of the PAR2 hyperpolarization signal transduction cascade. Likewise, discovering a relationship between PAR2-mediated Ca^{2+}-transient characteristics and TRPV may offer an explanation for preserved vasodilation at the signal transduction level.

1.2.14 Vascular endothelium signaling microdomains

Signaling microdomains have been discovered on the plasma membrane of the endothelial IEL projections. Microdomains are stabilized by caveolin scaffolding on lipid rafts and cooperatively propagate hyperpolarizing current from the endothelial to VSM layer (Edwards et al., 2007; Sandow et al., 2009; Triggle et al., 2012). In non-depolarized rodent mesenteric artery EDV was sensitive to apamin but not TRAM-34 (Crane et al., 2003). Yet at depolarizing potentials only the combination of apamin and TRAM-34 would inhibit EDHF-mediated EDV (Crane et al., 2003). Researchers hypothesize that different membrane potential effects on K_{Ca}-dependence mean that SK_{Ca} and IK_{Ca} occupy different membrane locations on the EC (Crane et al., 2003). SK_{Ca} is localized to caveolin-rich lipid rafts in close association with TRP subtypes V1, V4 and C1 and near endothelial homocellular gap junctions (Absi et al., 2007; Dora et al., 2008; Dora, 2010; Mendoza et al., 2010; Saliez et al., 2008; Sandow et al., 2009). Studies demonstrate that TRPV4 is localized to ECs of murine mesenteric arteries. Control arteries increased endothelial $[Ca^{2+}]_i$ when subjected to shear stress, while TRPV4 knockout mice showed no such response (Mendoza et al., 2010). In mesenteric artery endothelium TRPV4 are co-localized with caveolin-1 (Saliez et al., 2008). MEGJ connexin proteins (Cx) 37, 40 and 43 are co-localized with caveolin-1 in regions without TRPV4 (Saliez et al., 2008).

IK_{Ca} is in close association with MEGJs and Na^+/K^+-ATPase, occupying a second distinct microdomain near endothelial IEL projections. This domain is speculated to be near IP3R on the endothelial ER extensions (Ledoux et al., 2008). Intact pressurized rodent mesenteric arteries were probed for SK_{Ca}, IK_{Ca}, Na^+/K^+-ATPase and MEGJs (Dora et al., 2008). IK_{Ca} and Na^+/K^+-ATPase were preferentially expressed at the site of IEL projections on endothelium. Dora *et al.*, (2008) observed MEGJs on the endothelial IEL projections in the same region as IK_{Ca} and

Na^+/K^+-ATPase. MEGJs transport small molecules such as: IP_3, ATP, K^+, Na^+ and to a lesser extent Ca^{2+} and Mg^{2+}, but not large peptides or proteins (Behringer et al., 2012; Mather et al., 2005). MEGJ transport is proposed to be bi-directional and based on the concentration gradient (Sandow et al., 2004; Straub et al., 2011).

Microsignalling domain proteins SK_{Ca}, IK_{Ca} and TRPV are involved in PAR2-mediated vascular hyperpolarization. It is not known if PAR2 is associated with the same caveolin-rich domains. However PAR2 interacts with caveolin during receptor termination in clathrin-coated pits (Canto et al., 2012; Ramachandran et al., 2012b). Researchers have colocalized caveolae, PAR2 and TF-VIIa in cultured human breast carcinoma cells (Awasthi et al., 2007). Studies must be performed to determine if PAR2 is located on signaling microdomains and how PAR2-containing microdomains may interact with other lipid rafts in vascular hyperpolarization.

1.2.15 Summary

The *in vitro* effects of PAR2 activation on resistance artery preparations are well understood: PAR2 elicits relaxation and hyperpolarization, both of which are preserved in the face of endothelial dysfunction. Yet little research has been conducted on the receptor signal transduction in freshly isolated ECs. Studying PAR2 Ca^{2+}-events at the level of isolated ECs builds a foundation for *in situ* Ca^{2+}-transients and whole artery myograph studies. The focus of the study is to determine what purpose is served by PAR2 Ca^{2+}-transients in the setting of endothelial dysfunction. Using high-temporal resolution spinning disk confocal microscopy and the PAR2-KO model this study is the first to identify basic elements of Ca^{2+}-transients in EC PAR2 signaling. The study observed peripheral and central-repeating Ca^{2+}-transients in murine mesenteric ECs. I report that EC PAR2-mediated Ca^{2+}-signaling is preserved in Ang II-induced hypertension where M_3-mediated Ca^{2+}-events are attenuated. The 2fly experiments have been

controlled by comparison to ACh-induced Ca^{2+}-events. In addition, I investigated the role of IP3R and TRP channels in 2fly and ACh-activated ECs. Both IP3R and TRP channels play different but significant roles in PAR2 and ACh-mediated EC Ca^{2+}-dynamics. To explore the contribution of proteins associated with EDH I examined the expression of PAR2, eNOS, IP3R, SK_{Ca} and IK_{Ca} in fixed EC preparations. This study found the distribution of eNOS was attenuated in response to Ang II infusion, and concludes that the reduction may be responsible for the reduced vasodilation seen in endothelial dysfunction.

Dora, Garland, Ledoux, Segal, Taylor and others shaped the landscape of resistance vessel EDHF research. This work aims to contribute to the body of literature by contributing data from a family of GPCRs yet to be explored in detail at the Ca^{2+}-transient level. If the source of the preserved endothelial PAR2 functionality during disease can be pinpointed it could serve as a therapeutic target in hypertension, stroke and diabetes. It remains to be determined if various Ca^{2+}-transients lead to different mechanical activity in blood vessels. This work should provide a more complete picture from molecular signaling to mechanical reactivity following PAR2 activation.

Chapter 2: Materials and Methods

2.1 Mice

Littermate PAR-WT and PAR2-KO mice were bred from parental PAR2-WT, PAR2-KO and PAR2-HET crosses. All animals were genotyped to confirm identities prior to experiments. Male mice (11 to 13 weeks of age; 22 to 33 g) were used in all experiments. Mice were housed in a pathogen-free barrier facility from birth until experiments. Barrier temperature, humidity and light cycles were monitored by Animal Care Services in the Health Sciences Centre. All handling and experimental procedures involving animals were approved by the Institutional Animal Care Committee of Memorial University in accordance with guidelines of the Canadian Council of Animal Care.

2.2 Breeding Protocol

C57BL/6J (PAR-WT) and B6.Cg-*F2rl1*^{tm1Mslb}/J (PAR-KO) mice were initially purchased from Jackson Laboratory (Bar Harbor, ME). Multiple crosses of PAR-WT and PAR-KO mice were performed to yield F_2 C57BL/6J /B6.Cg-*F2rl1*^{tm1Mslb}/J (PAR2-HET) mice with different F_1 lineages. F_2 PAR2-HET were crossed to yield F_3 PAR2-WT and PAR2-KO animals. Additionally F_2 PAR2-WT and F_2 PAR2-KO were crossed to generate F_3 PAR2-WT and PAR2-KO animals. Mice were weaned at 21 days, tagged, separated by sex and a 2 mm tail clip was obtained for genotyping. To reduce variability between groups littermate F_3 and F_4 generations were used in experiments.

2.3 Materials

For the live-cell confocal protocol Fluo-4 AM was purchased from Invitrogen (Burlington, ON). Ruthenium red (sc-202328) and xestospongin C (sc-201505) were purchased from Santa Cruz Biotechnology (Dallas, TX). 2fly was purchased from Peptides International

(Louisville, KT). For the immunocytochemistry (ICC) protocol: bovine serum albumin (BSA) was purchased from EMD MilliPore (Billerica, MA). Primary antibodies: polyclonal eNOS anti-rabbit (ab66127), polyclonal KCNN3 (SK_{Ca}) anti-rabbit (ab83737), polyclonal KCNN4 (IK_{Ca}) anti-rabbit (ab83740) were purchased from Abcam, Inc. (Toronto, ON). Polyclonal IP3R anti-rabbit, pan isoform in mouse, (407140) was purchased from Calbiochem (Etobicoke, ON). Polyclonal PECAM-1 anti-goat (sc-1506) was purchased from Santa Cruz Biotechnology (Dallas, TX). The polyclonal PAR2 primary antibody, B5 anti-rabbit, was provided by Dr. Morely D. Hollenberg (Calgary, AB). Fluorescein (FITC)-conjugated AffinPure Goat Anti-Rabbit IgG secondary antibody (111-095-003) and Texas Red® dye-conjugated AffinPure Bovine Anti-Goat IgG secondary antibody (805-075-180) were purchased from Jackson ImmunoResearch Laboratories, Inc. (West Grove, PA). For the genotyping protocol, oligonucleotide primers were purchased from Eurofins MWG Operon (Huntsville, AL) while Taq polymerase, $MgCl_2$, DNAse-free water and 10 x PCR buffer were purchased from Bio Basic Inc. (Markham, ON). SYBR® Safe for deoxyribonucleic (DNA) gel staining and 1kb plus DNA ladder were purchased from Invitrogen (Burlington, ON). All other chemicals and reagents were purchased from Sigma-Aldrich (Oakville, ON).

2.4 Genotyping

Mice were genotyped from a modification of the supplier's protocol (Jackson Laboratory, Bar Harbor, ME). DNA extraction was accomplished by heating 2 mm tail clips in 50mM NaOH at 95 ˚C for 1 hour, adding Tris-HCl buffer (pH 7.5) and centrifuging at 10,000 x *g* for 2 min before extracting supernatant containing the DNA. DNA samples were kept in storage at -20 ˚C until used. PCR was carried out utilizing three oligonucleotide primers to target characteristic genes in PAR2-WT and PAR2-KO (Appendix A). The reaction mixture with primers amplified a

portion of exon 2 in the *par*2 gene present in PAR2-WT and a fragment of the *neomycin* gene present in PAR2-KO. PAR2-HETs were identified as containing amplified *par*2 exon 2 and *neomycin* gene fragments. Gel electrophoresis and DNA staining techniques were employed to identify the amplified DNA bands. Gels cast were 1.5% agarose w/v dissolved in tris borate ethylenediaminetetraacetic acid (TBE) buffer containing 10 µL SYBR® Safe DNA chelating dye.1kb plus DNA ladder, resolving to 100 bp increments, was run parallel to the PCR products to discern the sizes of fragments. Gels ran for 1.5 hours at 90 V to separate the DNA bands from at a distance ≥ 4 cm from the wells. Migrated PCR products were imaged with Alpha Imager® EP (Cell Biosciences, Santa Clara, CA) using trans-illumination with ultraviolet light.

2.5 Model of endothelial dysfunction: subcutaneous angiotensin II infusion

Endothelial dysfunction was induced by chronic administration of low doses of angiotensin II. Ang II was administered by subcutaneous infusion using micro-osmotic pumps (Chia et al., 2011) (Alzet, Cupertino, CA). Micro-osmotic pumps (model #: 1002, pump rate of 0.25 µl/h) were filled with saline (controls) or Ang II (Chia et al., 2011), then equilibrated for 12 h at 37 ºC as per manufacturer's recommendation (Alzet, Cupertino, CA). Male PAR2-WT and PAR2-KO were anesthetized with 2% isoflurane (2 L O_2/min). Pumps were implanted subcutaneously through a dorsal incision on the neck, into a pocket filled with saline along the flank, as described previously (McGuire et al., 2008). Surgeries to implant micro-osmotic pumps lasted 5-10 min and were followed by administration of 0.02 ml of i.m. duplocillin (benzylpenicillin procaine and benzylpenicillin benzathine suspension). After 5 min post-surgical recovery the mice were returned to the holding room in the animal care facility. Doses of Ang II (1.5 mg/kg/day), delivered over 14 days, were based on previous vascular reactivity studies with the Ang II model (Chia et al., 2011).

2.6 Endothelial and vascular smooth muscle cell isolation

Mice were euthanized by an overdose inhalation of isoflurane followed by cardiac puncture with a syringe for blood sampling (1.0 ml), containing 0.1 ml of heparin (10 units). Mesentery tissue was extracted and placed in 4 ºC endothelial cell (EC) isolation buffer with the following composition (mM): NaCl, 55; glutamate, 80; KCl, 6; $MgCl_2$, 2; $CaCl_2$ 1; 4-(2-hydroxyethyl)-1-piperazine ethanesulfonic acid (HEPES), 10; glucose, 10; pH 7.4. The mesenteric arteries were then stripped of fat and connective tissue and finely cut into small pieces. A modified cellular isolation procedure was then implemented, based on isolation of vascular smooth muscle cells for electrophysiology studies (Gauthier et al., 2002). The finely cut mesenteric arteries were placed in 4 ºC vascular smooth cell (VSMC) isolation buffer, a Ca^{2+}-free solution, with the following composition (mM): NaCl, 55; glutamate, 80; KCl, 5; $MgCl_2$, 2; ethylene glycol tetraacetic acid (EGTA), 0.1 mM; HEPES, 10; glucose, 10; pH 7.4. Dithiothreitol (DDT), 0.5 µg/µL; and protease papain, 0.5 µg/µL; were added to the VSMC isolation buffer and tissue mix. The tissue containing solution was then incubated for 30 min at 37 ºC with agitation. Then $CaCl_2$ (0.2 mM) and proteases collagenase IV 1.0 µg/µL, and neutral protease 1.0 µg/µL were added to the 1.0 mL final volume VSMC isolation buffer and tissue mix. The preparation was incubated for 25 min at 37 ºC with agitation. After incubation the preparation was washed twice with modified EC isolation buffer at 4 ºC. The following washing procedure was used, the preparation was centrifuged at 120 x *g* (Eppendorf micro-centrifuge 5415c at 1200 rpm) for 5 min and 800 µL supernatant was removed leaving only cell pellet and 200 µL of VSMC isolation buffer. The buffer was replaced with an equal volume (800 µL) of 2 mM [Ca^{2+}] EC isolation buffer and triturated with a 1000 µL pipette tip (cut at 45 º angle) to disperse and suspend the cells. The preparation was kept on ice at 4 ºC and contained a mix of isolated ECs and VSMCs.

2.7 Ca^{2+}-event imaging

Cell preparation

Aliquots (100 µL) of cells were transferred to separate tubes (1.5 mL) containing EC isolation buffer (900 µL) with 2 mM $[Ca^{2+}]_o$, plus Fluo-4 AM Ca^{2+}-indicator dye (10 µg/mL), then incubated at room temperature for 10 min at 37 ºC (pH 7.4). Following Fluo-4 AM incubation the preparation was transferred to a 35 mm uncoated glass FluoroDish® (Catalogue #: FD35-100, World Precision Instruments, Inc., Sarasota, FL) and cells were allowed to settle for 7 minutes. The FluoroDish® preparation was transferred to a confocal microscope set up and the cells were washed with EC isolation buffer, 2 mM $[Ca^{2+}]_o$ at 37 ºC and pH 7.4, for 10 min (1 ml/min). Cell Fluo-4 AM loading and incubation procedure was similar to other described protocols (Burdyga et al., 2003; Mumtaz et al., 2011; Socha et al., 2012; Stuyvers et al., 2005).

Microscope setup for Ca^{2+}-image sampling procedures

The Fluo-4 loaded cells were positioned in an experimental chamber on the stage of a motorized inverted microscope, Olympus IX81 (Olympus, Center Valley, PA). The microscope was equipped with 10x ocular, 10x, 40x and 60x objective lenses. The microscope also had a 1.6x magnifying extension in use for all experiments, total magnification 960x (60x objective lens). The microscope was attached to a Nipkow spinning disc unit (Yokogawa CSU-X1, Tokyo, Japan). Images were captured on a Fast 1394 Rolera-MGI Plus CCD camera (Q Imaging, Surrey, BC). Illumination for the Fluo-4 dye was provided by a FRAP-3D MAG Biosystems™ laser unit equipped with argon diode laser, 488 nm excitation (Microimaging Applications Group Worldwide, USA). 512 x 512 pixel images were captured using MAG Biosystems™ CSU software version 7.7.0.0 (Molecular Devices, Inc., Sunnyvale, CA). This setup is similar to that

used in previous work on cardiac purkinje fibers (Haq et al., 2013; Stuyvers et al., 2005). EC isolation buffer perfusion was driven by a Rabbit® Peristaltic pump (Rainin Instrument Company, Inc., France). In RR and XeC inhibitor experiments perfusion was provided by an 11Plus microperfusion apparatus (Harvard Apparatus, Holliston, MA).

Sampling procedure for PAR2 and M_3-mediated Ca^{2+}-events

After washing, cells were perfused (1 ml/min) with EC isolation buffer, 2 mM $[Ca^{2+}]_o$ at 37 ºC and pH 7.4, containing a range of 2fly concentrations (0.1 nM to 3 µM) or ACh (1 nM to 30 µM). Agonist concentrations corresponding to ED_{50} values were selected based on isometric tension assays of murine mesenteric arteries (Chia et al., 2011). Baseline was not reevaluated following agonist addition. After 1 min equilibration with agonist-containing buffer, individual cells were resolved at 960x magnification with 488 nm excitation using a 60x objective lens under oil-immersion. The calibration of raw images (512 x 512 pixels) was set to 6.825 pixels/µm. Ca^{2+}-events were measured through changes in Fluo-4 fluorescence intensity and were resolved in 2D at 30 fps on the mid planar region of the ECs. Acquisition of Ca^{2+}-events lasted for 7 min after agonist addition (10 s per cell). Baseline Ca^{2+}-events (free of agonist) was recorded in cells from each animal and served as the reference. A total of 20 animals were dedicated to this study alone; 5 each of saline and Ang II infused PAR2-WT and PAR2-KO. 10 cells were imaged for each concentration of 2fly, ACh, and baseline from 5 PAR2-WT and 5 PAR2-KO infused with saline or Ang II. Data with median CRC values of agonists [2fly] = 30 nM and [ACh] = 300 nM were collected from a sample of cells from each animal. Baseline activity was also recorded for a sample of cells from each animal. Ca^{2+}-events were acquired over a 10 s period from each cell with MAG Biosystems™ CSU software version 7.7.0.0 (Molecular Devices, Inc., Sunnyvale, CA). See Appendix B for a schematic of the protocol.

Sampling procedure for IP3R and TRP inhibition effects on Ca^{2+}-events

After washing, cells were perfused (1 ml total volume per FluoroDish®) with EC isolation buffer, $[Ca^{2+}]_o$ = 2 mM at 37 ºC (pH 7.4) containing either XeC, 2 µM and/or RR, 75 µM. Concentrations of XeC, $IC_{50} \approx 358$ nM for IP3R channels (Bishara et al., 2002; Gafni et al., 1997; Naser et al., 2013) and RR, $IC_{50} \approx 5$ nM for TRPV channels (Jornot et al., 1999; Mendoza et al., 2010; Phan et al., 2009) were selected based on our trials and other work shown to inhibit Ca^{2+}-events . Following a 10 min incubation period with XeC and/or RR, either 30 nM 2fly or 300 nM ACh were added to assess the role of IP3R and TRP channels in the PAR2 and M_3-mediated Ca^{2+}-responses. 30 nM 2fly and 300 nM ACh were selected because these agonist concentrations correspond to the approximate mid-point (EC_{50}) of the Ca^{2+}-event CRCs. Ca^{2+}-events were resolved in ECs as per the non-inhibitor study. 16 animals were dedicated to this study alone; 4 each of saline and Ang II infused PAR2-WT and PAR2-KO.10 cells were imaged for each combination of XeC, RR, 2fly, ACh and baseline from 4 PAR2-WT and 4 PAR2-KO infused with saline or Ang II. Ca^{2+}-events were acquired over a 10 s period from each cell with MAG Biosystems™ CSU software version 7.7.0.0 (Molecular Devices, Inc., Sunnyvale, CA). Refer to Appendix C for a schematic of this experimental protocol.

2.8 Protein expression study

Cell preparation

Following isolation the cell preparations were centrifuged at 120 x *g* (Eppendorf micro-centrifuge 5415c at 1200 rpm) for 5 min. The supernatant was decanted leaving behind 200 µL of EC isolation buffer and the cell pellet. The cell pellet was then incubated for 5 min with a 600 µL solution of 1.26% formaldehyde in phosphate buffered saline (PBS) at 4 ºC. 50:1

PBS:formaldehyde solution, where formaldehyde was 37 wt. % in water and PBS composition was as follows (mM): NaCl, 137; KCl, 2.7; Na_2HPO_4, 10; KH_2PO_4, 2.0; pH 7.4 at 4 ºC. After fixing, the preparation was centrifuged at 120 x *g* (Eppendorf micro-centrifuge 5415c at 1200 rpm) for 5 min and 600 µL of supernatant was decanted leaving the cell pellet. For cell membrane permeabilization and non-specific blocking of protein the preparation was incubated 5 min with 600 µL of 0.1% saponin and 3% BSA solution in PBS at 4 ºC. After permeabilization and blocking the preparation was centrifuged at 120 x *g* (Eppendorf micro-centrifuge 5415c at 1200 rpm) for 5 min and 800 µL of supernatant was decanted leaving behind the cell pellet. Cells were triturated with 800 µL of fresh PBS at 4 ºC and aliquots were distributed according to the number of primary antibodies tested. Primary antibody stocks were diluted as follows: polyclonal eNOS anti-rabbit, 5 µg/mL; polyclonal IP3R anti-rabbit, 1:1000; polyclonal SK_{Ca}, KCNN3 anti-rabbit, 1:2000; polyclonal IK_{Ca}, KCNN4 anti-rabbit, 1:2000; polyclonal PECAM-1 anti-goat, 1:500; polyclonal PAR2 primary antibody B5 anti-rabbit, 1:1000. Each preparation was dual-labeled with PECAM-1 that was stained with Texas Red®-containing secondary antibody, and one of the other above mentioned primary antibodies that was stained by Fluorescein isothiocyanate (FITC)-containing secondary antibody. All primary antibodies were fully cross reactive with mouse proteins. For each animal a negative staining control preparation was run, containing no primary antibody with FITC and Texas Red® secondary antibodies. Each preparation contained fixed, permeabilized and isolated ECs and VSMCs. Dilutions of primary antibodies were determined based on manufacturers' recommendation and preliminary testing by JCH in our laboratory. Cell preparations were left to incubate with primary antibodies overnight at 4 ºC. After 12-16 hrs preparations were centrifuged at 120 x *g* (Eppendorf micro-centrifuge 5415c at 1200 rpm) for 5 min and the supernatant removed, leaving behind pellets. 800 µL of

fresh PBS at 4 ºC was added and the cell preparations were incubated at 4 ºC for 1 hour 30 minutes with secondary antibodies: FITC-conjugated AffinPure Goat Anti-Rabbit IgG, 1:1000; Texas Red® dye-conjugated AffinPure Bovine Anti-Goat IgG, 1:500. Dilutions of secondary antibodies were determined based on manufacturers' recommendation and preliminary testing by JCH in our laboratory. Following secondary antibody incubation preparations were centrifuged at 120 x *g* (Eppendorf micro-centrifuge 5415c at 1200 rpm) for 5 min and the supernatant was decanted leaving behind the cell pellet. 500 µL of fresh PBS at 4 ºC was added and the cell preparations were finally moved to 8-well Lab-Tek II chamber covered glass slides (Thermo Fisher Scientific, Inc., Rochester, NY). Cell fixation protocol for ICC was modified from those used on cardiac myocytes and purkinje fibers (Stuyvers et al., 2005).

Microscope set up for immunocytochemistry in situ

The fluorescence of secondary antibodies was imaged using an inverted line-scan confocal microscope, Olympus Fluoview® FV1000 FV10-ASW (Olympus, Center Valley, PA). The microscope was equipped with 10x ocular, 10x, and 60x objective lenses. The microscope was attached to an Olympus Fluoview® control unit, main system line scanner for image resolution (Olympus, Center Valley, PA). Images were captured on a Spot RT CCD Cool Camera (Spot Imaging Solutions, Sterling Heights, MI). Illumination for FITC and Texas Red® dyes was provided by a MELESS Griot argon (488 nm excitation) and HeNe (520 nm excitation) diode laser unit (CIVI laser optics and MELESS Griot, Albuquerque, NM), powered by a FV10-MCPSU laser diode power supply system (Olympus, Center Valley, PA). 1024 x 1024 images, with 1.6x digital zoom, were captured on Olympus Fluoview® application software, version 5 (Olympus, Center Valley, PA). Total magnification of images collected was 960x. The calibration of raw images (1024 x 1024 pixels) was set at 121.951 pixels/µm.

Sampling procedure for secondary antibody fluorescence

Fluorescent signals from EC and VSMC were illuminated by dual 488 and 520 nm excitation. 2D images were line-scanned at a rate of 4 μs/pixel. Z-stacks through fixed and settled cells were acquired at 0.25 μm step thickness. Images were also attained for EC and VSMCs without primary antibodies but with FITC and Texas Red® to determine non-specific signals. 16 animals were dedicated to this study; 3 ECs from each well were acquired from 4 PAR2-WT and 4 PAR2-KO that were infused with saline or Ang II. All images and z-stacks were captured on Olympus Fluoview® software, version 5 (Olympus, Center Valley, PA).

2.9 Data processing

(a) Intracellular Ca^{2+}-events

All image processing was performed using the open source NIH software ImageJ version 1.47 (Research Services Branch, National Institutes of Health, Bethesda, MD). The dynamics of intracellular Ca^{2+} was imaged by capturing a series of 300 frames (512 x 512 pixels, 30 frames per second). Serial frames were stored as stacks of images and later converted to AVI files on MAG Biosystems^{TM} CSU software. Converted image stacks were then examined by a semi-automatic method to examine the spatial and temporal characteristics of Ca^{2+}-events. First the number of Ca^{2+}-release sites and the number of Ca^{2+}-events per site were counted frame by frame visually during a 10 s acquisition sequence. The "Z Profiler" plugin for ImageJ (Kevin (Gali) Baler and Wayne Rasband, National Institutes of Health, Bethesda, MD) was utilized to scan the entire image stack for confirmation of Ca^{2+}-release site number and Ca^{2+}-events per site. F/F_o ratio image stacks were created for each Ca^{2+}-event by dividing pixel by pixel ("Ratio Plus" ImageJ plugin) all images (F) in the stack by a frame (F_o) selected immediately before a transient

rise in fluorescence. F/Fo images reflected the actual rise in fluorescence that was directly proportional to the $[Ca^{2+}]_i$ variations. Image stacks were then smoothed (single pass) using the ImageJ "Gaussian Smoothing" function. Spatial properties of Ca^{2+}-events were analyzed using the "Dynamic Profiler" line scans. Finally, the temporal characteristics of Ca^{2+}-events in smoothed ratio images were captured using the "Z Profiler" ImageJ plugin. All spatial and temporal quantitative characteristics were exported using ImageJ to Microsoft Excel®, 2010 (Microsoft, Redmond, WA). The repetitive nature of individual central Ca^{2+}-release sites was determined by maintaining a small (< 0.5 μm) fixed Z-profiler region over the release site of interest. The 300 frame video was then cycled and all central Ca^{2+}-event initiations (determined by maximal fluorescence falling within the Z-profiler region) were counted.

Further intracellular Ca^{2+}-events was processed as follows:

(i) Non-propagating Ca^{2+}-event determination

All Ca^{2+}-events, peripheral and central-repeating, were determined to be non-propagating by analyzing the fluorescence (F/F_o) of discrete events spatially. The transition of fluorescence between cytosol and extracellular space localized the EC plasma membrane in transverse scans to determine cell boundaries. Dynamic profiles of Ca^{2+}-events across the cell, pixel-to-pixel, determined that from the point of origin of a Ca^{2+}-event there was no sustained rise in fluorescence. This is characteristic of Ca^{2+}-event diffusion and not CICR. This type of transverse line-scan to determine non-propagation is similar to that performed in the past with cardiac purkinje fibers (Stuyvers et al., 2005).

(ii) Spatial data processing

Dynamic Profiler data from ImageJ was graphed for all Ca^{2+}-events. Groups' spatial profiles were averaged and the mean curves were compared. Maxima (maximum amplitude or greatest F/F_o) were measured directly from the spatial graph. GraphPad Prizm version 4.0 interpolation function was utilized to determine Full-width at half-maximum amplitude (FWHM). Frequencies (Hz) of central-repeating Ca^{2+}-transients were calculated by dividing the number of events from a single central locus into the time period (10 s) of the video. Frequencies of each individual central Ca^{2+}-release site per cell were combined into a cell average, which was then combined into a group average (10 cells per group).

(iii) Temporal data processing

Z Profiler data from ImageJ was graphed for all Ca^{2+}-events. Groups' temporal profiles were averaged and the mean curves were compared. Total duration was determined by using GraphPad® Prizm version 4.0 interpolation function to intersect time (s) and fluorescence return to baseline ($F/F_o \approx 1$). Interpolation determined the time to rise to maximum amplitude from baseline ($t_{rise} = t_{MAXIMA} - t_o$) and time to decay to half maximum amplitude from event maxima ($t_{1/2} = t_{half\text{-}MAXIMA} - t_{MAXIMA}$).

(b) Protein expression in situ

All image processing was performed on ImageJ version 1.47 (Research Services Branch, National Institutes of Health, Bethesda, MD). As indicated above, the cells were sliced optically (z-stepping) by collecting vertical series of frames across the full thickness of the preparation. This operation was performed automatically (software controlled) by progressively changing the confocal plan (focus) by 0.25µm steps. First, the analysis of the immunodistribution begins with selection of the optical section that is close to the equator of EC . Red staining of EC membrane

protein PECAM-1 was used to position the plasma membrane. The cell equator was detected by tracking the greatest circumference of the cell across the z-stack images. Image stacks were smoothed (single pass) using the ImageJ "Gaussian Smoothing" function. Image J plugins were used to process dual channel (488 nm and 522 nm) images from the cell equator by a method similar to work by Edwin Moore and colleagues (Fletcher et al., 2010; Scriven et al., 2008; Scriven et al., 2005). Briefly, images were separated into 488 nm and 522 nm channels and converted from the grey scale intensity domain into the frequency domain using the "Fast Fourier Transform" function on ImageJ. The resulting power spectra were filtered by a baseline black mask to filter low-frequency noise from the image.

Power spectra were then de-convoluted using the inverse FFT function on Image J. "Dynamic Profiler" ImageJ plugin was then used to perform spatial line scans across images. The scan line was selected manually so that it covered the entire width of the cell at the center. Line scans were conducted at the same location at both wavelengths for all images. For KCNN3 and KCNN4 ICC experiments, scans were carried out at the periphery of the cell. The expression of the potassium channels was discontinuous around the plasma membrane and the circular 'free-hand' line-scan tool in Image J was utilized. This 'free-hand' tool allowed for the total fluorescence to be quantified on the EC equator periphery. Representative images were processed as above and converted from grey-scale (8-bit) to RGB (32 bit) pseudo-color scales.

Line scan data of each channel from processed ICC images were imported into GraphPad Prizm software version 4.0 (GraphPad, San Diego, CA). Fluorescent signal intensity grey value (scaled from 0 to 255) were expressed as % Maximum Fluorescence (255 grey value = 100%). The signal intensities distributed along the length axis of each cell was averaged across groups as % Cell Length. These processes were conducted to accommodate the expression changes across

differently sized cells. To determine protein distribution, peak signal FWHM and total area integrals were calculated. Area under the curve integration was calculated across the line scan from one end of the cell to the other (%Maximum Fluorescence x % Cell Length). KCNN3 and KCNN4 were heterogeneously expressed on the cell periphery in discrete populations. To fairly represent this discrete expression, peripheral scan integrals of total peripheral fluorescence were calculated for KCNN3 and KCNN4 (%Maximum Fluorescence x Cell circumference).

2.10 Statistical Analyses

GraphPad Prizm software version 4.0 (GraphPad, San Diego, CA) was used to generate graphs and to conduct the statistical analyses of all data. In results tables and graphs the statistical significant notations are: "a or *" $p < 0.05$; "b or **" $p < 0.01$; "c or ***" $p < 0.001$.

2fly and ACh concentration response curves (CRCs)

10 cells per data point from a total of 5 different animals across both *par*2 strains and treatments (saline or Ang II-treated) were used to construct each CRC. The software fit drug CRCs for each agonist to a four-parameter equation by nonlinear regression equation to calculate the variables E_{max}, pD_2, Bottom and Hill slope:

Number of Ca^{2+}-release sites/cell (or number of Ca^{2+}-events/release site/s) = Bottom + (E_{max} - Bottom) / (1 + 10 ^ (log EC_{50} - log[Drug]) * Hill slope)

Where: E_{max} is maximum number of Ca^{2+}-release sites/cell (or maximum number of Ca^{2+}-events/release site/s); pD_2 is negative $\log_{10}$ of curve EC_{50} value; Bottom is baseline level of Ca^{2+}-events (minimum response region); Hill slope is curve steepness (rate of change in the number of Ca^{2+}-events with increasing drug concentration); Drug is 2fly or ACh. CRC variables were compared by two-way ANOVA followed by Bonferroni post-hoc test.

Effect of XeC and RR on 2fly and ACh Ca^{2+}-response

10 cells per data point from a total of 4 different animals across both *par*2 strains and across treatments (saline or Ang II-treated) were used to evaluate each XeC and /or RR with 30 nM 2fly or 300 nM ACh combination. Data were arranged in bar graphs where maximum response in number of Ca^{2+}-release sites/cell or number of Ca^{2+}-events/release site/s were compared by two-way ANOVA followed by Bonferroni post-hoc test. Where S.E.M. = 0 unweighted two-way ANOVA was used. No variance was observed in some inhibitor preparations due to the low number of cells with Ca^{2+}-events.

Spatial and temporal characteristics of non-propagating Ca^{2+}-events

Ca^{2+}-event characteristics variables (amplitude, t_{rise}, $t_{1/2}$, FWHM and frequency) were compared by the following method: the means of two independent groups were compared by Student's t-test for unpaired data where $p < 0.05$ was considered significant. Statistical comparisons of the means of more than two independent groups were performed by two-way ANOVA followed by Bonferroni post-hoc test. n = the number of cells from each group.

Protein expression in situ

Secondary antibody parameters, relative maximum fluorescence (PAR2 and IP3R) and the integral of relative maximum fluorescence (eNOS, KCNN3 and KCNN4), were compared by two-way ANOVA (treatment x genotype) and compared by Bonfferoni post-hoc test. n = 6 cells from each group.

Chapter 3: Results

3.1 Genotyping of *par*2 strains

We determined the genotype of all mice using PCR (section 2.4) to identify carriers of the *par*2 gene. Agarose gel electrophoresis was conducted to separate amplified *par*2 and *neomycin* DNA fragments (Figure 4). *par*2 DNA bands were observed in all PAR2-WT and *neomycin* bands were found in all PAR2-KO mice used in this study.

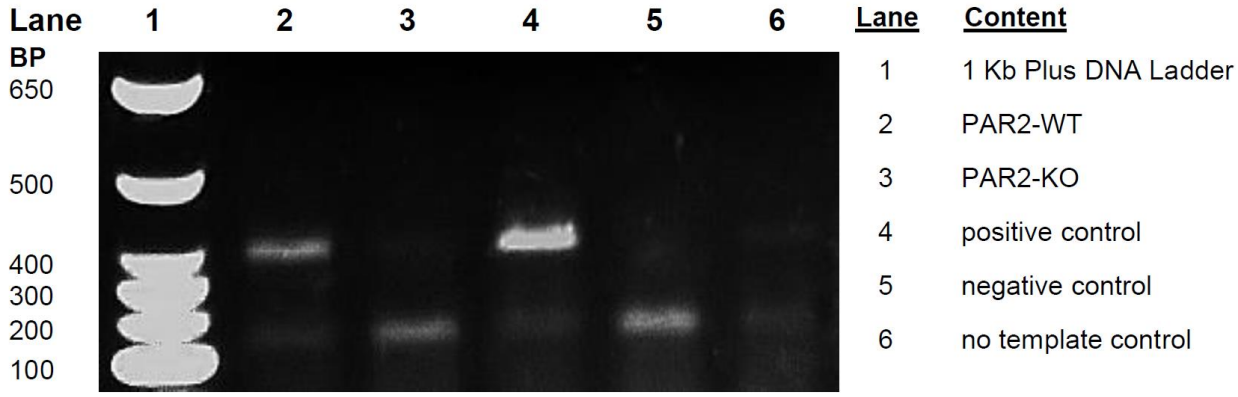

Figure 4. *par*2 genotyping gel experiment. Representative PCR products from mouse tail samples were separated by agarose gel electrophoresis and stained by SYBR® Safe (section 2.4). Positive identification of *par*2 gene (385 base pairs) in lanes 2 and 4. Positive identification for *neomycin* gene (198 base pairs) in lanes 3 and 5. Previously identified PAR2-WT (lane 4) and PAR2-KO (lane 5) were run as positive and negative controls, respectively. Lane 1 contains the 1 Kb Plus DNA Ladder used for band identification.

3.2 Morphology of endothelial cells

The mesenteric artery cellular isolation (section 2.6) contained a mix of endothelial and vascular smooth muscle cells. The typical dimensions of ECs from mesenteric arteries measured 13 ± 0.1 µm wide by 16 ± 0.1 µm long. Endothelial cells were generally round-oval and flat in shape with a smooth surface following isolation. VSMCs were considerably larger than ECs, with dimensions 3-5 times the length of ECs. The gross morphology of ECs and VSMCs under white light did not vary across *par*2 strains or with Ang II treatment (Figure 5).

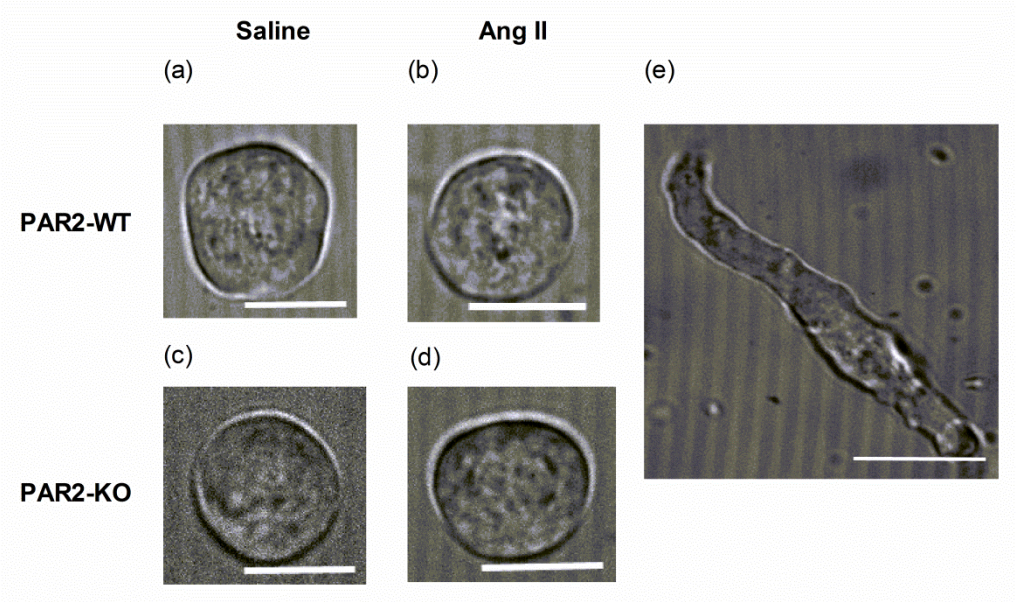

Figure 5. Gross morphology of representative endothelial and vascular smooth muscle cells isolated from mesenteric arteries in mice. Isolated endothelial cells from saline (a, c) and angiotensin II (b, d) treated PAR2-WT (a, b) and PAR2-KO (c, d) were imaged in transmitted light mode. A saline treated PAR2-WT vascular smooth muscle cell (e) is shown for comparison. Both endothelial and vascular smooth muscle cells were found in all preparations. Scale bars 10 µm, magnification 960 x.

3.3 Effect of PAR2 activation on Ca^{2+}-events of endothelial cells

To determine the effect of PAR2 activation on intracellular calcium activity, Fluo-4 fluorescent dye experiments were performed using a spinning-disk confocal microscope setup. Fluo-4 intensity is proportionate to free cytosolic $[Ca^{2+}]_i$. Changes in Ca^{2+}-events are inferred from relative elevations in Fluo-4 fluorescence. Endothelial dysfunction in PAR2-WT and PAR2-KO was produced by continuous subcutaneous infusion with Ang II for 14 days; saline was used in controls. In separate mesenteric arterial ECs, Ca^{2+}-Fluo 4 fluorescence data were recorded before and during exposure to different concentrations of PAR2 agonist 2fly (0.1 nM to 3 µM) or ACh (1 nM to 30 µM). ECs were constantly perfused with agonist in buffer containing 2 mM $[Ca^{2+}]_o$. At concentrations of $[Ca^{2+}]_o$ between 1-10 mM, preliminary work indicated that the number of Ca^{2+}-release sites or firing rates were relatively stable in our isolated ECs over a 10 s imaging sequence.

In PAR2-WT, we found that both 2fly and ACh increased the number of Ca^{2+}-release sites per cell and the Ca^{2+}-event firing rate in a concentration dependent manner (Figure 6). 2fly increased the number of Ca^{2+}-release sites 12-fold and Ca^{2+}-event firing rate 6-fold in PAR2-WT over PAR2-KO. In PAR2-WT, compared to 2fly, the number of Ca^{2+}-firing sites and firing rate were 50% lower in presence of ACh (Figure 6). PAR2 agonist 2fly enlisted the same number of Ca^{2+}-release sites per cell and had equivalent Ca^{2+}-event firing rates in Ang II treated PAR2-WT and controls (Figure 6).

Yet the recruitment of the Ca^{2+}-release sites by ACh was attenuated by 22% in Ang II PAR2-WT ($p < 0.001$, E_{max}, Figure 6b). Similarly for ACh, Ca^{2+}-event firing rate was decreased by 24% in Ang II PAR2-WT compared to controls ($p < 0.01$, E_{max}, Figure 6d). These attenuations in Ca^{2+}-events were not observed for 2fly CRCs. Notably, the same Ca^{2+}-event firing rate was measured in the presence of 2fly and ACh in Ang II and control PAR2-WT ($p > 0.05$, E_{max}, Figure 6c, 6d). The slope of the Ca^{2+}-event firing rate curve was 1.5-times steeper for 2fly than ACh ($p < 0.01$, Hill slope).

Data collected from PAR2-KO confirmed the specificity of 2fly for activating PAR2 (Figure 6a, 6c) and showed that *par2* genotype had no effect on Ca^{2+} activities elicited by ACh (Figure 6b, 6d). Curve-fit function variables for concentration response curves (CRCs) are located in supplement Tables S1 and S2.

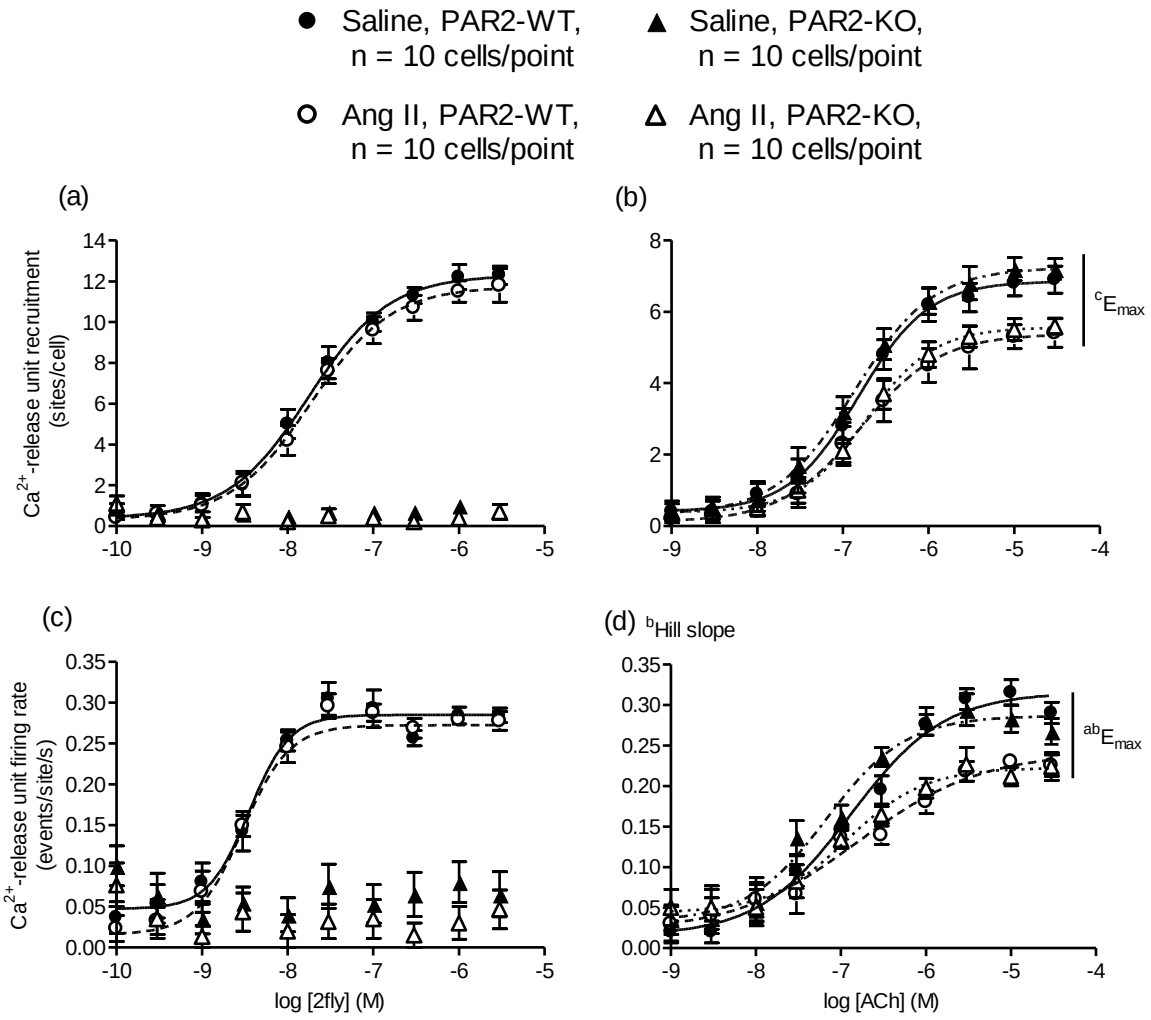

Figure 6. Effect of chronic angiotensin II infusion on PAR2 and M_3-mediated endothelial Ca^{2+}-events. Freshly isolated mesenteric endothelial cells from saline and angiotensin II-infused male PAR2-WT and PAR2-KO were perfused with varying concentrations of either (a, c) 2-furoyl-LIGRLO-amide (2fly) or (b, d) acetylcholine (ACh). Top graphs (a, b) represent the increase in Ca^{2+}-event sites by agonists, bottom graphs (c, d) represent change in Ca^{2+}-event site firing rate. Symbols are means ± S.E.M., n = number of endothelial cells per point, 5 animals per curve. Lines represent 4 parameter logistic curves which calculate the variables: pD_2, E_{max} and Hill slope. Variables were compared by 2 way ANOVA (treatment x genotype), followed by Bonferroni post-hoc testing. (b) $^{c}p < 0.001$, E_{max}, Ang II PAR2-WT and PAR2-KO vs Controls. (d) $^{b}p < 0.01$, E_{max}, Ang II PAR2-WT vs Controls. $^{a}p < 0.05$, E_{max}, Ang II PAR2-KO vs Controls. $^{b}p < 0.01$, Hill slope, PAR2-WT 2fly vs ACh.

3.4 Effects of inhibition of IP3R and TRPV channels on intracellular Ca^{2+}-activities

To determine the molecular nature of the Ca^{2+}-release units, endothelial cells were pretreated with an inhibitor of IP3R (xestospongin C, XeC, 2 µM) and/or transient receptor potential vanilloid channels (ruthenium red, RR, 75 µM) and then exposed to 2fly (30 nM) or ACh (300 nM). ECs were constantly perfused with the inhibitor and agonist combinations in buffer solution, 2mM $[Ca^{2+}]_o$. Ca^{2+}-events was then assessed as described in section 3.2, and compared to measurements from cells without channel inhibitors or agonist. Inhibition of IP3R with XeC abolished the 2fly and ACh-mediated increase of Ca^{2+}-release sites in PAR2-WT controls and Ang II ($p < 0.001$, Ca^{2+}-release sites/cell, Figure 7a, 7b). Inhibition of TRPV with RR partly reduced the 2fly and ACh mediated number of Ca^{2+}-release sites in PAR2-WT controls and Ang II (Figure 7a, 7b). Data collected from PAR2-KO confirmed that *par2* genotype had no effect on inhibition of Ca^{2+}-activities elicited by ACh in controls or Ang II. PAR2-KO did not show increased Ca^{2+}-events to PAR2 agonist 2fly. See supplement Tables S3-S5 for detailed statistics.

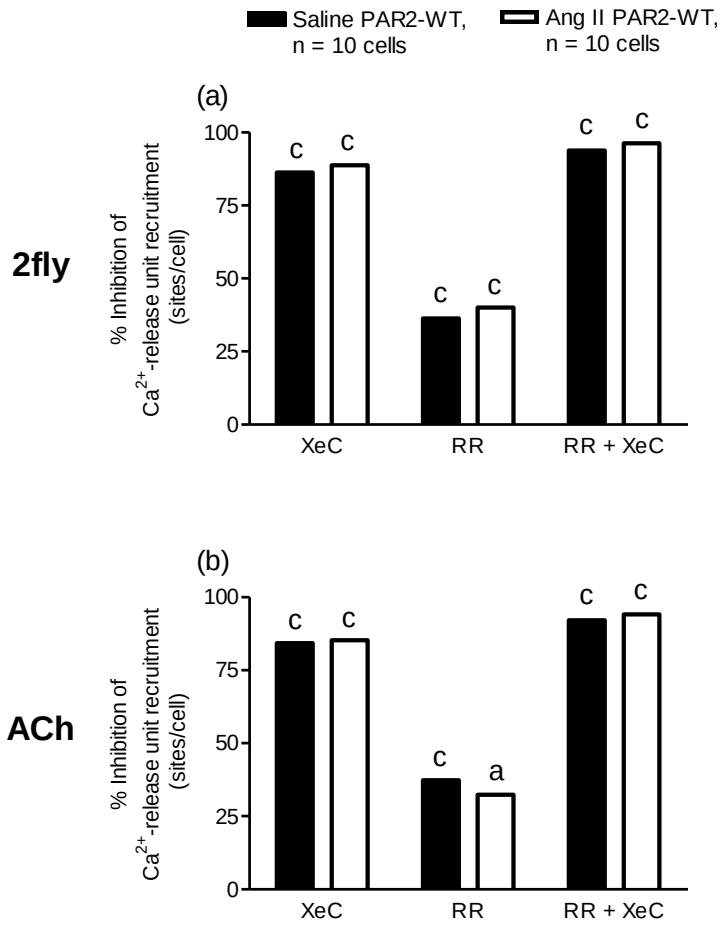

Figure 7. Effect of IP3R and TRPV channel inhibitors on Ca^{2+}-activities in endothelial cells from saline and Ang II-infused PAR2-WT mice. Freshly isolated mesenteric endothelial cells from saline and angiotensin II (Ang II) -infused male PAR2-WT were incubated with inhibitors xestospongin c (XeC, 2 µM) and/or ruthenium red (RR, 75 µM) and then exposed to agonists (a) 2-furoyl-LIGRLO-amide (2fly, 30 nM) or (b) acetylcholine (ACh, 300 nM). Controls = saline-treated PAR2-WT. Data were analyzed by 2 way ANOVA (inhibitor x genotype/treatment group) followed by Bonferonni post-hoc testing. Where S.E.M. = 0, unweighted 2 way ANOVA was used. n = 10 cells, 4 animals per group. (a) $^{c}p < 0.001$, Ca^{2+}-release site density, 2fly + XeC, + RR, + (RR + XeC) vs Controls. (b) $^{c}p < 0.001$, Ca^{2+}-release site density, ACh + XeC, + RR (saline) + (RR + XeC) vs Controls; $^{a}p < 0.05$, Ca^{2+}-release site density, ACh + RR (Ang II) vs Controls.

3.5 Specific Ca^{2+}-transients in endothelial cells

3.5.1 Identification of peripheral and central Ca^{2+}-transients

Ca^{2+}-transients induced by 2fly (3 µM) in saline PAR2-WT could be separated by plotting their frequency and amplitude distributions. The amplitude distribution histogram (Figure 8) revealed two distinct groups in the overall population of Ca^{2+}-transients induced by 2fly (3 µM). Group 1 was composed of Ca^{2+}-events with amplitude $F/F_o = 1.77 \pm 0.01$and group 2 encompassed Ca^{2+}-transients of larger amplitudes $F/F_o = 3.14 \pm 0.02$ ($p < 0.001$, Amplitude, Figure 8 and Table 4). Interestingly, most events of group 1 were found at the periphery of the cell, whereas the vast majority of group 2 events were located at the cell centre. The distribution of Ca^{2+}-events was skewed towards more peripheral events.

Interestingly, there was a higher proportion of peripheral events recruited by 2fly (3 µM) than by ACh (30 µM), 87% vs 69% of total events respectively (Table 4). The same amplitude difference between Ca^{2+}-transient types was also found for baseline and ACh-induced Ca^{2+}-events in all other treatment and genotype groups. Choice of agonist did not affect the dynamic (amplitude, FWHM) or kinetic (t_{rise}, $t_{1/2}$) parameters of either type of Ca^{2+}-transient compared to baseline (Table 4). Ang II treatment had no effect on the distribution or characteristics of peripheral and central Ca^{2+}-events.

Line-scans of 2fly (3 µM) induced peripheral and central Ca^{2+}-transients over a 300 frame (10 s) acquisition period are depicted in a 2D heat map (Figure 9). Surface plots of peripheral and central Ca^{2+}-transients (Figure 10) illustrate kinetic and dynamic differences between the two event types. Three characteristics differentiated each type of event. First, the time to rise from baseline to maximum amplitude was shorter for peripheral than central events ($p < 0.001$, t_{rise}*:* 80 ± 1 ms vs 98 ± 1 ms). Second, the time to fall from maximum amplitude to

half maximum amplitude was longer for peripheral than central events ($p < 0.001$, $t_{1/2}$: 205 ± 1 ms vs 115 ± 1 ms). Third, a regular frequency was measured in the occurrence of large central events (0.64 ± 0.12 Hz) and Ca^{2+}-release clearly originated from the same locus within the cells. This was confirmed by consecutively analyzing central events through different vertical confocal planes. Ca^{2+}-transient parameters were unaffected by the choice of agonist (Figure 11, Table 4). Endothelial dysfunction produced by Ang II, and *par2* genotype did not affect the characteristics of events. See Table 4 for spatial and temporal characteristics of Ca^{2+}-transients.

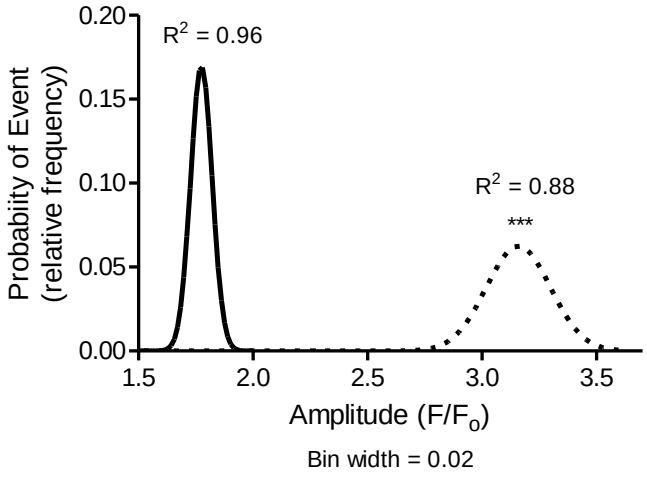

Figure 8. Distinct peripheral and central Ca^{2+}-transients induced by 2fly in saline treated PAR2-WT. Ca^{2+}-transients analyzed from 2-furoyl-LIGRLO-amide (2fly, 3 µM) induced events in saline treated PAR2-WT endothelial cells. Controls = saline-treated PAR2-WT. The curves shown represent the best fit Gaussian distribution for the frequency distribution data (bin width $F/F_o = 0.02$) of peripheral Ca^{2+}-events (left, solid curve) and central-repeating Ca^{2+}-transients (right, hatched curve). 2fly amplitude distributions are not significantly different from Ca^{2+}-events induced spontaneously at baseline or by acetylcholine (ACh, 30 µM). ***$p < 0.001$, Amplitude, central vs peripheral.

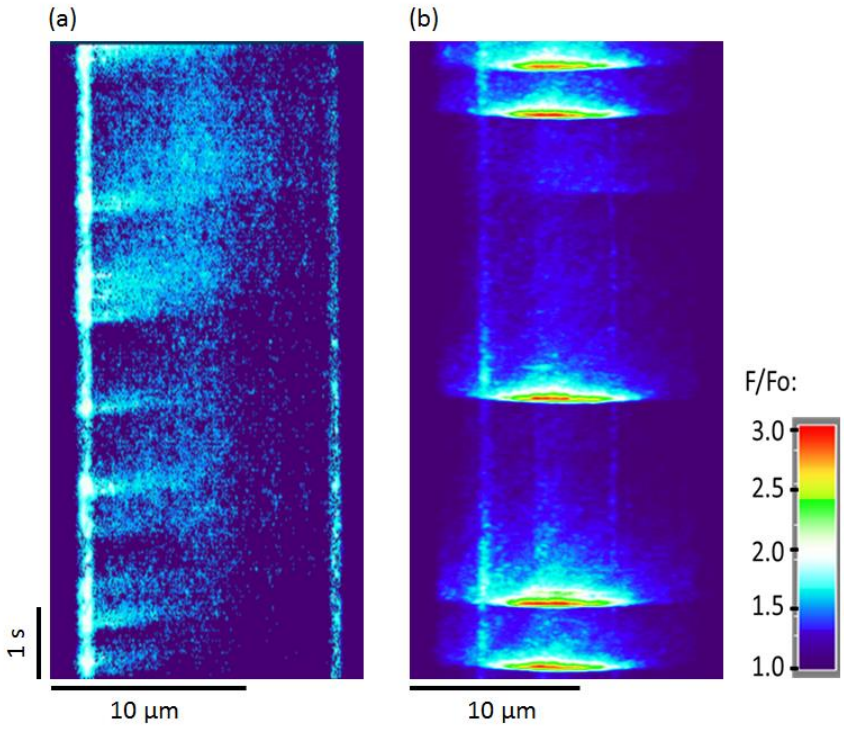

Figure 9. Representative line scan images of peripheral and central-repeating Ca^{2+}-transients induced by 2fly in saline treated PAR2-WT. Ca^{2+}-transients induced by 2-furoyl-LIGRLO-amide (2fly, 3 µM) collected over a 10 s acquisition period in saline treated PAR2-WT endothelial cells. FWHM, full width at half maximum amplitude. (a) Peripheral Ca^{2+}-transients with average amplitude $F/F_o \approx 1.77$, (FWHM 20 % cell length); (b) central-repeating Ca^{2+}-transients with average amplitude $F/F_o \approx 3.14$, (FWHM 34 % cell length). The characteristics of Ca^{2+}-transients were not significantly different across agonist, genotype or treatment groups (see Table 4).

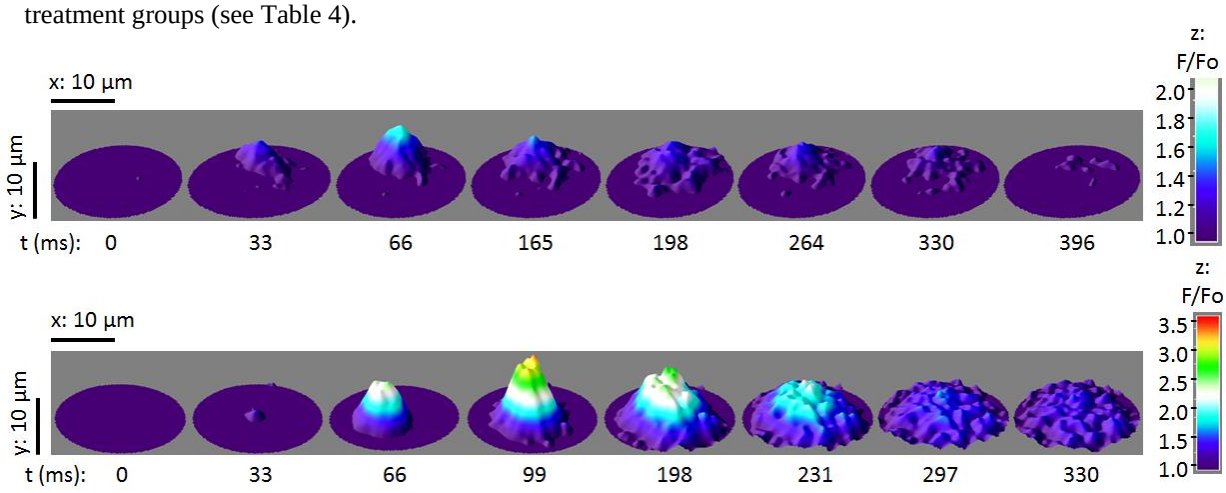

Figure 10. 3D surface plot of peripheral and central Ca^{2+}-transients induced by 2fly in saline treated PAR2-WT. Ca^{2+}-transients induced by 2-furoyl-LIGRLO-amide (2fly, 3 µM) collected over a 10 s acquisition period in saline treated PAR2-WT endothelial cells. t_{rise}, time to rise to maximum amplitude; $t_{1/2}$; half-life of Ca^{2+}-transients. (a) Representative plot of peripheral Ca^{2+}-transients with average $t_{rise} \approx 80$ ms , $t_{1/2} \approx 205$ ms ; (b) Representative plot of central Ca^{2+}-transients with average $t_{rise} \approx 98$, $t_{1/2} \approx 115$. The t_{rise} and $t_{1/2}$ of Ca^{2+}-transients were not significantly different across agonist, genotype or treatment groups (see Table 4).

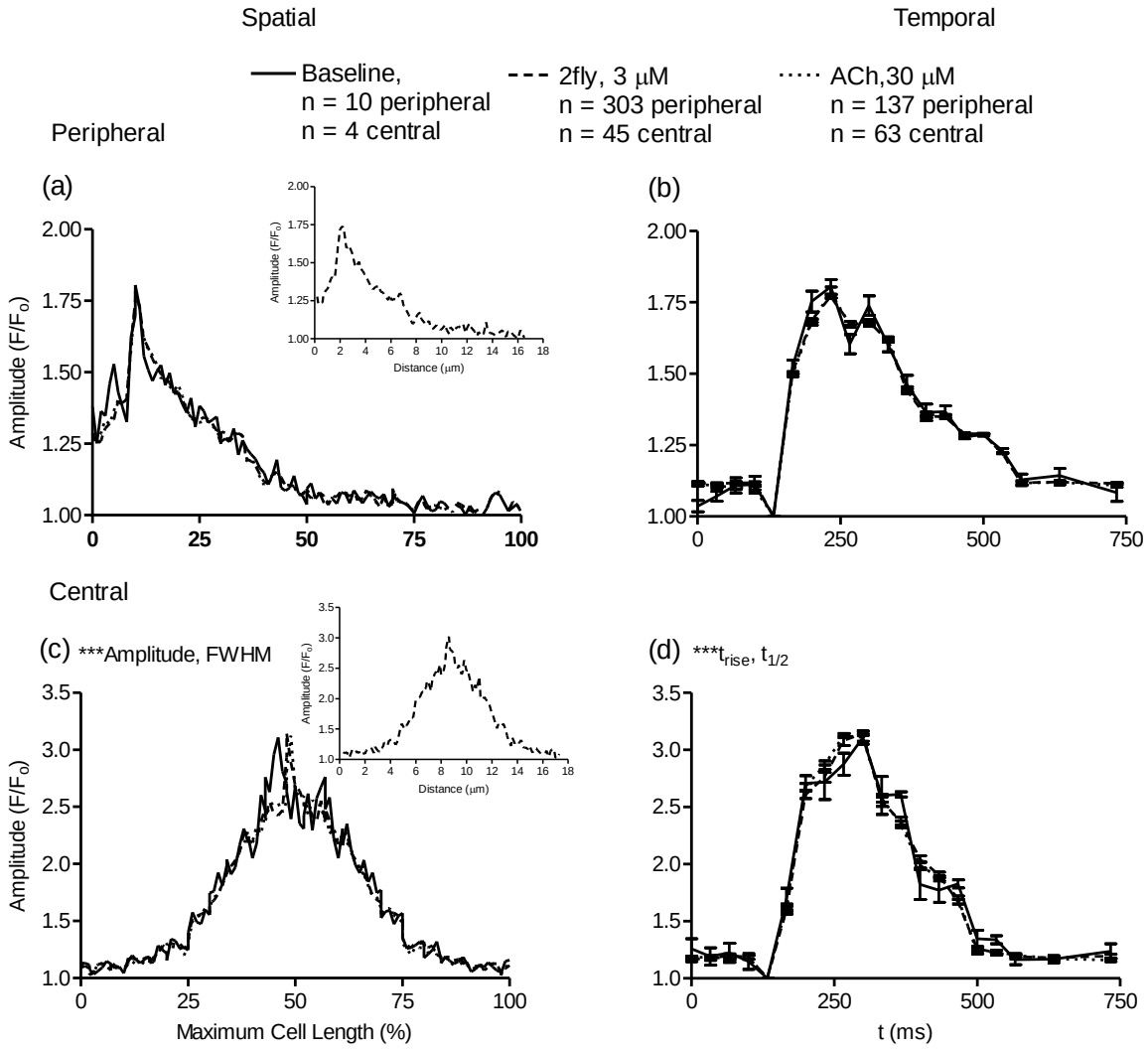

Figure 11. Average spatial and temporal characteristics of peripheral and central Ca^{2+}-transients from saline treated PAR2-WT. Freshly isolated mesenteric endothelial cells from saline treated PAR2-WT were exposed to 2-furoyl-LIGRLO-amide (2fly, 3 μM), acetylcholine (ACh, 30 μM) or at baseline (without agonist). Average characteristics of peripheral (a, b) and central (c, d) Ca^{2+}-transients' spatial (a, c) and temporal (b, d) profiles are presented. Values are means ± S.E.M., n = number of Ca^{2+}-events from 10 cells, 5 animals per group. S.E.M. calculated from number of cells with Ca^{2+}-transients present. Values were obtained by line scan analysis of Ca^{2+}-events in freshly isolated PAR2-WT mesenteric endothelial cells. Data were analyzed by 2 way ANOVA (Ca^{2+}-event type x genotype/treatment group) followed by Bonferonni post-hoc testing. (a) *Insert:* Sample raw plot of peripheral 2fly-induced Ca^{2+}-transient amplitude measured across the space of an endothelial cell. (c) *Insert:* Sample raw plot of central 2fly-induced Ca^{2+}-transient amplitude measured across the space of an endothelial cell. $^{***}p < 0.001$, Amplitude; FWHM, central vs peripheral. (d) $^{***}p < 0.001$, t_{rise}; $t_{1/2}$, central vs peripheral.

Ca^{2+}-Event Type	Treatment	Genotype	Agonist	n	Amplitude (F/F_o)	FWHM (% max cell length)	t_{rise} (ms)	$t_{1/2}$ (ms)	Frequency[ac] (Hz)
Peripheral	Saline	PAR2-WT	Baseline	10	1.80 ± 0.03	20 ± 1	80 ± 2	203 ± 3	N/A
			2fly	303	1.77 ± 0.01	20 ± 1	80 ± 1	205 ± 1	N/A
			ACh	137	1.78 ± 0.02	20 ± 1	80 ± 1	206 ± 1	N/A
		PAR2-KO	Baseline	9	1.81 ± 0.03	20 ± 2	78 ± 2	203 ± 2	N/A
			2fly	9	1.75 ± 0.03	19 ± 1	78 ± 3	203 ± 3	N/A
			ACh	126	1.76 ± 0.01	20 ± 1	80 ± 1	205 ± 1	N/A
	Ang II	PAR2-WT	Baseline	5	1.78 ± 0.04	22 ± 2	81 ± 3	205 ± 3	N/A
			2fly	289	1.77 ± 0.01	20 ± 1	80 ± 1	204 ± 1	N/A
			ACh	92	1.80 ± 0.02	20 ± 1	80 ± 1	204 ± 1	N/A
		PAR2-KO	Baseline	6	1.79 ± 0.05	19 ± 2	79 ± 3	203 ± 2	N/A
			2fly	7	1.76 ± 0.04	20 ± 2	81 ± 2	206 ± 2	N/A
			ACh	93	1.78 ± 0.03	20 ± 1	81 ± 1	206 ± 1	N/A
Central***	Saline	PAR2-WT	Baseline	4	3.11 ± 0.06	33 ± 1	101 ± 4	113 ± 4	0.02 ± 0.02
			2fly	45	3.14 ± 0.02	34 ± 1	98 ± 1	115 ± 1	0.64 ± 0.12[c]
			ACh	63	3.12 ± 0.02	33 ± 1	99 ± 1	115 ± 1	0.82 ± 0.18[c]
		PAR2-KO	Baseline	3	3.17 ± 0.05	31 ± 2	93 ± 2	116 ± 5	0.03 ± 0.02
			2fly	3	3.16 ± 0.07	32 ± 1	99 ± 4	112 ± 2	0.02 ± 0.01
			ACh	65	3.14 ± 0.02	33 ± 1	100 ± 1	116 ± 1	0.77 ± 0.06[c]
	Ang II	PAR2-WT	Baseline	3	3.19 ± 0.05	31 ± 1	102 ± 3	112 ± 1	0.02 ± 0.02
			2fly	43	3.14 ± 0.02	33 ± 1	101 ± 1	115 ± 1	0.52 ± 0.11[c]
			ACh	30	3.14 ± 0.02	33 ± 1	99 ± 2	115 ± 1	0.32 ± 0.06[a]
		PAR2-KO	Baseline	3	3.21 ± 0.05	33 ± 2	102 ± 2	112 ± 4	0.02 ± 0.02
			2fly	4	3.11 ± 0.12	36 ± 1	99 ± 5	117 ± 2	0.04 ± 0.02
			ACh	33	3.13 ± 0.02	33 ± 1	100 ± 2	113 ± 2	0.34 ± 0.04[a]

Table 4. Effect of PAR2 and M_3 activation on characteristics of peripheral and central Ca^{2+}-events from mice with and without endothelial dysfunction. Values are means ± S.E.M., n = number of Ca^{2+}-events from 10 cells, 5 animals per group. S.E.M. calculated from number of cells with Ca^{2+}-transients present. S.E.M. = 0 indicates that all cells observed had the same number of Ca^{2+}-release sites or rate.2-furoyl-LIGRLO-amide (2fly, 3 μM); acetylcholine (ACh, 30 μM); Baseline (without agonist); FWHM, full width at half-maximum Ca^{2+}-event amplitude (% maximum cell length). Values were obtained by line scan analysis of Ca^{2+}-events in freshly isolated PAR2-WT and PAR2-KO mesenteric endothelial cells. Data were analyzed by 2 way ANOVA (Ca^{2+}-event type x genotype/treatment group) followed by Bonfferoni post-hoc testing. Where S.E.M. = 0, unweighted 2 way ANOVA was used. [c]$p < 0.001$, Frequency, saline and Ang II PAR2-WT 2fly vs baseline. [c]$p < 0.001$, Frequency, saline PAR2-WT and PAR2-KO ACh vs baseline. [a]$p < 0.05$, Frequency, Ang II PAR2-WT and PAR2-KO ACh vs baseline. [***]$p < 0.001$, all parameters, central vs peripheral.

3.5.2 Effect of endothelial dysfunction on PAR2 and M_3-mediated peripheral and central Ca^{2+}-transients

To assess whether agonists and endothelial dysfunction had different effects on peripheral and central Ca^{2+}-events, data from Figure 6 were reanalyzed based on the location of Ca^{2+}-events. 2fly, compared to ACh, was a more potent activator of endothelial cells for both types of Ca^{2+} events (Figure 12a, 12b). Activation of peripheral events occurred at lower concentrations of 2fly and ACh than for central events.

PAR2 agonist 2fly (Figures 13a, 14a), recruited the same number of sites of peripheral and central Ca^{2+} events per cell in PAR2-WT controls and Ang II. ACh compared to 2fly produced half the number of sites of peripheral and central Ca^{2+} events per cell. ACh peripheral and central Ca^{2+}-transients (Figure 13b, 14b) were decreased by 22% and 23%, respectively in Ang II treated PAR2-WT ($p < 0.05$, peripheral, E_{max}; $p < 0.01$, central, E_{max}). Similarly for ACh (Figures 13d, 14d), the firing rate of peripheral and central Ca^{2+}-release units in PAR2-WT were decreased by 20-50% in Ang II treated cells compared to controls.

Data collected from PAR2-KO confirmed the specificity of 2fly for PAR2 recruitment of both peripheral and central Ca^{2+}-transients (Figure 13a, 13c and 14a, 14c). PAR2-KO data demonstrated that the *par2* genotype had no effect on peripheral or central Ca^{2+}-events elicited by ACh in controls or Ang II (Figure 13b, 13d and 14b, 14d). Curve-fit function variables for CRCs are located in supplement Table S6 and Table S7.

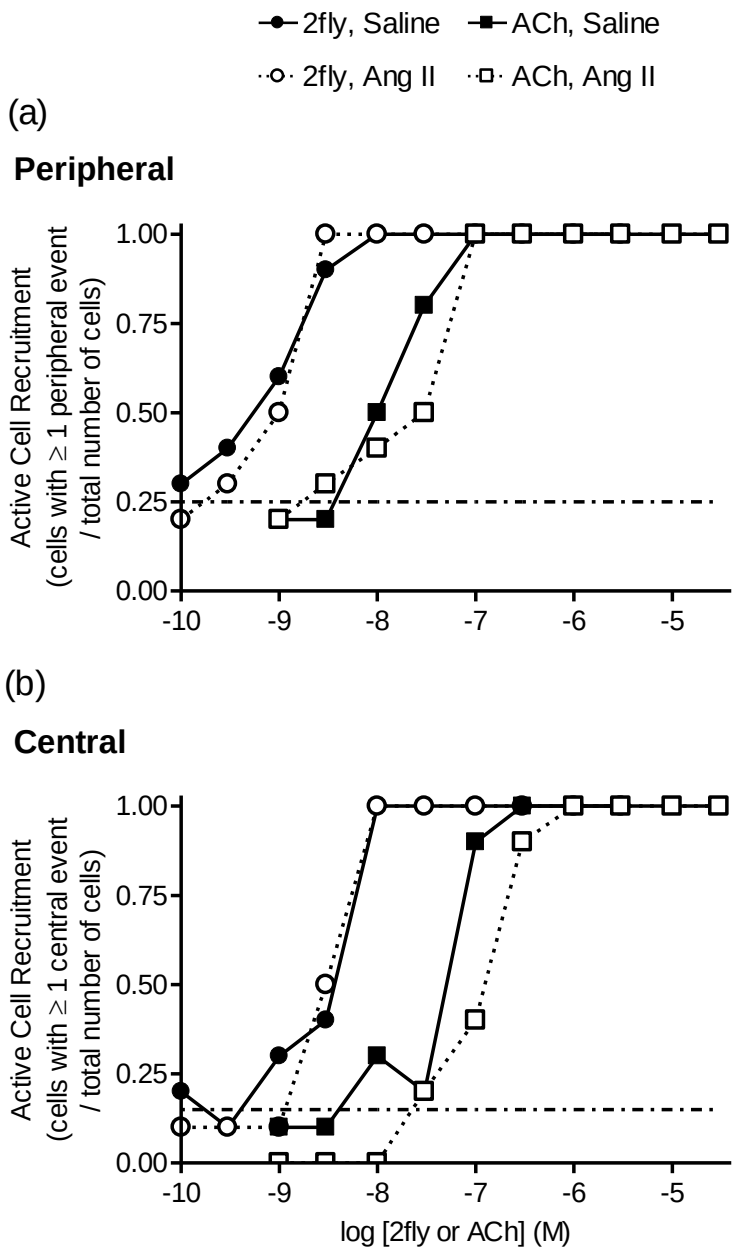

Figure 12. PAR2-activating peptide 2fly vs ACh activation of Ca^{2+}-release units in mesenteric arterial endothelial cells from PAR2-WT. Concentration-response data from PAR2-WT of 2-furoyl-LIGRLO-amide (2fly) vs acetylcholine (ACh) recruitment of cells displaying (**a**) peripheral and (**b**) central Ca^{2+}-release units. 2fly activation of PAR2 is a more potent mechanism for endothelial cell Ca^{2+}-events recruitment than M_3 activation by ACh. *n* = 10 cells per group at each concentration of agonist. Horizontal dashed line indicates the mean response rate under baseline (no agonist) conditions in cells from wild-type saline-treated mice (*n* = 20 cells).

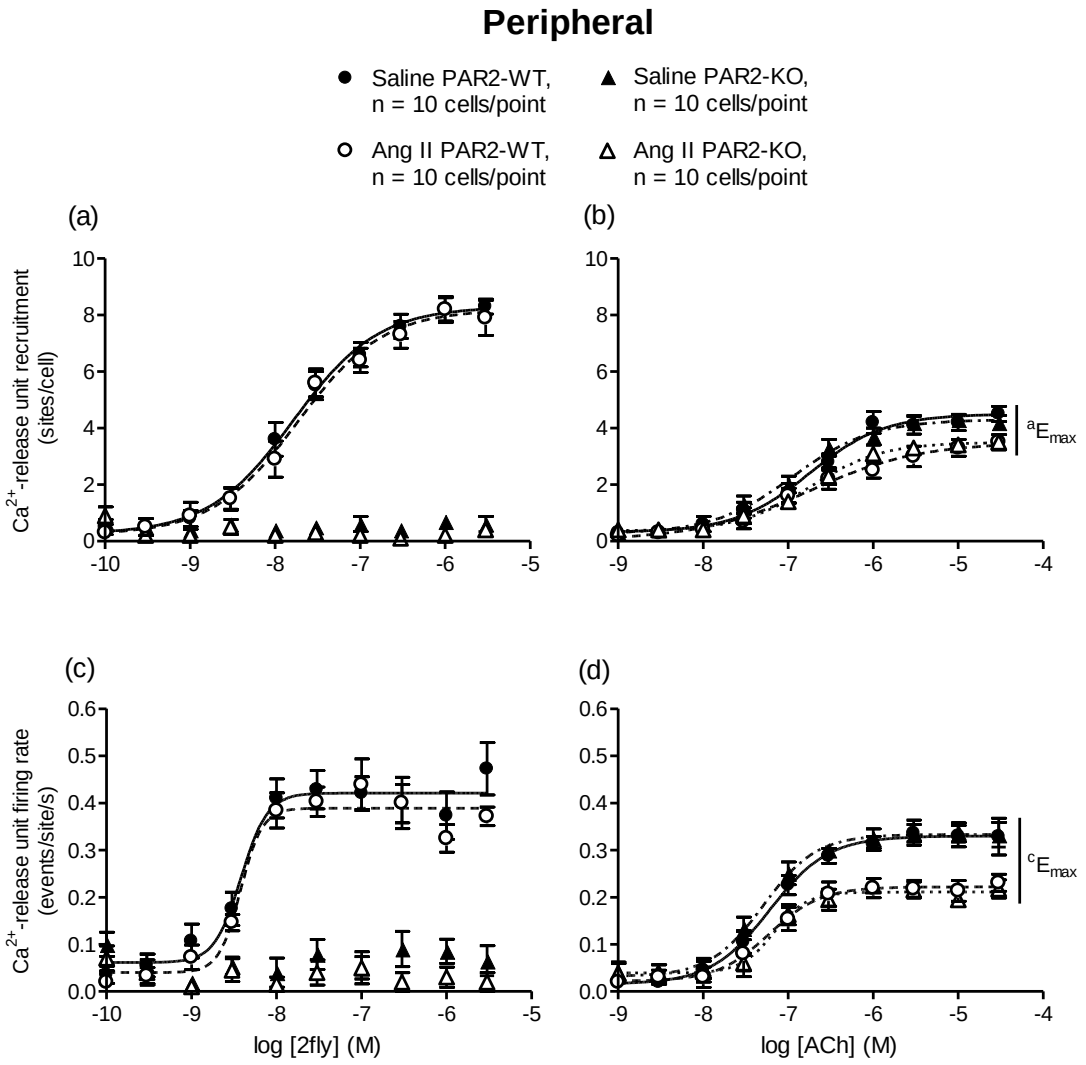

Figure 13. Effect of angiotensin II infusion on PAR2 and M_3-mediated peripheral Ca^{2+}-transients in endothelial cells. Freshly isolated mesenteric endothelial cells from saline and angiotensin II-infused male PAR2-WT and PAR2-KO were perfused with varying concentrations of either (a, c) 2-furoyl-LIGRLO-amide (2fly) or (b, d) acetylcholine (ACh). Top graphs (a, b) represent peripheral Ca^{2+}-event site recruitment by agonists, bottom graphs (c, d) represent peripheral Ca^{2+}-transient release rate by agonists. Symbols are means ± S.E.M., n = number of endothelial cells per point, 5 animals per curve. Lines represent 4 parameter logistic curves which calculate the variables: pD_2, E_{max} and Hill slope. Variables were compared by 2 way ANOVA (treatment x genotype), followed by Bonferroni post-hoc testing. (b) $^{a}p < 0.05$, E_{max}, Ang II PAR2-WT and PAR2-KO vs Controls. (d) $^{c}p < 0.001$, E_{max}, Ang II PAR2-WT and PAR2-KO vs Controls.

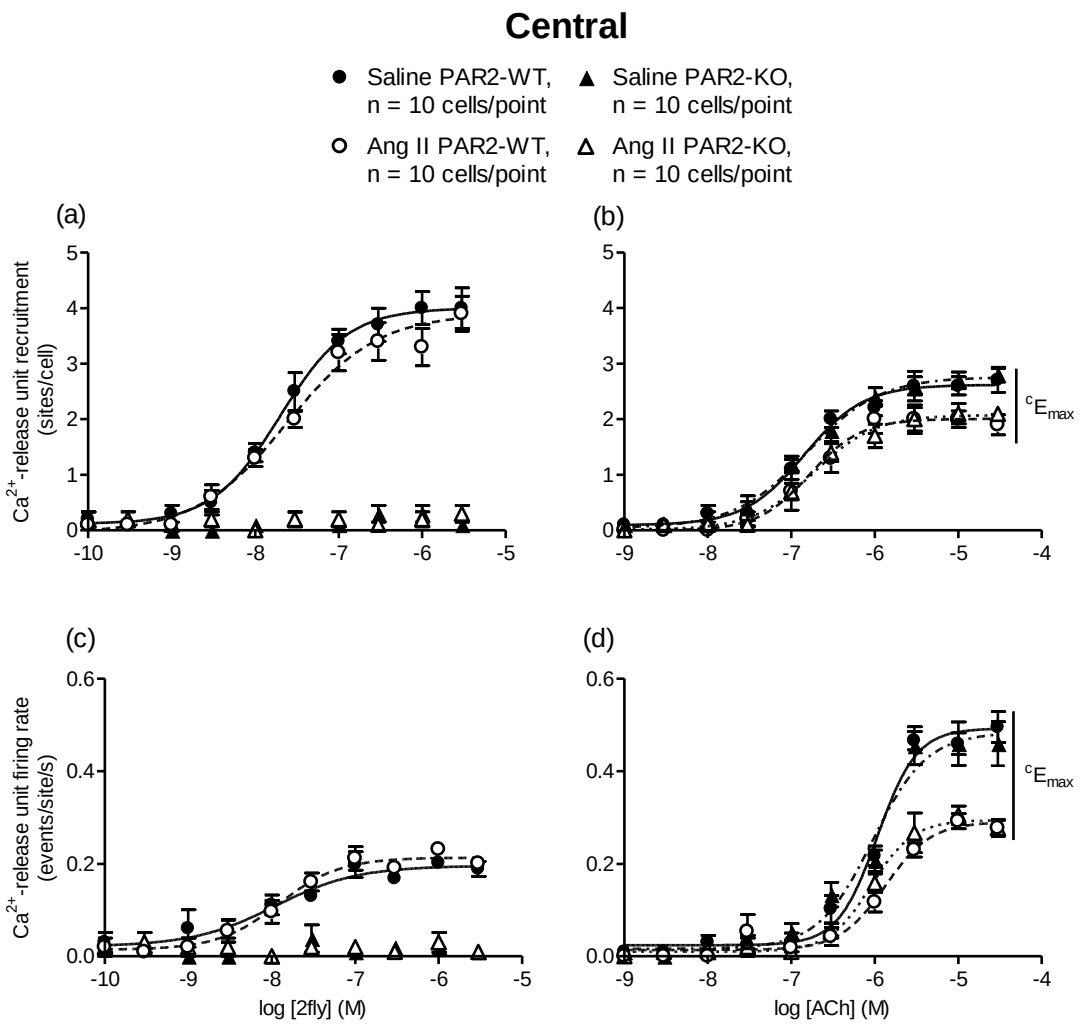

Figure 14. Effect of angiotensin II infusion on PAR2 and M_3-mediated central Ca^{2+}-transients in endothelial cells. Freshly isolated mesenteric endothelial cells from saline and angiotensin II-infused male PAR2-WT and PAR2-KO were perfused with varying concentrations of either (a, c) 2-furoyl-LIGRLO-amide (2fly) or (b, d) acetylcholine (ACh). Top graphs (a, b) represent central Ca^{2+}-event site recruitment by agonists, bottom graphs (c, d) represent central Ca^{2+}-transient release rate by agonists. Symbols are means ± S.E.M., n = number of endothelial cells per point, 5 animals per curve. Controls = saline-treated PAR2-WT. Lines represent 4 parameter logistic curves which calculate the variables: pD_2, E_{max} and Hill slope. Variables were compared by 2 way ANOVA (treatment x genotype), followed by Bonferroni post-hoc testing. (b) $^{c}p < 0.001$, E_{max}, Ang II PAR2-WT and PAR2-KO vs Controls. (d) $^{c}p < 0.001$, E_{max}, Ang II PAR2-WT and PAR2-KO vs Controls.

3.5.3 Effect of IP3R and TRPV channel inhibition on peripheral and central Ca^{2+}-transient events in endothelial cells

To determine whether the molecular characteristics of the Ca^{2+}-release units for peripheral events differed from central events, the data from Figure 10 were re-analyzed by event type. Inhibition of IP3R with XeC decreased the Ca^{2+}-release site density by 2fly and ACh of peripheral and central Ca^{2+}-release units in Ang II-treated and control PAR2-WT ($p < 0.001$, Ca^{2+}-release site density, Figure 15). TRPV inhibitor RR reduced PAR2-mediated peripheral and central Ca^{2+}-release site density (Figure 15a, c). For M_3 receptor-mediated events, only central Ca^{2+}-events in control PAR2-WT showed partial attenuation to RR ($p < 0.01$, Ca^{2+}-release site density, Figure 15d). The combination of XeC + RR affected Ca^{2+}-release site recruitment similarly to XeC alone.

Endothelial dysfunction did not alter the inhibition by XeC, RR, and RR + XeC of peripheral Ca^{2+}-release by 2fly or ACh in PAR2-WT ($p > 0.05$, Ca^{2+}-release site density, Figure 15a, 15b). Inhibition of central Ca^{2+}-release site density by XeC and RR + XeC was not different across treatment groups ($p > 0.05$, Ca^{2+}-release site density, Figure 15c, 15d). In ACh central Ca^{2+}-events, release site density was attenuated by RR in control PAR2-WT but not in Ang II treated animals. Data collected from PAR2-KO confirmed that *par2* genotype had no effect on inhibition of peripheral or central Ca^{2+}-events elicited by ACh in controls or Ang II. See supplement Tables S8-S13 for detailed statistics separated by Ca^{2+}-transient type.

The inhibitors also attenuated the dynamic and kinetic characteristics of the Ca^{2+}-events. IP3R inhibition with XeC reduced 2fly-induced peripheral Ca^{2+}-transient amplitude by 32% and FWHM by 55%, and increased the rise time of events (Figure 16a, 16b). XeC had similar, but more profound effects on central Ca^{2+}-transients (Figure 16c, 16d). RR attenuated the FWHM of

2fly-induced peripheral Ca^{2+}-transients by 20%, but did not change the amplitude or temporal parameters (Figure 16a, 16b). Interestingly, TRPV channel inhibition with RR had different effects on central Ca^{2+}-transients. RR attenuated the amplitude, but not FWHM, of PAR2-mediated central Ca^{2+}-transients by 32% (Figure 16c). There was no effect of RR on the temporal characteristics of central Ca^{2+}-transients (Figure 16d). The combination of RR and XeC produced the similar effects as XeC alone. The effects of inhibitors on Ang II treated EC Ca^{2+}-transients were similar to controls. There was no combination effect of treatment (saline or Ang II) and inhibitors on the spatial or temporal characteristics of Ca^{2+}-transients. See supplement Tables S14-S17 for detailed statistics of the inhibitory study Ca^{2+}-event characteristics.

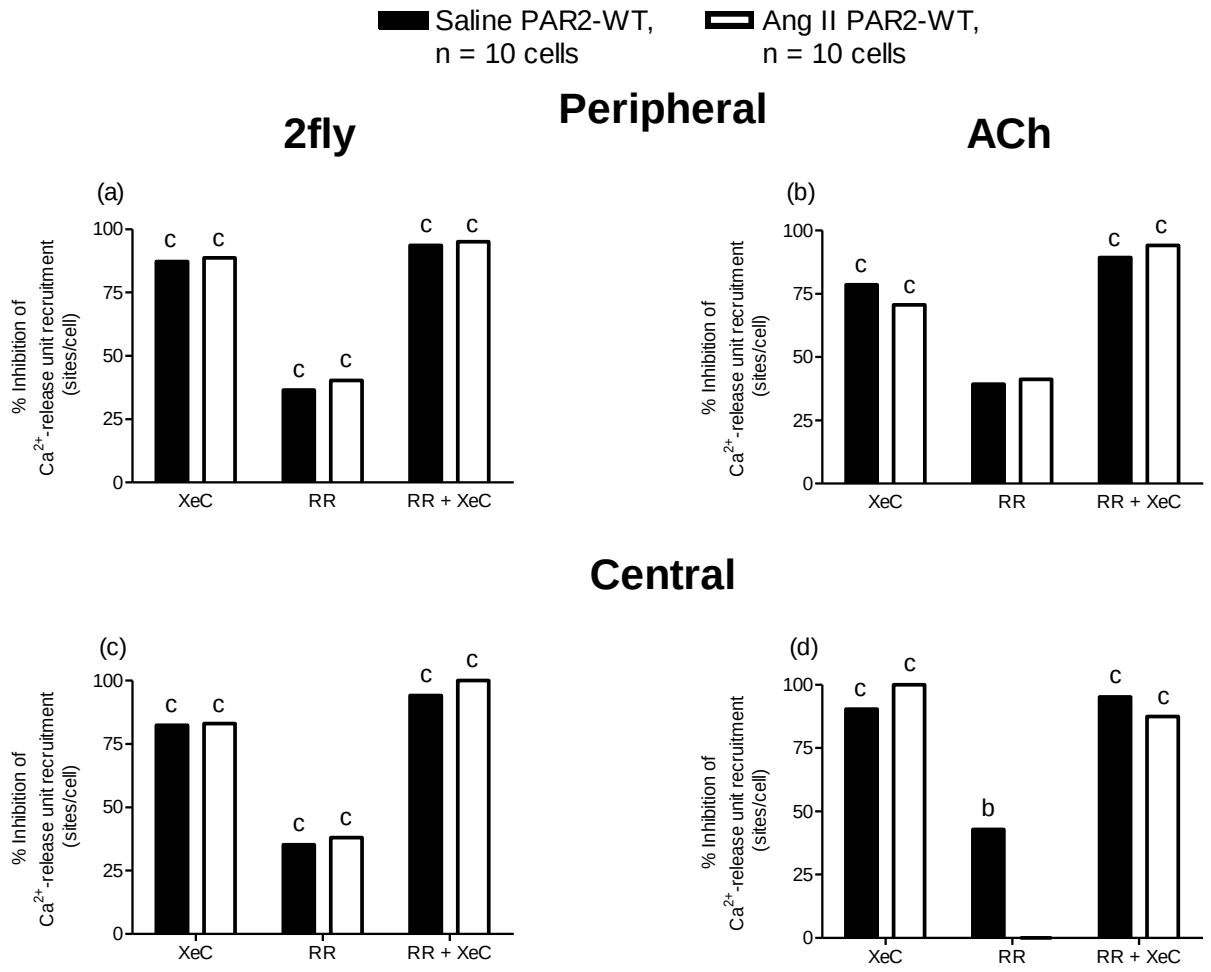

Figure 15. Effect of IP3R and TRPV channel inhibitors on peripheral Ca^{2+}-activities in endothelial cells from saline and Ang II-infused PAR2-WT. Freshly isolated mesenteric endothelial cells from saline and angiotensin II (Ang II) -infused male PAR2-WT were incubated with inhibitors xestospongin c (XeC, 2 μM) and or ruthenium red (RR, 75 μM) and then exposed to agonists (a,c) 2-furoyl-LIGRLO-amide (2fly, 30 nM) or (b,d) acetylcholine (ACh, 300 nM). Ca^{2+}-events were separated by type: peripheral (a,b) and central (c,d). Controls = saline-treated PAR2-WT. Data were analyzed by 2 way ANOVA (inhibitor x genotype/treatment group) followed by Bonferonni post-hoc testing. Where S.E.M. = 0, unweighted 2 way ANOVA was used. n = 10 cells, 4 animals per group. (a) $^{c}p < 0.001$, Ca^{2+}-release site density, 2fly + XeC, + RR, + (RR + XeC) vs Controls. (b) $^{c}p < 0.001$, Ca^{2+}-release site density, ACh + XeC, + (RR + XeC) vs Controls. (c) $^{c}p < 0.001$, Ca^{2+}-release site density, 2fly + XeC, + RR, + (RR + XeC) vs Controls. (d) $^{c}p < 0.001$, Ca^{2+}-release site density, ACh + XeC, + (RR + XeC) vs Controls; $^{b}p < 0.01$, Ca^{2+}-release site density, ACh + RR (saline) vs Controls.

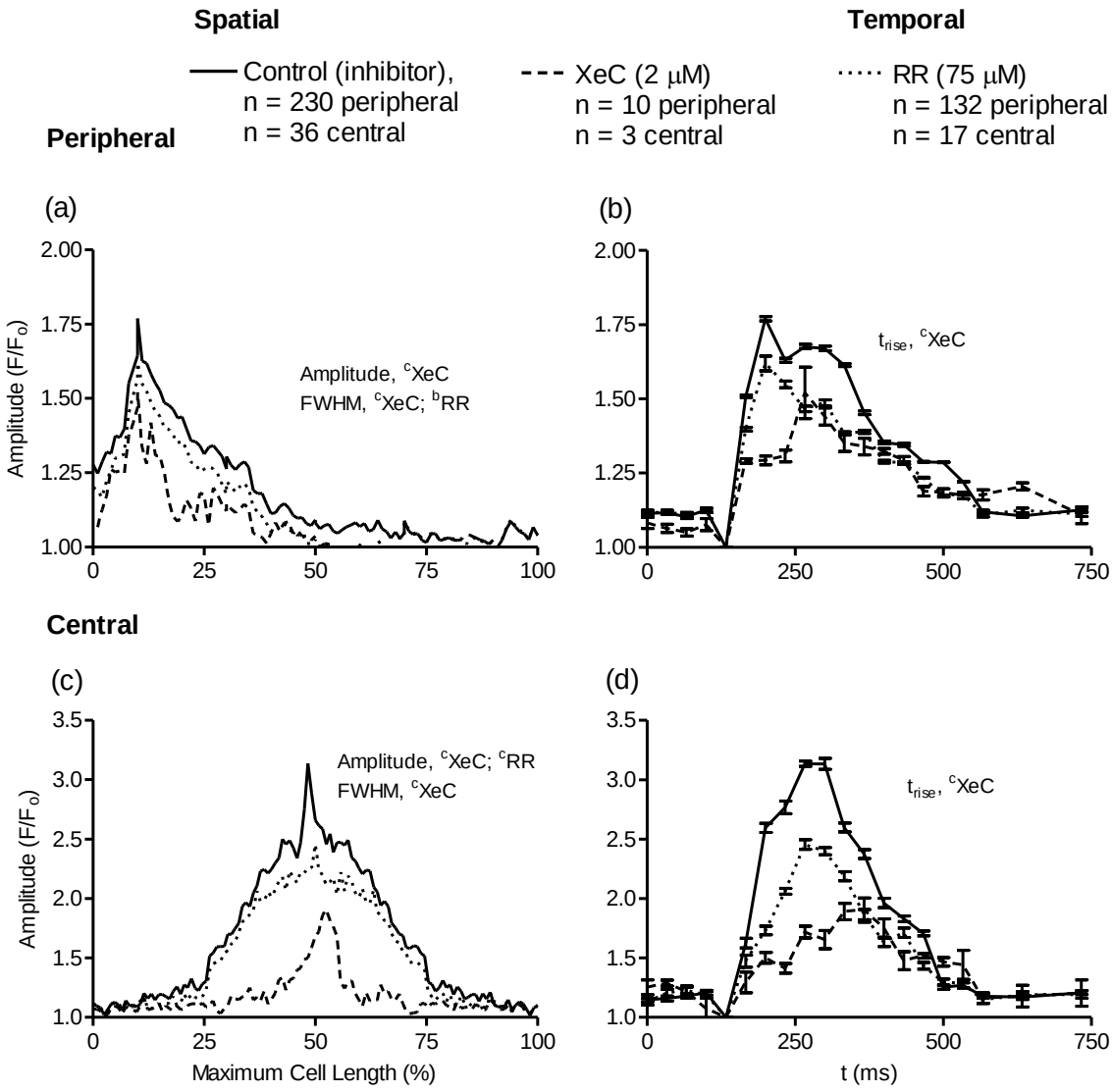

Figure 16. Effect of inhibitors XeC and RR on characteristics of PAR2-mediated peripheral and central Ca^{2+}-event profiles from saline-infused PAR2-WT. Freshly isolated mesenteric endothelial cells from saline treated PAR2-WT were exposed to combinations of xestospongin c (XeC, 2 μM) or ruthenium red (RR, 75 μM) and Control (no inhibitor) plus 2-furoyl-LIGRLO-amide (2fly, 3μM). Peripheral (a, b) and central (c, d) Ca^{2+}-transients spatial (a, c) and temporal (b, d) characteristics were assessed. Values are means ± S.E.M., n = number of Ca^{2+}-events from 10 cells, 5 animals per group. S.E.M. calculated from number of cells with Ca^{2+}-transients present. Values were obtained by line scan analysis of Ca^{2+}-events in freshly isolated PAR2-WT mesenteric endothelial cells. Controls = saline-treated PAR2-WT. Data were analyzed by 2 way ANOVA (Ca^{2+}-event type x genotype/treatment group) followed by Bonferonni post-hoc testing. Where S.E.M. = 0, unweighted 2 way ANOVA was used. (a) $^{c}p < 0.001$, Amplitude; FWHM, XeC vs Controls. $^{b}p < 0.01$, FWHM, RR vs Controls. (b) $^{c}p < 0.001$, t_{rise}, XeC vs Controls. (c) $^{c}p < 0.001$, Amplitude; FWHM, XeC vs Controls. $^{c}p < 0.001$, Amplitude, RR vs Controls. (d) $^{c}p < 0.001$, t_{rise}, XeC vs Controls.

3.6 Effects of endothelial dysfunction on the subcellular distribution of PAR2, IP3R, eNOS, SK_{ca} and IK_{ca} in endothelial cells

3.6.1 Identification of endothelial cells

Immunocytochemistry experiments were carried out to determine the effects of Ang II treatment on protein expression in endothelial cells. In addition to morphology, ECs were identified by probing for platelet endothelial cell adhesion molecule type 1 (PECAM-1) located on the plasma membrane. In all ICC experiments positive PECAM-1 signal verified the identity of endothelial cells (Figure 17) and delineated the periphery of the plasma membrane (Figure 18). Primary antibody for PECAM-1 was detected by staining with a Texas Red secondary antibody. VSMCs did not express red fluorescent signal when determined at 522 nm in the presence of PECAM-1 and Texas Red antibody. PECAM-1 staining did not vary across *par*2 genotype or with Ang II treatment.

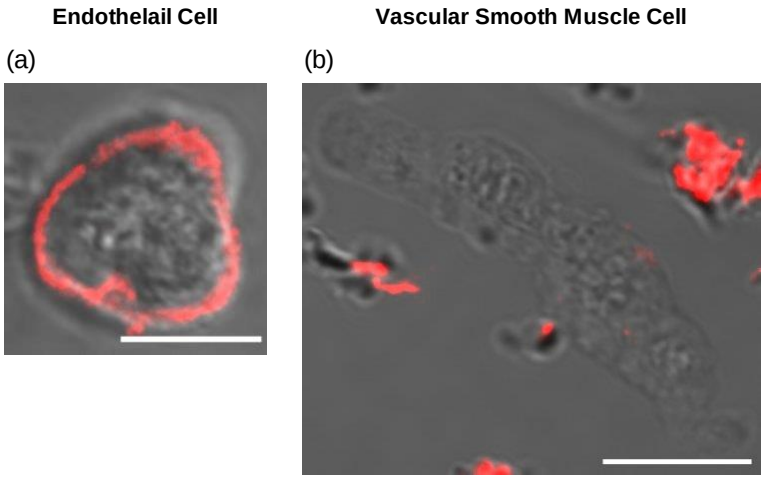

Figure 17. Texas Red staining of PECAM-1 identified endothelial cells. Isolated and fixed saline treated PAR2-WT endothelial cell (a) and vascular smooth muscle cell (b) probed with PECAM-1 primary antibody and Texas Red fluorescent secondary antibody. Images are Texas Red channels at 522 nm superimposed on white light images from the same cell plane. Positive PECAM-1 probing presents as a red colored signal. Red signal not on cells indicates the presence of debris which absorbed Texas Red secondary antibody. White line at bottom right of images is a scale bar = 10 µm. Magnification 960 x.

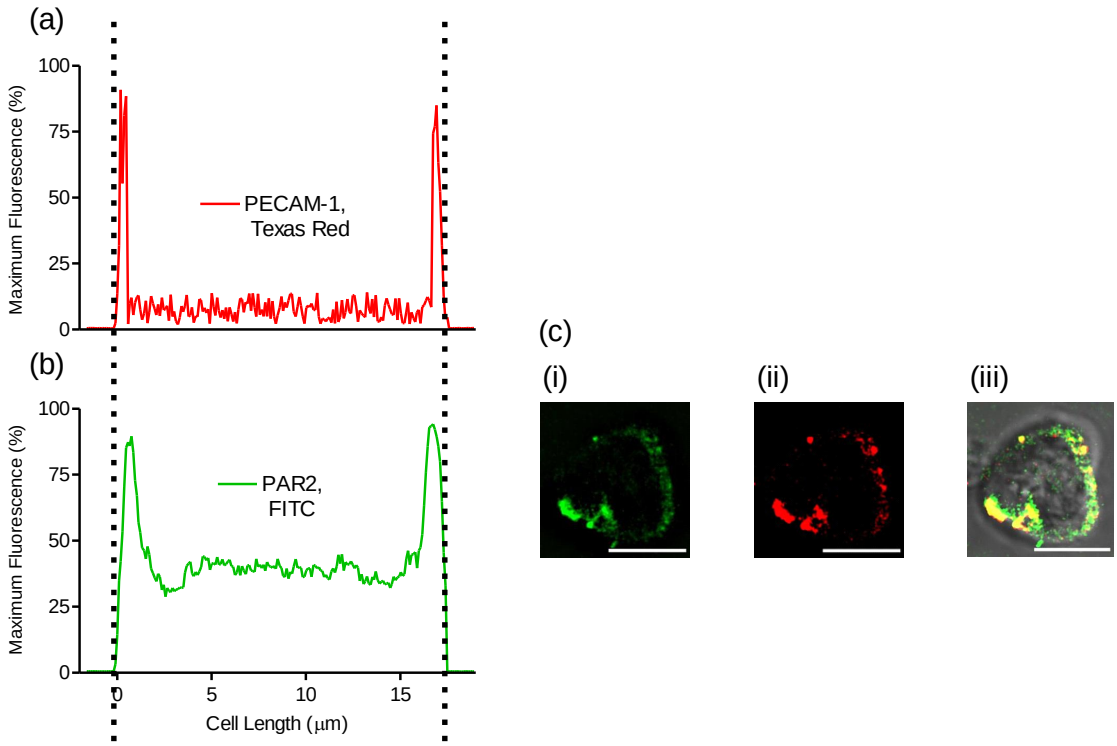

Figure 18. Identification of PAR2 on the plasma membrane in PAR2-WT endothelial cells. Plasma membranes of endothelial cells were demarcated by peak intensity of peripheral Texas Red signal. FITC, fluorescein isothiocyanate. Position zero (μm) is the origin of the line scan analysis for PECAM-1 fluorescent signal. (a) PECAM-1 Texas Red signal on the periphery of a representative saline treated PAR2-WT endothelial cell. (b) FITC signal for the same cell (below) demonstrates that PAR2 lies on the plasma membrane. (c) Saline treated PAR2-WT endothelial cell probed for PECAM-1 and PAR2. (i) PAR2 signal, green FITC; (ii) PECAM-1, Texas Red and (iii) FITC, Texas Red and white light composite image. Yellow signal indicates colocalization of PAR2 and PECAM-1. White line at bottom right of images is a scale bar = 10 μm. Magnification 960 x.

3.6.2 Effect of *par*2 genotype and endothelial dysfunction on protein expression in mesenteric endothelial cells

PAR2 expression

To determine whether an increase in PAR2 expression preserved the Ca^{2+}-signals by PAR2 agonist, PAR2 specific immunofluorescence across cells was compared between Ang II and saline treated PAR2-WT. Staining of PAR2 in ECs from saline and Ang II PAR2-WT overlapped with PECAM-1 near the periphery, and was observed to a lesser extent heterogeneously throughout the cell (Figure 19a-d). PAR2 immunofluorescence specificity in PAR2-WT was confirmed by comparing to PAR2-KO cells (Figure 19e-h). We found that the distribution of PAR2 immunofluorescence in Ang II treated ECs were unchanged from that of saline controls (Figure 20).

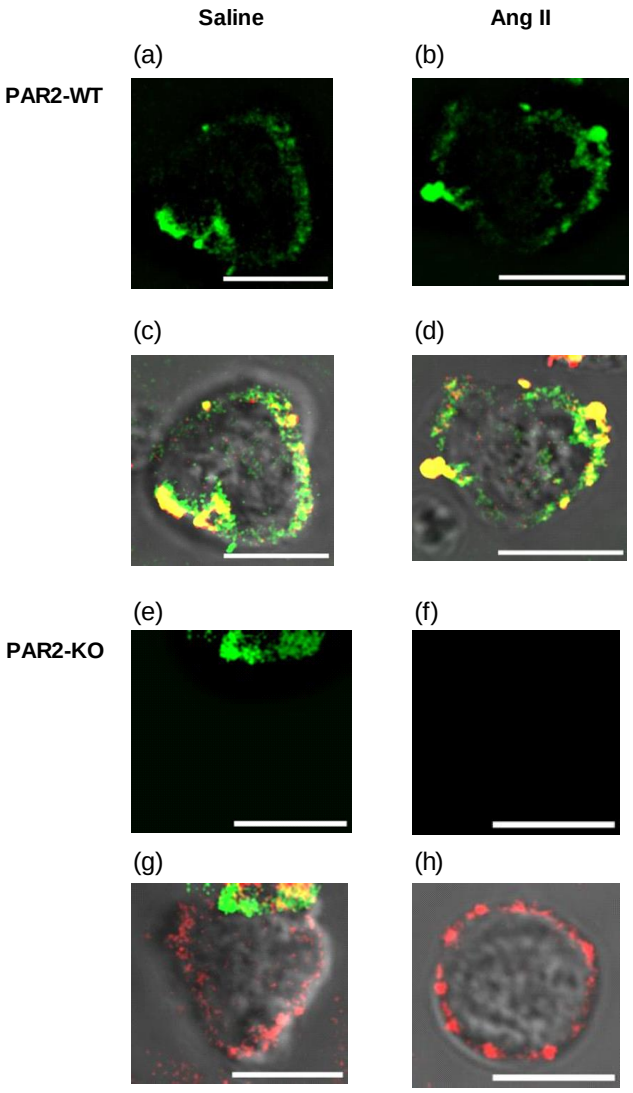

Figure 19. PAR2 immunocytochemistry staining from mesenteric endothelial cells across *par*2 genotypes and treatment groups. Isolated and fixed mesenteric endothelial cells from saline (a, c, e, g) and angiotensin II (b, d, f, h) treated PAR2-WT (a-d) and PAR2-KO (e-h) were probed with primary antibody for PAR2 and PECAM-1. Secondary antibody labeling with Texas Red (PECAM-1, red) and FITC, fluorescein isothiocyanate, (PAR2, green) reveal the location of PAR2 and PECAM-1 proteins in each group. Top panels (a, b, e, f) are FITC channel images showing the location of PAR2 signal only; bottom panels (c, d, g, h) are white light, FITC and Texas Red composite channel images showing the location of gross cellular structures, PAR2 and PECAM-1. Yellow signal indicates colocalization of PAR2 and PECAM-1. Acellular structures with red, green or yellow fluorescent signals are debris that have absorbed secondary antibody. There are no significant differences in green FITC PAR2 signal distribution between Ang II and saline PAR2-WT (a-d). PAR2-KO did not express green FITC PAR2-signal. White line at bottom right of images is a scale bar = 10 µm. Magnification 960 x.

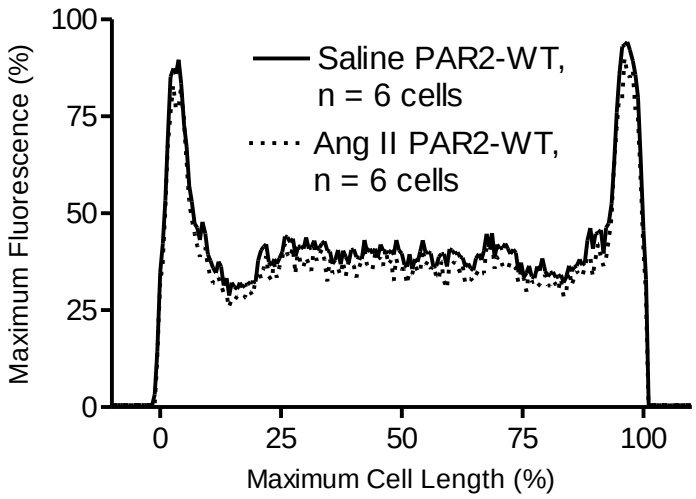

Figure 20. Spatial distribution of PAR2 in PAR2-WT endothelial cells with and without endothelial dysfunction. Isolated and fixed endothelial cells from saline or angiotensin II treated PAR2-WT and PAR2-KO were incubated with primary antibody specific for PAR2. FITC, fluorescein isothiocyanate fluorescent conjugate secondary antibody was detected at 498 nm under line scan confocal microscopy. The confocal plane presented is from the center of a z-stack series of images. Lines are means, n = 6 cells, 4 animals per group. PAR2 staining is congruent with the peripheral boundary of endothelial cells. There was no difference in the distribution of PAR2 fluorescent signal between PAR2-WT treatment groups. PAR2-KO endothelial cells did not stain with F ITC PAR2 fluorescent secondary antibody (not shown).

IP3R expression

Based on the live cell imaging data using XeC, IP3R were the predominant Ca^{2+}-release unit protein in endothelial cells. We investigated whether endothelial dysfunction altered the expression of these channels by measuring the distribution of IP3R pan-isoform immunostaining in endothelial cells (Figure 21a-h). We found IP3R immunofluorescence distributed as two different levels of intensity throughout confocal plane of an endothelial cell. The highest intensity level of IP3R staining corresponded to the periphery of the cells, inside the plasma membrane (i.e. PECAM-1 staining). A lower intensity level of IP3R signal was distributed throughout the interior of the cell. We did not find a difference between saline and Ang II treated PAR2-WT for the distribution of IP3R (Figure 22). PAR2-KO ICC experiments confirmed that the *par*2 gene did not affect the expression of pan-isoform IP3R antibody.

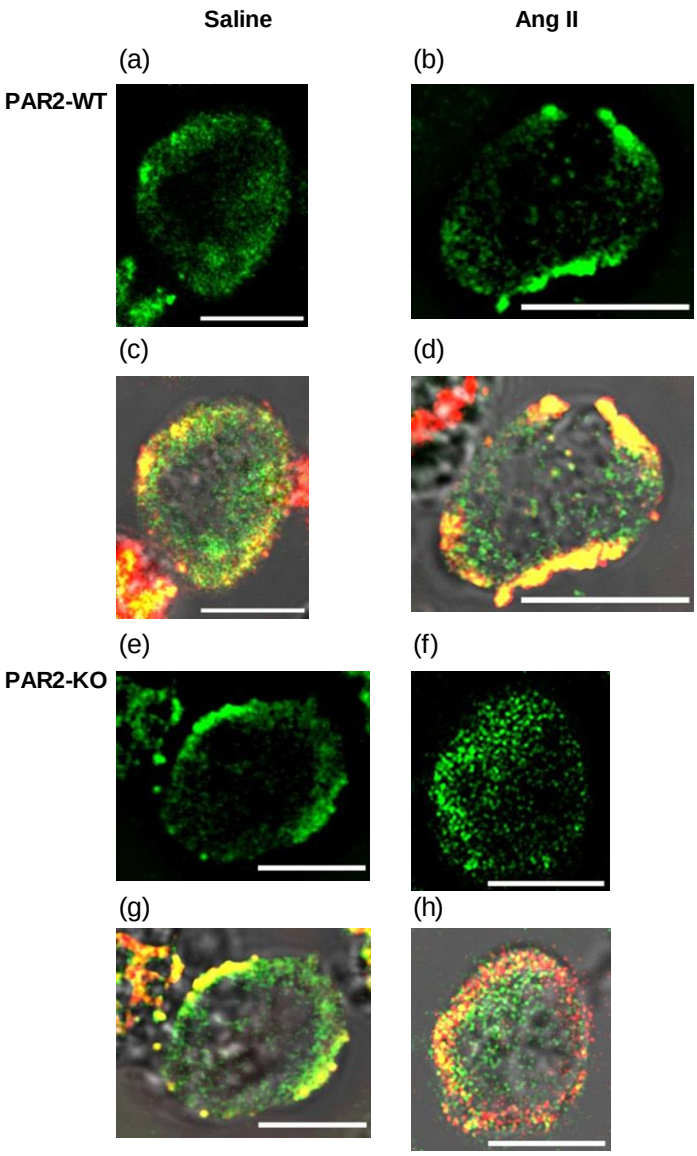

Figure 21. IP3R immunocytochemistry staining from mesenteric endothelial cells across *par*2 genotypes and treatment groups. Isolated and fixed mesenteric endothelial cells from saline (a, c, e, g) and angiotensin II (b, d, f, h) treated PAR2-WT (a-d) and PAR2-KO (e-h) were probed with primary antibody for pan-IP3R subtypes and PECAM-1. Secondary antibody labeling with Texas Red (PECAM-1, red) and FITC, fluorescein isothiocyanate, (IP3R, green) reveal the location of IP3R and PECAM-1 proteins in each group. Top panels (a, b, e, f) are FITC channel images showing the location of IP3R signal only; bottom panels (c, d, g, h) are white light, FITC and Texas Red composite channel images showing the location of gross cellular structures, IP3R and PECAM-1. Yellow signal indicates colocalization of IP3R and PECAM-1. Acellular structures with red, green or yellow fluorescent signals are debris that have absorbed secondary antibody. There are no significant differences in green FITC IP3R signal distribution between Ang II and saline PAR2-WT (a-d). There were no differences between PAR2-WT and PAR2-KO IP3R expression (a-h). White line at bottom right of images is a scale bar = 10 μm. Magnification 960 x.

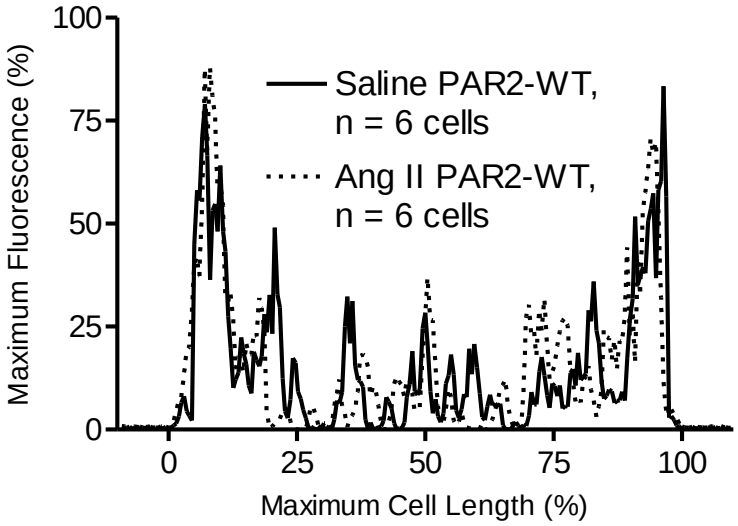

Figure 22. Spatial distribution of IP3R in PAR2-WT endothelial cells with and without endothelial dysfunction. Isolated and fixed endothelial cells from saline or angiotensin II treated PAR2-WT and PAR2-KO were incubated with primary antibody specific for IP3R. FITC, fluorescein isothiocyanate fluorescent conjugate secondary antibody was detected at 498 nm under line scan confocal microscopy. The confocal plane presented is from the center of a z-stack series of images. Lines are means, n = 6 cells, 4 animals per group. IP3R staining is congruent with the subplasmalemmal region of endothelial cells. A lower level of IP3R expression was noted throughout the cell. There was no difference in the distribution of IP3R fluorescent signal between PAR2-WT and PAR2-KO treatment groups (not shown).

Expression of downstream Ca^{2+}-signaling targets: eNOS, SK_{ca} and IK_{ca}

We also assessed the distribution of several known Ca^{2+}-sensitive downstream targets of PAR2 signals within the endothelial cells from mice with and without endothelial dysfunction. Immunofluorescence staining for eNOS (Figure 23 and Figure 24), but not SK_{ca} (Figure 25) or IK_{ca} (Figure 26), was differently distributed in Ang II treated cells than in control cells. Specifically, we found the spread of immunofluorescence for eNOS from the peripheral edges to the centre of the cells was reduced in Ang II treated cells compared to controls (Figure 24). The expression of both SK_{ca} and IK_{ca} appeared as discrete loci of fluorescence that were discontinuous around the peripheral edges of endothelial cells. Immunofluorescence staining for SK_{ca} and IK_{ca} (Figure 27) in Ang II treated cells were unchanged compared to saline controls. There was no effect of the *par*2 genotype on the expression of the downstream Ca^{2+}-signaling target proteins.

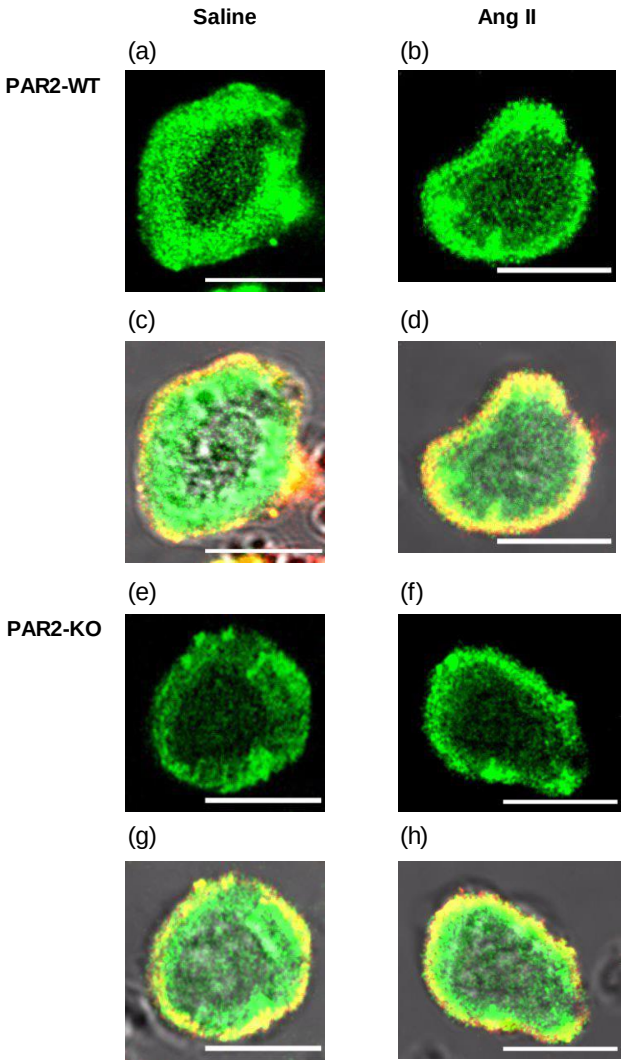

Figure 23. eNOS immunocytochemistry staining from mesenteric endothelial cells across *par*2 genotypes and treatment groups. Isolated and fixed mesenteric endothelial cells from saline (a, c, e, g) and angiotensin II (b, d, f, h) treated PAR2-WT (a-d) and PAR2-KO (e-h) were probed with primary antibody for eNOS and PECAM-1. Secondary antibody labeling with Texas Red (PECAM-1, red) and FITC, fluorescein isothiocyanate, (eNOS, green) reveal the location of eNOS and PECAM-1 proteins in each group. Top panels (a, b, e, f) are FITC channel images showing the location of eNOS signal only; bottom panels (c, d, g, h) are white light, FITC and Texas Red composite channel images showing the location of gross cellular structures, eNOS and PECAM-1. Yellow signal indicates colocalization of eNOS and PECAM-1. Acellular structures with red, green or yellow fluorescent signals are debris that have absorbed secondary antibody. Angiotensin II treatment reduced PAR2-WT eNOS penetration by 30% and PAR2-KO eNOS expression by 29%, $p < 0.001$. *par*2 genotype had no effect on eNOS fluorescent signal distribution. White line at bottom right of images is a scale bar = 10 µm. Magnification 960 x.

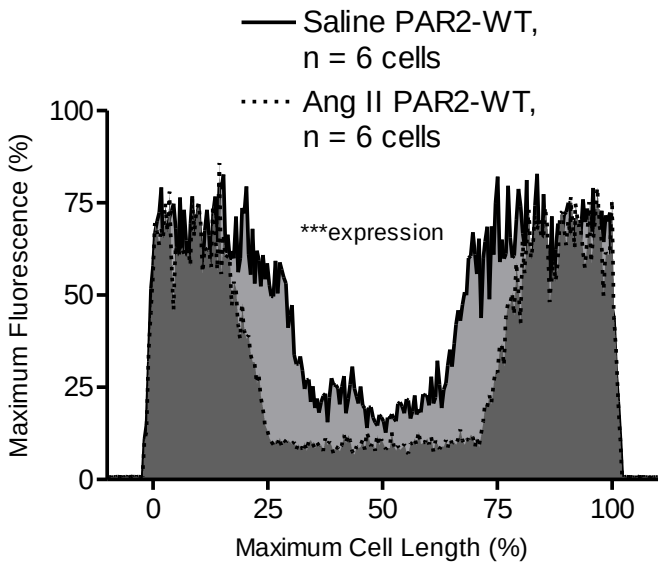

Figure 24. Spatial distribution of eNOS in PAR2-WT endothelial cells with and without endothelial dysfunction. Isolated and fixed endothelial cells from saline or angiotensin II treated PAR2-WT and PAR2-KO were incubated with primary antibody specific for eNOS. FITC, fluorescein isothiocyanate fluorescent conjugate secondary antibody was detected at 498 nm under line scan confocal microscopy. The confocal plane presented is from the center of a z-stack series of images. Lines are means, n = 6 cells, 4 animals per group. eNOS staining was expressed continuously at the periphery and penetrated into the cell. Lower density fluorescence from eNOS FITC secondary antibody was observed throughout the center of cells. Solid line with light grey fill is the integral of area under the curve from saline treated PAR2-WT. Hatched line with dark grey fill is the integral of area under the curve from angiotensin II treated PAR2-WT. Integrals were calculated as (Maximum Fluorescence (%) x Maximum Cell Length (%)): 5072 ± 43 saline PAR2-WT; 3561 ± 35 Ang II PAR2-WT. $^{***}p < 0.001$, Integral of eNOS expression, Ang II PAR2-WT vs saline PAR2-WT. PAR2-KO immunocytochemistry revealed that there was no effect of the *par*2 genotype on the distribution of eNOS staining (not shown).

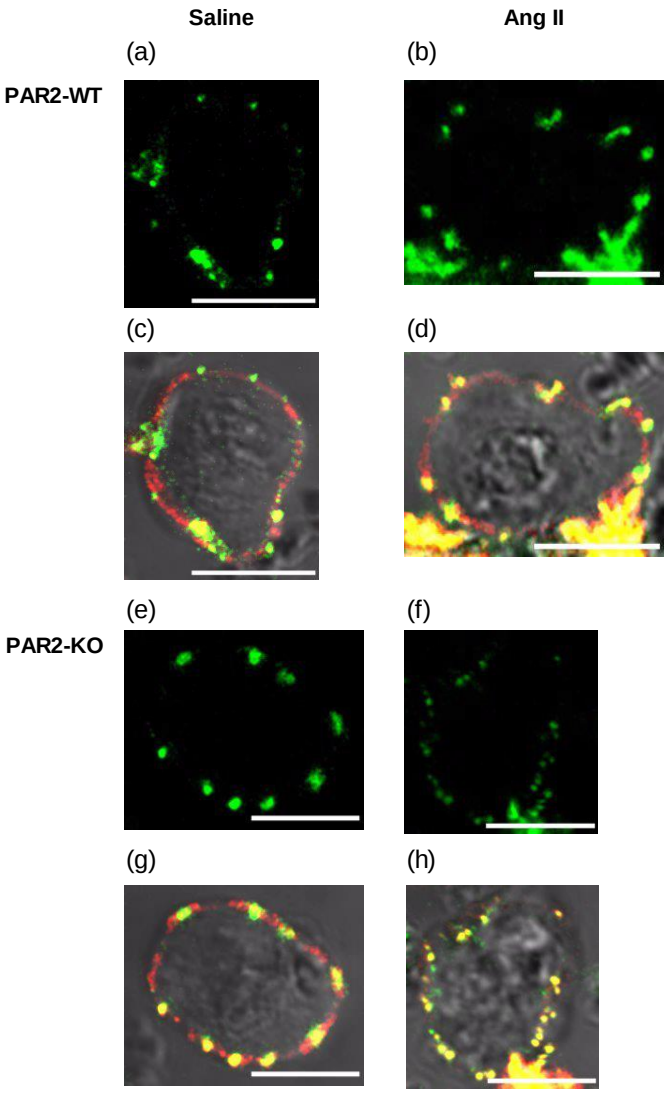

Figure 25. SK_{ca} immunocytochemistry staining from mesenteric endothelial cells across *par*2 genotypes and treatment groups. Isolated and fixed mesenteric endothelial cells from saline (a, c, e, g) and angiotensin II (b, d, f, h) treated PAR2-WT (a-d) and PAR2-KO (e-h) were probed with primary antibody for SK_{ca} and PECAM-1. Secondary antibody labeling with Texas Red (PECAM-1, red) and FITC, fluorescein isothiocyanate, (SK_{ca}, green) reveal the location of SK_{ca} and PECAM-1 proteins in each group. Top panels (a, b, e, f) are FITC channel images showing the location of SK_{ca} signal only; bottom panels (c, d, g, h) are white light, FITC and Texas Red composite channel images showing the location of gross cellular structures, SK_{ca} and PECAM-1. Yellow signal indicates colocalization of SK_{ca} and PECAM-1. Acellular structures with red, green or yellow fluorescent signals are debris that have absorbed secondary antibody. Angiotensin II treatment and *par*2 genotype had no effect on SK_{ca} distribution. White line at bottom right of images is a scale bar = 10 µm. Magnification 960 x.

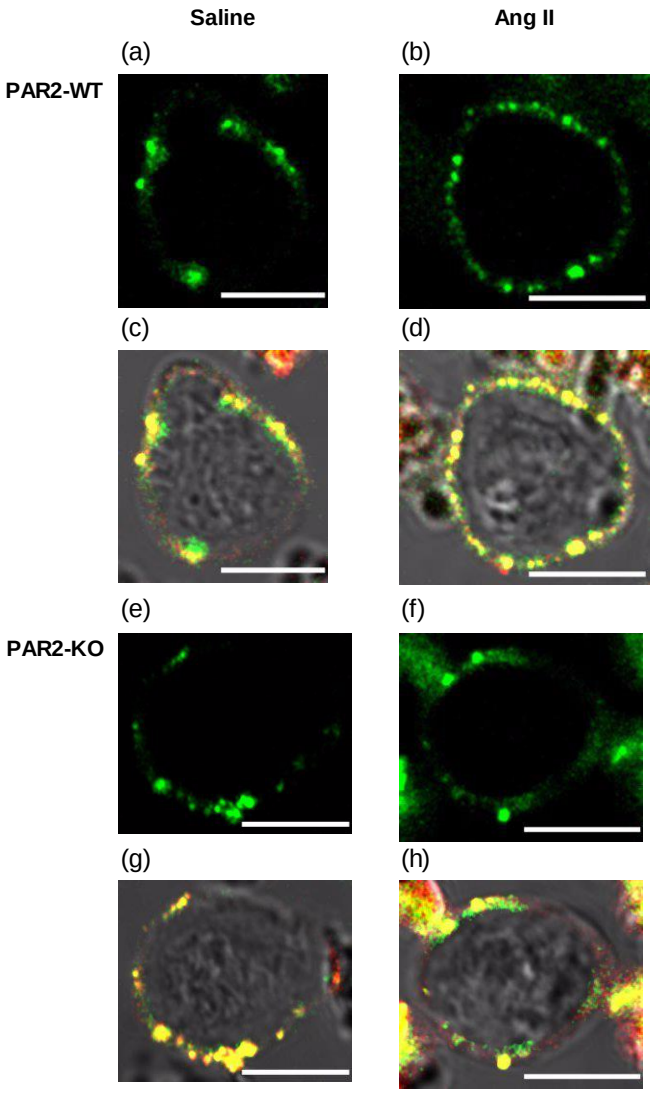

Figure 26. IK_{ca} immunocytochemistry staining from mesenteric endothelial cells across *par*2 genotypes and treatment groups. Isolated and fixed mesenteric endothelial cells from saline (a, c, e, g) and angiotensin II (b, d, f, h) treated PAR2-WT (a-d) and PAR2-KO (e-h) were probed with primary antibody for IK_{ca} and PECAM-1. Secondary antibody labeling with Texas Red (PECAM-1, red) and FITC, fluorescein isothiocyanate, (IK_{ca}, green) reveal the location of IK_{ca} and PECAM-1 proteins in each group. Top panels (a, b, e, f) are FITC channel images showing the location of IK_{ca} signal only; bottom panels (c, d, g, h) are white light, FITC and Texas Red composite channel images showing the location of gross cellular structures, IK_{ca} and PECAM-1. Yellow signal indicates colocalization of IK_{ca} and PECAM-1. Acellular structures with red, green or yellow fluorescent signals are debris that have absorbed secondary antibody. Angiotensin II treatment and *par*2 genotype had no effect on IK_{ca} distribution. White line at bottom right of images is a scale bar = 10 µm. Magnification 960 x.

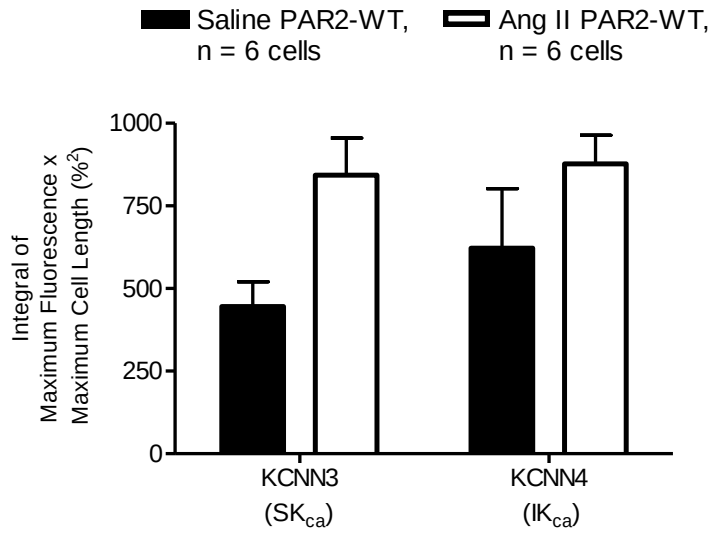

Figure 27. Expression of KCNN3 (SK_{ca}) and KCNN4 (IK_{ca}) in PAR2-WT endothelial cells with and without endothelial dysfunction. Isolated and fixed endothelial cells from saline or angiotensin II treated PAR2-WT and PAR2-KO were incubated with primary antibody specific for SK_{ca} or IK_{ca}. FITC, fluorescein isothiocyanate fluorescent conjugate secondary antibody was detected at 498 nm under line scan confocal microscopy. The confocal plane presented is from the center of a z-stack series of images. Bars are means ± S.E.M. n = 6 cells, 4 animals per group. SK_{ca} and IK_{ca} expression was observed as discrete regions of fluorescence congruent with the plasma membrane and did not penetrate into the cell. For comparison: peripheral line-scan analysis integrated the fluorescence of secondary antibody (FITC) with the circumference of cells. There was no effect of *par*2 genotype (not shown) or angiotensin II treatment on SK_{ca} or IK_{ca} staining.

Chapter 4: Discussion

4.1 Main findings

This study is the first to investigate the Ca^{2+}-signals elicited by PAR2 activation with and without endothelial dysfunction in single isolated endothelial cells from small caliber arteries. The first hypothesis tested the effects of Ang II treatment on PAR2 and muscarinic –induced Ca^{2+}-events in murine small caliber ECs. The primary finding is that endothelial dysfunction attenuates muscarinic but not PAR2-mediated Ca^{2+}-events. Ang II treatment did not change PAR2 Ca^{2+}-event CRC variables compared to controls, yet CRCs from M_3 Ca^{2+}-event numbers were reduced in Ang II-treated mice. Analysis of the Ca^{2+}-events uncovered two separate populations of Ca^{2+}-transients in the isolated ECs. These events are referred to as peripheral (i.e. near the plasma membrane) and central (i.e. in the center of the cell) Ca^{2+}-transients.

The second hypothesis tested if IP3R and TRPV channels contribute to the Ca^{2+}-events observed in our ECs. I found that the Ca^{2+}-events of both events was entirely abolished by IP3R inhibitor XeC, but less attenuated by TRPV channel inhibitor RR. These results show that both peripheral and central Ca^{2+}-transients are primarily dependent on IP3R channel activity, and less on Ca^{2+}-entry through TRPV channels.

The third hypothesis used immunocytochemistry to test if protein expression and distribution of PAR2 and IK_{ca} was increased in PAR2-WT with endothelial dysfunction. The third hypothesis also tested if eNOS expression was attenuated in response to experimental endothelial dysfunction. We found that the expression and distribution of PAR2, PECAM-1, IP3R, SK_{ca} and IK_{ca} were unchanged across treatment groups. Endothelial dysfunction attenuated the expression of eNOS in both *par*2 genotypes. Interestingly, the study revealed two separate pools of IP3R expression in our ECs, which may account for the differences between peripheral

and central Ca^{2+}-transients. Collectively the data suggest that PAR2 Ca^{2+}-signaling is preserved in our model of endothelial dysfunction. Yet an attenuation of muscarinic signaling was detected under the same conditions.

4.2 Main limitations of the experimental design and techniques

The main limitations to the experimental design and techniques used in this thesis include: use of fluorescent indicator dye Fluo-4 without another reference standard, the effect of out-of-plane Ca^{2+}-events on confocal measurements, endothelial cell sensitivity to the laser used for imaging and only measuring two GPCR responses (PAR2 and M_3). A disadvantage to the use of fluorescent indicators (Fluo-4) include challenges in the standardization (Takahashi et al., 1999). Furthermore, fluorescent molecules have incomplete affinities for $[Ca^{2+}]_i$. An inherent limitation to the general use of confocal imaging (both line scan and 2D) includes the possible acquisition of Ca^{2+}-events outside the confocal plane of focus. Such events can radiate into the confocal plane and create artifacts or increased background noise. We expect these effects to be minimized in our preparation because ECs had a relatively small thickness of 4 μm, where the confocal plane was 25% of this thickness at 1 μm. In addition F/F_0 image division for each Ca^{2+}-event analyzed removed most of the background noise during the events. Our isolated ECs were sensitive to the 488 nm laser excitation. After exposures of more than 10 s cells were observed to form vacuoles and leak fluorescent contents into the surrounding medium. Therefore all exposures were limited to 10 s or less. It is possible that not all forms of Ca^{2+}-event phenomena were captured due to the short exposure times. Finally we only measured responses to two GPCRs, PAR2 and M_3. It is possible that the Ang II-induced attenuation of M_3-mediated Ca^{2+}-events would not have been observed for another GPCR, like the bradykinin B_2 receptor. A more

comprehensive evaluation of other endothelial cell GPCR Ca^{2+}-events will allow for a listing of pathways that are preserved or attenuated by Ang II-induced endothelial cell dysfunction.

4.3 Identification of two distinct Ca^{2+}-transient types in isolated small caliber arterial endothelial cells

In this study I resolved the Ca^{2+} -signals elicited by PAR2 activation at the single EC level. It is well established that PAR2 agonists cause transient increases in global cytosolic $[Ca^{2+}]_i$ (Al-Ani et al., 1999a; Kanke et al., 2009), but previous studies have relied on cells in cultured conditions and intracellular Ca^{2+} measuring techniques with limited resolution. We obtained new understanding of PAR2 Ca^{2+}-signals by applying 2D spinning disk confocal fluorescence imaging techniques on freshly isolated single ECs. In our EC preparations, Ca^{2+} transients were a composition of two distinct types of events. PAR2 agonist 2fly increased the activity of both types of events in a concentration-dependent manner. The temporal and spatial characteristics of each event type were the same at baseline and when elicited by agonists, which indicates that PAR2 increases the open probability of Ca^{2+} channels. Chronic infusion with Ang II, *par*2 genotype and choice of agonist did not influence the kinetic or dynamic characteristics of either event.

The first type of event, referred to as peripheral Ca^{2+}-transients, originated just below the level of the EC plasma membrane. We characterized these events as sporadic, with no repetitive firing pattern at individual sites (i.e. no measurable frequency). The peripheral Ca^{2+}-transients we describe have similar properties to *Xenopus* oocyte EC 'puffs' described by other researchers (Sun et al., 1998; Thomas et al., 2000; Yao et al., 1995). These 'puffs' have also been described *in situ* in murine mesenteric artery EC tubes (Socha et al., 2012). It is important to note that variance in analytic techniques across laboratories make comparison of amplitude (F/F_o) data

challenging. With this variability in image analysis throughout the literature it is possible that the same cytosolic $[Ca^{2+}]_i$ could result in two different F/F_o. Nevertheless, our isolated EC peripheral transients shared IP3R CRU origin with the described *in situ* EC 'puffs' (Socha et al., 2012). These similarities suggest that the peripheral Ca^{2+}-transients observed by us in isolated ECs are possibly translatable to intact vessels.

The second type of event, central Ca^{2+}-transients, were observed near the cell center at the edge of the nucleus. These events typically arose from single loci, generating a measureable frequency of large Ca^{2+}-releases. Ca^{2+}-events similar to our central transients have been described in the literature as 'pulsars' (Ledoux et al., 2008; Nausch et al., 2012). However, 'pulsars' have been identified as originating near EC projections in the internal elastic lamina of small caliber arteries *in situ* (Dora et al., 2008; Ledoux et al., 2008). Much like our central Ca^{2+}-transients in isolated ECs, pulsars have a rapid decay that is ~ 69% of the t_{rise}, frequency and fixed release locus within the EC (Ledoux et al., 2008). An explanation for the different subcellular locations of our central Ca^{2+}-transients and pulsars could be the EC isolation technique. Isolation of the ECs disrupts the *in situ* 3D structure of the internal elastic lamina projections and the underlying ER. I isolated the central Ca^{2+}-transients as originating from the cell center by detecting a focal point of Fluo-4 signal during event initiation. This focal point (less than 5 pixels in diameter) was selected prior to image smoothing to improve localization of events. I expect that if central Ca^{2+}-transients originated in an out-of-focus plane that they would have partially diffused upon entering the confocal plane and would not have a concentrated fluorescent origin.

Aside from their oscillatory nature, central transients had nearly double the amplitude and 150% the area of their peripheral counterpart. Even though greater $[Ca^{2+}]_i$ was released by the

central transients, the half-life was nearly 50% the duration of peripheral transients. This may indicate that SERCA pumps are in higher density or working with greater capacity at the centrally located ER. Indeed, SERCA has been uncovered as a major player in the maintenance of oscillatory Ca^{2+}-event activity in ECs (Mumtaz et al., 2011). In rat artery ECs the initiation of Ca^{2+}-waves via 'puff'-like' events was found to be more reliant on inositol triphosphate release, while oscillatory Ca^{2+}-releases were intimately dependent on SERCA activity (Mumtaz et al., 2011). SERCA3 is the main inwardly-rectifying ER Ca^{2+}-pump in the endothelium (Khan et al., 2000). Yet the discovery of other vascular endothelial SERCA subtypes such as SERCA2b (Mountian et al., 1999) and the identification of three IP3R isoforms (Grayson et al., 2004) may account for the observation of multiple Ca^{2+}-transient types.

The literature describes cell wide Ca^{2+}-waves that propagate within and between ECs (Burdyga et al., 2003; Mumtaz et al., 2011; Uhrenholt et al., 2007). It should be noted that we did not observe any propagating Ca^{2+}-waves. Current research describes these Ca^{2+}-waves as typically initiating from 'puffs' or subplasmalemmal Ca^{2+}-events (Isshiki et al., 2004). Experiments in other laboratories report EC Ca^{2+}-waves captured over 1 min exposures to lasers, while our exposures to argon-gas laser pulses were 10 s in duration. We found that our ECs began to vacuolize and die after $\geq$ 10 s exposure to the laser on low-intensity settings. It is possible that our isolation technique sensitized the ECs to reactive oxygen species generation during Fluo-4 laser excitement. Indeed, the maximum frame rate for Ca^{2+}-event acquisition was 30 fps, it is possible that events occurring under $1/30^{th}$ s would go unnoticed. The scope of such rapid events includes reports of some subplasmalemmal events (Isshiki et al., 2004) or blips (Cheng et al., 2008). Still our work indicates that 2fly can elicit isolated Ca^{2+}-transients that are similar to those described by classical M_3 receptor activation of vessels *in situ*. The finding that

choice of agonist does not alter the dynamic or kinetic properties of Ca^{2+}-events suggests that it is the number, and not the characteristics, of peripheral and central Ca^{2+}-transients that shape vascular responses in small caliber arteries.

4.4 PAR2-mediated Ca^{2+}-events is protected from endothelial dysfunction

Ca^{2+}-signals elicited by PAR2, but not by acetylcholine, are protected from endothelial dysfunction in our model. I found that both peripheral and central PAR2-mediated Ca^{2+}-transients' site recruitment and firing rates were preserved in Ang II treated PAR2-WT ECs. We report 'classic' characteristics of endothelial dysfunction, described in blood vessels of the Ang II infusion model (Chia et al., 2011), are present in single ECs. Specifically, we show that acetylcholine elicits Ca^{2+}-signals in ECs from PAR2-WT controls that are decreased in cells from Ang II treated mice. This finding aligns with previous studies with intact small caliber arteries (Chia et al., 2011), where PAR2 dependent responses in endothelial cells were protected from endothelial dysfunction caused by Ang II. In reference to its potency and efficacy in intact tissues, the pD_2 values for the activation of both PAR2 Ca^{2+}-events (peripheral, 7.8 and central, 7.7) correlate with published pD_2 values for vasodilation of small caliber arteries (Kagota et al., 2011; McGuire et al., 2007). It appears that the single endothelial cell measurements of Ca^{2+}-events replicate pharmacological action of the intact tissues.

Other studies suggest numerous mechanisms, including those originating in both endothelial and non-endothelial cells, that contribute to endothelial dysfunction (Fernandez-Alfonso et al., 2013; Kagota et al., 2011; Kanikarla-Marie et al., 2014). Previous studies on ApoE (-/-) mice demonstrate that selective inhibition of NO synthase attenuates ACh, but not

SLIGRL-induced relaxation of murine mesenteric arteries (Beleznai et al., 2011). This and other work (McGuire JJ et al., 2002; McLean et al., 2002) suggests that PAR2 can maintain hyperpolarization of the vasculature during endothelial dysfunction, leading to preserved vasodilation. Our data indicate that this level of PAR2 signal transduction maintenance may originate at the level of, or earlier than, endothelial Ca^{2+}-events. Banquet *et al.,* (2011) have suggested that attenuations to muscarinic receptor response during endothelial dysfunction may originate prior to eNOS phosphorylation at Ser(1177) (Banquet et al., 2011). Due to the protection of PAR2, but the reduction in M_3 receptor-mediated Ca^{2+}-signaling, our study provides support for the notion that an upstream target closer to receptor activation is a significant site of lesion for muscarinic receptor signals in ECs.

The effect of PAR2 agonist was to increase the open probability of Ca^{2+} channels, specifically IP3R which were inhibited by XeC. In the isolated EC preparations PAR2 agonist 2fly has a greater capacity for increasing recruitment of Ca^{2+} channels than ACh. Even in cells from PAR2-WT, ACh recruited half as many Ca^{2+} channels as 2fly. It has been reported previously that the maximal endothelium-mediated hyperpolarization of vascular smooth muscle by PAR2 agonist was greater than by ACh in intact tissues (McGuire et al., 2004a). This again demonstrates the direct translation of our single cell data to *in situ* whole vessel studies. On one hand, the single cell level provides cellular specificity for investigation. On the other hand, the single cell level restricted the scope of our study to endothelial cells alone. Our freshly isolated Ang II treated EC model may reveal other targets of endothelial dysfunction resistance. Such targets may have potential for *de novo* pharmaceutical development (i.e. to reverse and/or attenuate dysfunction).

4.5 PAR2-mediated endothelial Ca^{2+}-transients depend on IP3R and TRPV

Our investigation of the molecular nature of Ca^{2+}-release in the ECs revealed that both peripheral and central transients were completely dependent on IP3R channels, while they only partially relied on Ca^{2+}-entry across TRPV channels. Blocking IP3R could entirely account for Ca^{2+}-signals elicited by ACh and 2fly. Experiments using IP3R inhibitor XeC completely abolished PAR2 and M_3 receptor-mediated Ca^{2+}-events in ECs. We found a TRPV sensitive inhibition of Ca^{2+}-signals elicited by ACh and 2fly, which may be produced by the cooperative activity of TRPV4 sparklets in endothelial cells. Sparklets were observed under conditions of IP3R block in whole tissues (Sonkusare et al., 2012). In various cell types and cell lines under cultured conditions, Ca^{2+} signals of different magnitude are explained by incrementally higher levels of inositol triphosphate, leading to progressive recruitment of local single IP3R channels (blips), close-by multiple channels (puffs), and then globally propagating (waves) channel activation (Foskett et al., 2007).

PAR2 (Chen et al., 2011; Poole et al., 2013) and M_3 receptor (Aure et al., 2010; Sonkusare et al., 2012) activation sensitizes TRPV channels leading to rises in intracellular $[Ca^{2+}]_i$. Specifically, sensitization of TRPV1 and TRPV4 has been correlated to PAR2 signaling in non-endothelial cells (Chen et al., 2011). Though our technique did not isolate individual EC sparklets as described in the literature, a degree of sensitivity to TRPV inhibitor RR was still observed. GPCR sensitization of TRPV Ca^{2+}-influx channels may play a role in the filling of intracellular Ca^{2+}-stores (Ma et al., 2010) or initiate Ca^{2+}-events which underpin vascular hyperpolarization (Sullivan et al., 2013). RR reduced the recruitment, but not the firing rates of Ca^{2+} channels; this supports the notion of an indirect effect of RR on IP3R-mediated Ca^{2+}-release. RR inhibition of TRPV could potentially inhibit Ca^{2+}-stores/handling which results in a lower capacity for Ca^{2+}-release once IP3R were activated.

4.6 Expression of PAR2 and downstream target proteins

Our immunocytochemistry experiments reveal two pools of fluorescence signal for PAR2 and IP3R. The more peripheral pool of expression is near the plasma membrane, defined by PECAM-1 fluorescence labelling. A second pool of both proteins, albeit lower in fluorescence signal, is heterogeneous throughout the cell center. Studies with vascular and cardiac cell types found nuclear membranes express seven transmembrane GPCRs (i.e. AT1 and ET-1), which can be activated by ligands to elicit Ca^{2+}-signals (Bkaily et al., 2003; Gangopadhyay et al., 2010). Interior cell expression of PAR2 has been described in RPC lines, a model of retinal pigment cells (Zhu et al., 2006). In murine lung fibroblast cell culture, antibody H99 bound ectopic PAR2 green fluorescent protein is congruent with cell nuclei (Adams et al., 2012). Others who have used the PAR2 polyclonal antibody B5 used in this study have not reported central staining in murine neurons (Kelso et al., 2006). It is possible that we are the first to present central cellular expression of PAR2 in freshly isolated murine mesenteric ECs, or that the central fluorescence is an artifact of our methods (despite a lack of PAR2 fluorescent signal in PAR2-KO). All three IP3R isoforms are heterogeneously expressed in ECs, with IP3R1 expression predominating around the plasma membrane (Grayson et al., 2004). The distinct pools of IP3R expression may explain the different kinetic characteristics of peripheral versus central Ca^{2+}-events. Based on these results we propose a cooperative relationship between GPCRs and IP3R pools that may contribute to the differences in recruitment of CRUs.

Endothelial dysfunction did not change PAR2, IP3R, SK_{Ca} or IK_{Ca} expression in ECs; however it did reduce the distribution of eNOS. Research showed that eNOS is down regulated during endothelial dysfunction in mesenteric arteries (Caliman et al., 2013; Mukohda et al., 2013). Our results show that the penetration of eNOS expression from the level of the plasma

membrane toward the cell center is reduced with endothelial dysfunction. The integral of eNOS antibody fluorescence in experimental ECs was reduced by 29%, suggesting a global reduction due to Ang II infusion. Our anti-eNOS antibody was not specific for the phosphorylated protein. Therefore we cannot be certain that our observations in Ang II treated mice strictly correlate to a reduction of phosphorylated (active) eNOS. Future studies should compare the ratio of active to total eNOS in vascular endothelial cells from Ang II treated mice. We did not compare the distribution of eNOS following activation of PAR2 or M_3. For upcoming studies it would be informative to compare the data from Figure 24 to endothelial cell immunocytochemistry after exposure to 2fly or ACh.

In small caliber arteries, key studies have suggested that expression of IP3R are distributed near the downstream targets of their Ca^{2+}-signals: SK_{Ca} and IK_{Ca} (Dora et al., 2008; Sandow et al., 2006). SK_{Ca} was found to be widely distributed on the cell surface whereas IK_{Ca} was localized to MEGJs (Dora et al., 2008). These data infer the potential for different pools of IP3R to associate with Ca^{2+}-sensitive targets. Our immunocytochemistry signals of SK_{Ca} and IK_{Ca} appear similar and are found in discrete bundles of fluorescence at the EC plasma membrane. It is possible that these focal points of intense K_{Ca} expression correspond to the former locations of endothelial projections before the mesenteric cells were enzymatic dispersed. Further investigation with Cx37, 40 and 43 staining (Saliez et al., 2008; Sandow et al., 2006) may be useful to determine if "islands" of potassium channel expression are associated with the location of MEGJs hemi-channels.

4.7 Conclusion

Our study is the first to examine the kinetics and dynamics of PAR2-mediated Ca^{2+}-events in freshly isolated endothelial cells. We have described methods that reliably produce

viable endothelial cells from resistance vasculature in mice, whose Ca^{2+}-signaling is comparable to *in situ* preparations. Taken together our data suggest that PAR2 Ca^{2+}-signaling is preserved in endothelial dysfunction that results in a selective lesion to the activation of IP3R by ACh. This study has also demonstrated that EC GPCRs, PAR2 and M_3 receptor , trigger Ca^{2+}-events from IP3R which are dependent on TRPV activity.

The preserved PAR2 activation of IP3R mediated Ca^{2+}-signals in small caliber arteries may provide an endothelial dysfunction resistant pathway of EC-VSMC communication. The comparable EC_{50} values for Ca^{2+} and isometric tension CRCs indicate that our model of single cell endothelial dysfunction is translatable to physiological models like diabetes. Our work on single cell PAR2 Ca^{2+}-events provide a foundation for future studies combining electrophysiology (electrical potential) of small caliber arteries mounted in myographs (mechanical forces) on confocal microscopes (Ca^{2+}-signaling). Simultaneous experiments following PAR2 activation may establish a more holistic understanding for the preservation of PAR2 signaling in endothelial dysfunction.

Chapter 5: Appendices

5.1 Appendix A

#	Primer	Sequence (5' to 3')	T_m ($^{\circ}C$)
1	IMR5332 (Mutant)	GCCAGAGGCCACTTGTGTAG	64.5
2	IMR7419 (Forward)	TCAAAGACTGCTGGTGGTTG	60.4
3	IMR7420 (Reverse)	GGTCCAACAGTAAGGCTGCT	62.5

Product from (1) and (2) = 198 bp fragment → MUT→ *neomycin* gene present

Product from (2) and (3) = 345 bp fragment → WT→ *F2rL*1, *par*2, gene exon 2 present

Table 5. Oligonucleotide primer sets used in the genotyping of mice. T_m represents the melting temperature for the primers. Modified from McGuire Laboratory, 2013.

5.2 Appendix B

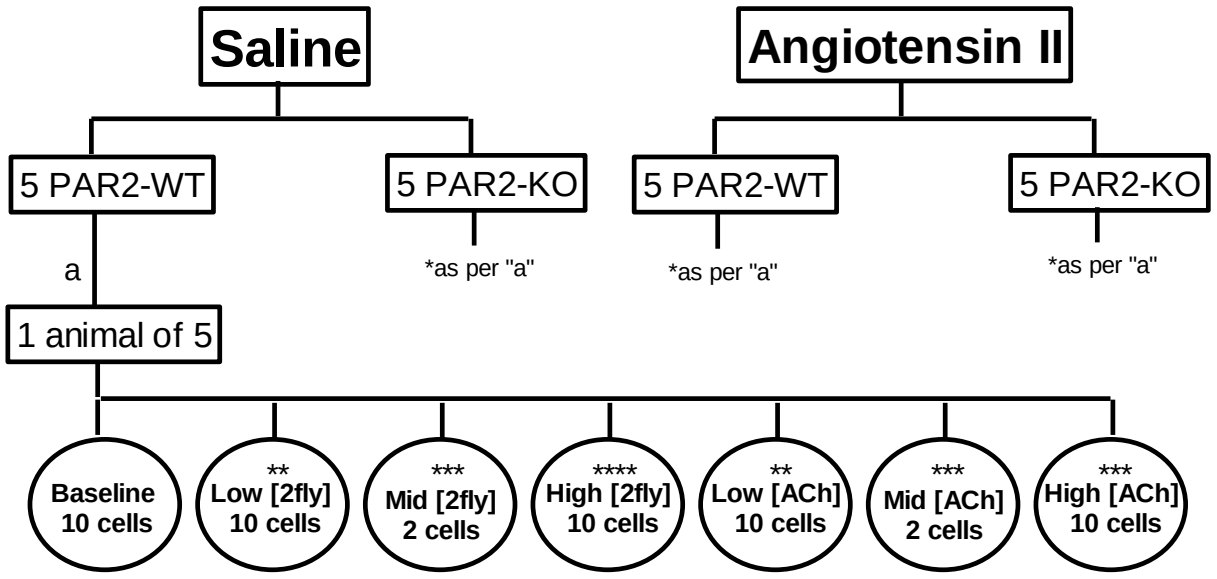

* Each treatment/genotype group underwent the same protocol as per line "a" from saline treated PAR2-WT

** Low [2fly] indicates concentrations between 0.1 nM and 10 nM
Low [ACh] indicates concentrations between 1 nM and 100 nM

*** Mid [2fly] indicates concentration of 30 nM
Mid [ACh] indicates concentration of 300 nM
2 cells from each animal were taken for each mid [2fly] and [ACh] measurement. 10 cells total from each group were used to create mid points in 2fly and ACh concentration response curves representing all animals.

**** High [2fly] indicates concentrations between 100 nM and 3 μM
High [ACh] indicates concentrations between 1 μM and 30 μM

Figure 28. Protocol for 2fly and ACh calcium signaling concentration response curve experiments. Saline and angiotensin II treated mice were processed as per methods section 2.7. 2fly, 2-furoyl-LIGRLO-amide; ACh, acetylcholine. Baseline, no agonist present.

5.3 Appendix C

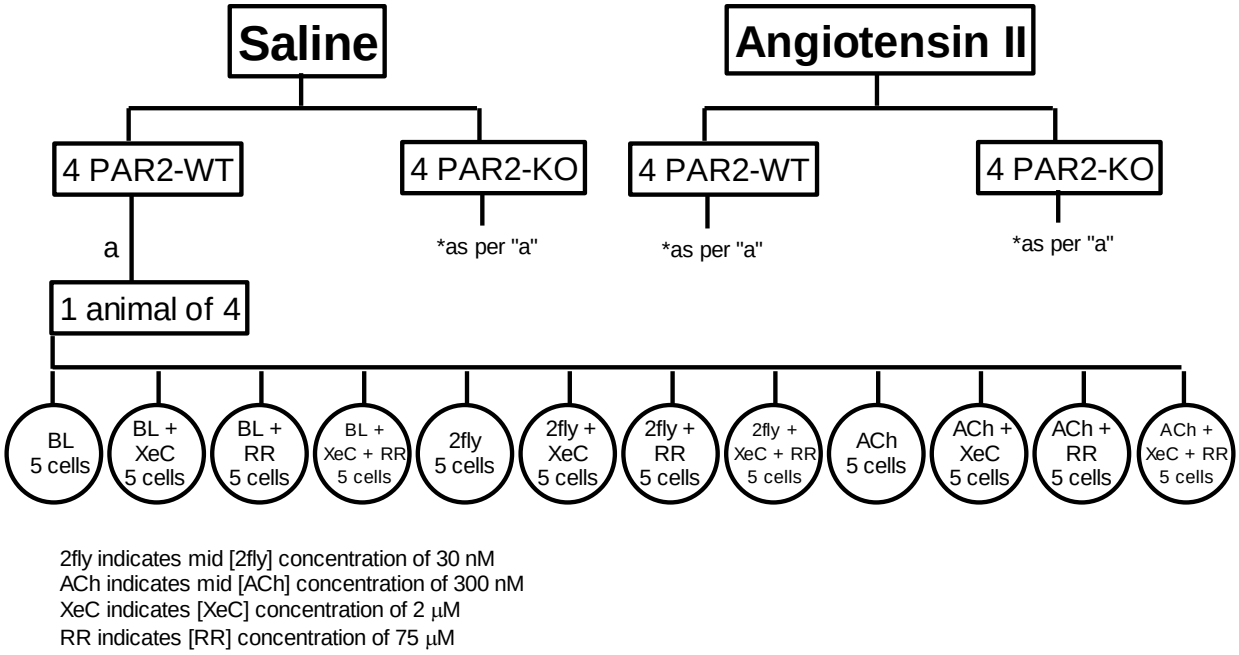

Figure 29. Protocol for IP3R and TRPV inhibitor experiments. Saline and angiotensin II treated mice were processed as per methods section 2.7. Inhibitors of IP3R: XeC, xestospongin-c; and TRPV channels: RR, ruthenium red were used to examine the contribution of these proteins to endothelial calcium signaling. The effects of these inhibitors were examined without agonist present: BL, baseline; and in the presence of PAR2 agonist: 2fly, 2-furoyl-LIGRLO-amide; and with M_3 agonist: ACh, acetylcholine.

5.4 Appendix D

Supplemental Data

Agonist	Treatment	Genotype	n	pD_2 (M)	E_{max}[c] (Ca^{2+}-release sites/cell)	Hill slope
2fly	Saline	PAR2-WT	5	7.8 ± 0.1	12.3 ± 0.4	0.9 ± 0.1
		PAR2-KO	5	N/A	N/A	N/A
	Ang II	PAR2-WT	5	7.2 ± 0.1	11.7 ± 0.5	0.9 ± 0.2
		PAR2-KO	5	N/A	N/A	N/A
ACh	Saline	PAR2-WT	5	6.8 ± 0.1	6.9 ± 0.3[c]	1.1 ± 0.2
		PAR2-KO	5	6.9 ± 0.1	7.2 ± 0.3	1.0 ± 0.2
	Ang II	PAR2-WT	5	6.8 ± 0.1	5.4 ± 0.3[cc]	0.9 ± 0.3
		PAR2-KO	5	6.7 ± 0.1	5.6 ± 0.2[c]	1.1 ± 0.2

Table S1. Characteristics for 2fly and acetylcholine Ca^{2+}-event concentration response curves of angiotensin II and saline treated mice. Values are means ± S.E.M., n = number of mice per curve, 10 cells per point. 2fly, 2-furoyl-LIGRLO-amide; ACh, acetylcholine. Variables were determined by curve fitting 2fly and acetylcholine-induced Ca^{2+}-event recruitment data from PAR2-WT and PAR2-KO to a 4 parameter logistic curve. Data were analyzed by 2 way ANOVA (treatment x genotype) followed by Bonfferoni post-hoc testing. [c]$p < 0.001$, E_{max}, Ang II PAR2-WT and PAR2-KO vs saline PAR2-WT and PAR2-KO. [c]$p < 0.001$, E_{max}, saline and Ang II PAR2-WT 2fly vs saline and Ang II PAR2-WT ACh.

Agonist	Treatment	Genotype	n	pD_2 (M)	E_{max}[ab] (Ca^{2+}-event/site/s)	Hill slope[b]
2fly	Saline	PAR2-WT	5	8.4 ± 0.1	0.29 ± 0.01	1.8 ± 0.6
		PAR2-KO	5	N/A	N/A	N/A
	Ang II	PAR2-WT	5	8.5 ± 0.1	0.28 ± 0.01	1.6 ± 0.4
		PAR2-KO	5	N/A	N/A	N/A
ACh	Saline	PAR2-WT	5	6.9 ± 0.1	0.32 ± 0.01	0.8 ± 0.2[b]
		PAR2-KO	5	7.2 ± 0.1	0.29 ± 0.01	0.9 ± 0.3
	Ang II	PAR2-WT	5	6.8 ± 0.2	0.24 ± 0.02[b]	0.6 ± 0.2[b]
		PAR2-KO	5	6.9 ± 0.2	0.22 ± 0.01[a]	1.0 ± 0.3

Table S2. Characteristics for 2fly and acetylcholine Ca^{2+}-event site firing rate concentration response curves of angiotensin II and saline treated mice. Values are means ± S.E.M., n = number of mice per curve, 10 cells per point. 2fly, 2-furoyl-LIGRLO-amide; ACh, acetylcholine. Variables were determined by curve fitting 2fly and acetylcholine-induced Ca^{2+}-event site firing rate data from PAR2-WT and PAR2-KO to a 4 parameter logistic curve. Data were analyzed by 2 way ANOVA (treatment x genotype) followed by Bonfferoni post-hoc testing. [b]$p < 0.01$, E_{max}, Ang II PAR2-WT vs saline PAR2-WT; [a]$p < 0.05$, E_{max}, Ang II PAR2-KO vs saline PAR2-KO. [b]$p < 0.01$, Hill slope, saline and Ang II PAR2-WT 2fly vs saline and Ang II PAR2-WT ACh.

Agonist	Inhibitor	Treatment	Genotype	n	Ca^{2+}-release sites/cell
Baseline	Control	Saline	PAR2-WT	10	0.5 ± 0.3
			PAR2-KO	10	0.3 ± 0.2
		Ang II	PAR2-WT	10	0.5 ± 0.3
			PAR2-KO	10	0.3 ± 0.2
	XeC	Saline	PAR2-WT	10	0.1 ± 0
			PAR2-KO	10	0.5 ± 0.2
		Ang II	PAR2-WT	10	0.3 ± 0.2
			PAR2-KO	10	0.2 ± 0.1
	RR	Saline	PAR2-WT	10	0.5 ± 0.2
			PAR2-KO	10	0.3 ± 0.2
		Ang II	PAR2-WT	10	0.5 ± 0.2
			PAR2-KO	10	0.3 ± 0.2
	RR + XeC	Saline	PAR2-WT	10	0.2 ± 0
			PAR2-KO	10	0.2 ± 0.1
		Ang II	PAR2-WT	10	0.3 ± 0.2
			PAR2-KO	10	0.4 ± 0.2

Table S3. Effect of IP3R and TRP channel inhibitors on baseline Ca^{2+}-events in endothelial cells from saline and Ang II-infused mice. Values are means ± S.E.M., n = 10 cells, 4 animals per group. S.E.M. = 0 indicates only 1 cell from 10 observed had Ca^{2+}-events, or that all cells observed had the same number of Ca^{2+}-release sites. Baseline, baseline no agonist; Control, no inhibitor present; RR, ruthenium red (75 µM); XeC, xestospongin c (2 µM). Values were obtained by measuring number of Ca^{2+}-releases in freshly isolated PAR2-WT and PAR2-KO mesenteric endothelial cells. Data were analyzed by 2 way ANOVA (inhibitor x genotype/treatment group) followed by Bonferonni post-hoc testing. Where S.E.M. = 0, unweighted 2 way ANOVA was used. No differences were observed across the inhibitors and treatment groups, $p > 0.05$.

Agonist	Inhibitor	Treatment	Genotype	n	Ca^{2+}-release sites/cell[c]
2fly	Control	Saline	PAR2-WT	10	8 ± 0.4
			PAR2-KO	10	0.4 ± 0.2
		Ang II	PAR2-WT	10	8 ± 0.6
			PAR2-KO	10	0.3 ± 0.2
	XeC	Saline	PAR2-WT	10	1.1 ± 0.3[c]
			PAR2-KO	10	0.4 ± 0.2
		Ang II	PAR2-WT	10	0.9 ± 0.3[c]
			PAR2-KO	10	0.3 ± 0.2
	RR	Saline	PAR2-WT	10	5.1 ± 0.4[c]
			PAR2-KO	10	0.4 ± 0.2
		Ang II	PAR2-WT	10	4.8 ± 0.5[c]
			PAR2-KO	10	0.5 ± 0.2
	RR + XeC	Saline	PAR2-WT	10	0.5 ± 0.3[c]
			PAR2-KO	10	0.5 ± 0.3
		Ang II	PAR2-WT	10	0.3 ± 0.2[c]
			PAR2-KO	10	0.2 ± 0.1

Table S4. Effect of IP3R and TRP channel inhibitors on PAR2-mediated Ca^{2+}-events in endothelial cells from saline and Ang II-infused mice. Values are means ± S.E.M., n = 10 cells, 4 animals per group. S.E.M. = 0 indicates only 1 cell from 10 observed had Ca^{2+}-events, or that all cells observed had the same number of Ca^{2+}-release sites. 2fly, 2-furoyl-LIGRLO-amide (30 nM); Control, no inhibitor present; RR, ruthenium red (75 μM); XeC, xestospongin c (2 μM). Values were obtained by measuring number of Ca^{2+}-releases in freshly isolated PAR2-WT and PAR2-KO mesenteric endothelial cells. Data were analyzed by 2 way ANOVA (inhibitor x genotype/treatment group) followed by Bonfferoni post-hoc testing. Where S.E.M. = 0, unweighted 2 way ANOVA was used. $^{c}p < 0.001$, Ca^{2+}-release sites/cell, XeC saline and Ang II PAR2-WT vs Controls; $^{c}p < 0.001$, Ca^{2+}-release sites/cell, RR saline and Ang II PAR2-WT vs Controls; $^{c}p < 0.001$, Ca^{2+}-release sites/cell, RR + XeC saline and Ang II PAR2-WT vs Controls.

Agonist	Inhibitor	Treatment	Genotype	n	Ca^{2+}-release sites/cell[ac]
ACh	Control	Saline	PAR2-WT	10	5.1 ± 0.3
			PAR2-KO	10	5.4 ± 0.4
		Ang II	PAR2-WT	10	3.4 ± 0.4
			PAR2-KO	10	3.3 ± 0.4
	XeC	Saline	PAR2-WT	10	0.8 ± 0.2[c]
			PAR2-KO	10	1 ± 0.3[c]
		Ang II	PAR2-WT	10	0.5 ± 0.2[c]
			PAR2-KO	10	0.6 ± 0.3[c]
	RR	Saline	PAR2-WT	10	3.2 ± 0.3[c]
			PAR2-KO	10	3.4 ± 0.5[c]
		Ang II	PAR2-WT	10	2.3 ± 0.3[a]
			PAR2-KO	10	2.7 ± 0.3
	RR + XeC	Saline	PAR2-WT	10	0.4 ± 0.2[c]
			PAR2-KO	10	0.4 ± 0.3[c]
		Ang II	PAR2-WT	10	0.2 ± 0.1[c]
			PAR2-KO	10	0.5 ± 0.3[c]

Table S5. Effect of IP3R and TRP channel inhibitors on M_3-mediated Ca^{2+}-events in endothelial cells from saline and Ang II-infused mice. Values are means ± S.E.M., n = 10 cells, 4 animals per group. S.E.M. = 0 indicates only 1 cell from 10 observed had Ca^{2+}-events, or that all cells observed had the same number of Ca^{2+}-release sites. ACh, acetylcholine (300 nM); Control, no inhibitor present; RR, ruthenium red (75 µM); XeC, xestospongin c (2 µM). Values were obtained by measuring number of Ca^{2+}-releases in freshly isolated PAR2-WT and PAR2-KO mesenteric endothelial cells. Data were analyzed by 2 way ANOVA (inhibitor x genotype/treatment group) followed by Bonfferoni post-hoc testing. Where S.E.M. = 0, unweighted 2 way ANOVA was used. [c]$p < 0.001$, Ca^{2+}-release sites/cell, XeC saline and Ang II PAR2-WT and PAR2-KO vs Controls. [c]$p < 0.001$, Ca^{2+}-release sites/cell, RR saline PAR2-WT and PAR2-KO vs Controls; [a]$p < 0.05$, Ca^{2+}-release sites/cell, RR Ang II PAR2-WT vs Controls. [c]$p < 0.001$, Ca^{2+}-release sites/cell, RR + XeC saline and Ang II PAR2-WT and PAR2-KO vs Controls.

Ca^{2+}-event	Agonist	Treatment	Genotype	n	pD_2 (M)	E_{max}^{abc}(Ca^{2+}-release sites/cell)	Hill slope
Peripheral	2fly	Saline	PAR2-WT	5	7.8 ± 0.1	8.3 ± 0.5	0.9 ± 0.1
			PAR2-KO	5	N/A	N/A	N/A
		Ang II	PAR2-WT	5	7.7 ± 0.1	8.2 ± 0.6	0.9 ± 0.1
			PAR2-KO	5	N/A	N/A	N/A
	ACh	Saline	PAR2-WT	5	6.7 ± 0.1	4.5 ± 0.3	1.0 ± 0.2
			PAR2-KO	5	6.9 ± 0.1	4.3 ± 0.2	0.9 ± 0.2
		Ang II	PAR2-WT	5	6.8 ± 0.2	3.5 ± 0.3[a]	0.7 ± 0.1
			PAR2-KO	5	6.7 ± 0.1	3.5 ± 0.2[a]	1.0 ± 0.2
Central	2fly	Saline	PAR2-WT	5	7.7 ± 0.1	4.0 ± 0.4	1.1 ± 0.2
			PAR2-KO	5	N/A	N/A	N/A
		Ang II	PAR2-WT	5	7.6 ± 0.1	3.9 ± 0.3	0.8 ± 0.1
			PAR2-KO	5	N/A	N/A	N/A
	ACh	Saline	PAR2-WT	5	6.8 ± 0.1	2.6 ± 0.1	1.2 ± 0.3
			PAR2-KO	5	6.8 ± 0.1	2.8 ± 0.1	1.0 ± 0.2
		Ang II	PAR2-WT	5	6.8 ± 0.1	2.0 ± 0.1[b]	1.4 ± 0.5
			PAR2-KO	5	6.7 ± 0.1	2.1 ± 0.1[c]	1.2 ± 0.3

Table S6. Characteristics for 2fly and acetylcholine peripheral and central Ca^{2+}-event concentration response curves of angiotensin II and saline treated mice. Values are means ± S.E.M., n = number of mice per curve. 2fly, 2-furoyl-LIGRLO-amide; ACh, acetylcholine. Variables were determined by curve fitting 2fly and acetylcholine-induced Ca^{2+}-event recruitment data from PAR2-WT and PAR2-KO to a 4 parameter logistic curve. Data were analyzed by 2 way ANOVA (treatment x genotype) followed by Bonfferoni post-hoc testing. [c]$p < 0.001$, central E_{max}, Ang II PAR2-KO vs saline PAR2-KO. [b]$p < 0.01$, central E_{max}, Ang II PAR2-WT vs saline PAR2-WT. [a]$p < 0.05$, peripheral E_{max}, Ang II PAR2-WT and PAR2-KO vs saline PAR2-WT and PAR2-KO.

Ca^{2+}-event	Agonist	Treatment	Genotype	n	pD_2 (M)	E_{max}[c](Ca^{2+}-event/site/s)	Hill slope
Peripheral	2fly	Saline	PAR2-WT	5	8.4 ± 0.1	0.42 ± 0.02	2.8 ± 1.6
			PAR2-KO	5	N/A	N/A	N/A
		Ang II	PAR2-WT	5	8.4 ± 0.1	0.39 ± 0.02	3.4 ± 2.5
			PAR2-KO	5	N/A	N/A	N/A
	ACh	Saline	PAR2-WT	5	7.2 ± 0.1	0.33 ± 0.01	1.3 ± 0.3
			PAR2-KO	5	7.3 ± 0.1	0.33 ± 0.01	1.4 ± 0.3
		Ang II	PAR2-WT	5	7.2 ± 0.1	0.22 ± 0.01[c]	1.4 ± 0.6
			PAR2-KO	5	7.2 ± 0.1	0.21 ± 0.01[c]	2.2 ± 0.9
Central	2fly	Saline	PAR2-WT	5	8.0 ± 0.2	0.20 ± 0.02	0.9 ± 0.4
			PAR2-KO	5	N/A	N/A	N/A
		Ang II	PAR2-WT	5	7.9 ± 0.1	0.21 ± 0.01	1.2 ± 0.4
			PAR2-KO	5	N/A	N/A	N/A
	ACh	Saline	PAR2-WT	5	6.0 ± 0.1	0.50 ± 0.02	1.8 ± 0.4
			PAR2-KO	5	6.0 ± 0.1	0.48 ± 0.03	1.3 ± 0.3
		Ang II	PAR2-WT	5	5.9 ± 0.1	0.29 ± 0.02[c]	1.6 ± 0.4
			PAR2-KO	5	6.0 ± 0.1	0.30 ± 0.01[c]	1.7 ± 0.5

Table S7. Characteristics for 2fly and acetylcholine peripheral and central Ca^{2+}-event site firing rate concentration response curves of angiotensin II and saline treated mice. Values are means ± S.E.M., n = number of mice per curve. 2fly, 2-furoyl-LIGRLO-amide; ACh, acetylcholine. Variables were determined by curve fitting 2fly and acetylcholine-induced Ca^{2+}-event site firing rate data from PAR2-WT and PAR2-KO to a 4 parameter logistic curve. Data were analyzed by 2 way ANOVA (treatment x genotype) followed by Bonfferoni post-hoc testing. [c]$p < 0.001$, peripheral E_{max}, Ang II PAR2-WT and PAR2-KO vs saline PAR2-WT and PAR2-KO. [c]$p < 0.001$, central E_{max}, Ang II PAR2-WT and PAR2-KO vs saline PAR2-WT and PAR2-KO.

Ca^{2+}-event	Inhibitor	Treatment	Genotype	n	Ca^{2+}-release sites/cell
Baseline Peripheral	Control	Saline	PAR2-WT	10	0.4 ± 0.2
			PAR2-KO	10	0.3 ± 0.2
		Ang II	PAR2-WT	10	0.4 ± 0.2
			PAR2-KO	10	0.3 ± 0.2
	XeC	Saline	PAR2-WT	10	0
			PAR2-KO	10	0.4 ± 0.2
		Ang II	PAR2-WT	10	0.1 ± 0
			PAR2-KO	10	0.1 ± 0
	RR	Saline	PAR2-WT	10	0.4 ± 0.2
			PAR2-KO	10	0.3 ± 0.2
		Ang II	PAR2-WT	10	0.3 ± 0.2
			PAR2-KO	10	0.2 ± 0.1
	RR+ XeC	Saline	PAR2-WT	10	0.1 ± 0
			PAR2-KO	10	0.2 ± 0.1
		Ang II	PAR2-WT	10	0.2 ± 0.1
			PAR2-KO	10	0.4 ± 0.2

Table S8. Effect of IP3R and TRP channel inhibitors on baseline peripheral Ca^{2+}-events in endothelial cells from saline and Ang II-infused mice. Values are means ± S.E.M., n =10 cells, 4 animals per group. S.E.M. = 0 indicates only 1 cell from 10 observed had Ca^{2+}-events, or that all cells observed had the same number of Ca^{2+}-release sites. Control, no inhibitor present; Baseline (no agonist); RR, ruthenium red (75 μM); XeC, xestospongin c (2 μM). Values were obtained by measuring number of Ca^{2+}-releases in freshly isolated PAR2-WT and PAR2-KO mesenteric endothelial cells. Data were analyzed by 2 way ANOVA (inhibitor x genotype/treatment group) followed by Bonfferoni post-hoc testing. Where S.E.M. = 0, unweighted 2 way ANOVA was used. $p > 0.05$, no differences between groups.

Ca^{2+}-event	Inhibitor	Treatment	Genotype	n	Ca^{2+}-release sites/cell
Baseline Central	Control	Saline	PAR2-WT	10	0.1 ± 0
			PAR2-KO	10	0
		Ang II	PAR2-WT	10	0.1 ± 0
			PAR2-KO	10	N/A
	XeC	Saline	PAR2-WT	10	0.1 ± 0
			PAR2-KO	10	0
		Ang II	PAR2-WT	10	0.2 ± 0.1
			PAR2-KO	10	0.1 ± 0
	RR	Saline	PAR2-WT	10	0.1 ± 0
			PAR2-KO	10	0.1 ± 0
		Ang II	PAR2-WT	10	0.2 ± 0.1
			PAR2-KO	10	0.1 ± 0
	RR+ XeC	Saline	PAR2-WT	10	0.1 ± 0
			PAR2-KO	10	0
		Ang II	PAR2-WT	10	0
			PAR2-KO	10	0

Table S9. Effect of IP3R and TRP channel inhibitors on baseline central Ca^{2+}-events in endothelial cells from saline and Ang II-infused mice. Values are means ± S.E.M., n =10 cells, 4 animals per group. S.E.M. = 0 indicates only 1 cell from 10 observed had Ca^{2+}-events, or that all cells observed had the same number of Ca^{2+}-release sites. Control, no inhibitor present; Baseline (no agonist); RR, ruthenium red (75 µM); XeC, xestospongin c (2 µM). Values were obtained by measuring number of Ca^{2+}-releases in freshly isolated PAR2-WT and PAR2-KO mesenteric endothelial cells. Data were analyzed by 2 way ANOVA (inhibitor x genotype/treatment group) followed by Bonfferoni post-hoc testing. Where S.E.M. = 0, unweighted 2 way ANOVA was used. $p > 0.05$, no differences between groups.

Ca^{2+}-event	Inhibitor	Treatment	Genotype	n	Ca^{2+}-release sites/cell[c]
2fly Peripheral	Control	Saline	PAR2-WT	10	6.3 ± 0.3
			PAR2-KO	10	0.3 ± 0.2
		Ang II	PAR2-WT	10	6.2 ± 0.6
			PAR2-KO	10	0.2 ± 0.1
	XeC	Saline	PAR2-WT	10	0.8 ± 0.2[c]
			PAR2-KO	10	0.4 ± 0.2
		Ang II	PAR2-WT	10	0.7 ± 0.3[c]
			PAR2-KO	10	0.2 ± 0.1
	RR	Saline	PAR2-WT	10	4 ± 0.3[c]
			PAR2-KO	10	0.4 ± 0.2
		Ang II	PAR2-WT	10	3.7 ± 0.4[c]
			PAR2-KO	10	0.3 ± 0.2
	RR+ XeC	Saline	PAR2-WT	10	0.4 ± 0.2[c]
			PAR2-KO	10	0.3 ± 0.2
		Ang II	PAR2-WT	10	0.3 ± 0.2[c]
			PAR2-KO	10	0.2 ± 0.1

Table S10. Effect of IP3R and TRP channel inhibitors on PAR2-mediated peripheral Ca^{2+}-events in endothelial cells from saline and Ang II-infused mice. Values are means ± S.E.M., n =10 cells, 4 animals per group. S.E.M. = 0 indicates only 1 cell from 10 observed had Ca^{2+}-events, or that all cells observed had the same number of Ca^{2+}-release sites. 2fly, 2-furoyl-LIGRLO-amide (30 nM); Control, no inhibitor present; RR, ruthenium red (75 μM); XeC, xestospongin c (2 μM). Values were obtained by measuring number of Ca^{2+}-releases in freshly isolated PAR2-WT and PAR2-KO mesenteric endothelial cells. Data were analyzed by 2 way ANOVA (inhibitor x genotype/treatment group) followed by Bonfferoni post-hoc testing. Where S.E.M. = 0, unweighted 2 way ANOVA was used. $^{c}p < 0.001$, Ca^{2+}-release sites/cell, XeC, RR and RR + XeC saline and Ang II PAR2-WT vs Controls.

Ca^{2+}-event	Inhibitor	Treatment	Genotype	n	Ca^{2+}-release sites/cell[c]
2fly Central	Control	Saline	PAR2-WT	10	1.7 ± 0.2
			PAR2-KO	10	0.1 ± 0
		Ang II	PAR2-WT	10	1.8 ± 0.1
			PAR2-KO	10	0
	XeC	Saline	PAR2-WT	10	0.3 ± 0.2[c]
			PAR2-KO	10	N/A
		Ang II	PAR2-WT	10	0.3 ± 0.2[c]
			PAR2-KO	10	0
	RR	Saline	PAR2-WT	10	1.1 ± 0.1[c]
			PAR2-KO	10	0.1 ± 0
		Ang II	PAR2-WT	10	1.1 ± 0.1[c]
			PAR2-KO	10	0.1 ± 0
	RR+ XeC	Saline	PAR2-WT	10	0.1 ± 0[c]
			PAR2-KO	10	0.1 ± 0
		Ang II	PAR2-WT	10	0[c]
			PAR2-KO	10	0

Table S11. Effect of IP3R and TRP channel inhibitors on PAR2-mediated central Ca^{2+}-events in endothelial cells from saline and Ang II-infused mice. Values are means ± S.E.M., n =10 cells, 4 animals per group. S.E.M. = 0 indicates only 1 cell from 10 observed had Ca^{2+}-events, or that all cells observed had the same number of Ca^{2+}-release sites. 2fly, 2-furoyl-LIGRLO-amide (30 nM); Control, no inhibitor present; RR, ruthenium red (75 µM); XeC, xestospongin c (2 µM). Values were obtained by measuring number of Ca^{2+}-releases in freshly isolated PAR2-WT and PAR2-KO mesenteric endothelial cells. Data were analyzed by 2 way ANOVA (inhibitor x genotype/treatment group) followed by Bonfferoni post-hoc testing. Where S.E.M. = 0, unweighted 2 way ANOVA was used. [c]$p < 0.001$, Ca^{2+}-release sites/cell, XeC saline and Ang II PAR2-WT vs Controls. [c]$p < 0.001$, Ca^{2+}-release sites/cell, RR saline and Ang II PAR2-WT vs Controls. [c]$p < 0.001$, Ca^{2+}-release sites/cell, RR + XeC saline PAR2-WT vs Controls.

Ca^{2+}-event	Inhibitor	Treatment	Genotype	n	Ca^{2+}-release sites/cell[c]
ACh Peripheral	Control	Saline	PAR2-WT	10	2.8 ± 0.2
			PAR2-KO	10	2.9 ± 0.2
		Ang II	PAR2-WT	10	1.7 ± 0.2
			PAR2-KO	10	1.7 ± 0.2
	XeC	Saline	PAR2-WT	10	0.6 ± 0.3[c]
			PAR2-KO	10	0.5 ± 0.2[c]
		Ang II	PAR2-WT	10	0.5 ± 0.2[c]
			PAR2-KO	10	0.2 ± 0.1[c]
	RR	Saline	PAR2-WT	10	1.7 ± 0.2[c]
			PAR2-KO	10	1.8 ± 0.2[c]
		Ang II	PAR2-WT	10	1 ± 0.1
			PAR2-KO	10	1.4 ± 0.2
	RR+ XeC	Saline	PAR2-WT	10	0.3 ± 0.2[c]
			PAR2-KO	10	0.3 ± 0.2[c]
		Ang II	PAR2-WT	10	0.1 ± 0[c]
			PAR2-KO	10	0.3 ± 0.2[c]

Table S12. Effect of IP3R and TRP channel inhibitors on M_3-mediated peripheral Ca^{2+}-events in endothelial cells from saline and Ang II-infused mice. Values are means ± S.E.M., n =10 cells, 4 animals per group. S.E.M. = 0 indicates only 1 cell from 10 observed had Ca^{2+}-events, or that all cells observed had the same number of Ca^{2+}-release sites. ACh, acetylcholine (300 nM); Control, no inhibitor present; RR, ruthenium red (75 µM); XeC, xestospongin c (2 µM). Values were obtained by measuring number of Ca^{2+}-releases in freshly isolated PAR2-WT and PAR2-KO mesenteric endothelial cells. Data were analyzed by 2 way ANOVA (inhibitor x genotype/treatment group) followed by Bonfferoni post-hoc testing. Where S.E.M. = 0, unweighted 2 way ANOVA was used. $^{c}p < 0.001$, Ca^{2+}-release sites/cell, XeC saline and Ang II PAR2-WT and PAR2-KO vs Controls. $^{c}p < 0.001$, Ca^{2+}-release sites/cell, RR saline PAR2-WT and PAR2-KO vs Controls. $^{c}p < 0.001$, Ca^{2+}-release sites/cell, RR + XeC saline and Ang II PAR2-WT and PAR2-KO vs Controls.

Ca^{2+}-event	Inhibitor	Treatment	Genotype	n	Ca^{2+}-release sites/cell[abc]
ACh Central	Control	Saline	PAR2-WT	10	2.1 ± 0.3
			PAR2-KO	10	2.5 ± 0.3
		Ang II	PAR2-WT	10	0.8 ± 0.2
			PAR2-KO	10	1.1 ± 0.3
	XeC	Saline	PAR2-WT	10	0.2 ± 0.1[c]
			PAR2-KO	10	0.2 ± 0.1[c]
		Ang II	PAR2-WT	10	0[c]
			PAR2-KO	10	0.3 ± 0.2[a]
	RR	Saline	PAR2-WT	10	1.2 ± 0.2[b]
			PAR2-KO	10	1.1 ± 0.3[c]
		Ang II	PAR2-WT	10	0.8 ± 0.2
			PAR2-KO	10	0.8 ± 0.2
	RR+ XeC	Saline	PAR2-WT	10	0.1 ± 0[c]
			PAR2-KO	10	0.2 ± 0.1[c]
		Ang II	PAR2-WT	10	0.1 ± 0
			PAR2-KO	10	0[c]

Table S13. Effect of IP3R and TRP channel inhibitors on M_3-mediated central Ca^{2+}-events in endothelial cells from saline and Ang II-infused mice. Values are means ± S.E.M., n =10 cells, 4 animals per group. S.E.M. = 0 indicates only 1 cell from 10 observed had Ca^{2+}-events, or that all cells observed had the same number of Ca^{2+}-release sites. ACh, acetylcholine (300 nM); Control, no inhibitor present; RR, ruthenium red (75 µM); XeC, xestospongin c (2 µM). Values were obtained by measuring number of Ca^{2+}-releases in freshly isolated PAR2-WT and PAR2-KO mesenteric endothelial cells. Data were analyzed by 2 way ANOVA (inhibitor x genotype/treatment group) followed by Bonfferoni post-hoc testing. Where S.E.M. = 0, unweighted 2 way ANOVA was used. [c]$p < 0.001$, Ca^{2+}-release sites/cell, XeC saline PAR2-WT and PAR2-KO vs Controls; [a]$p < 0.05$, Ca^{2+}-release sites/cell , XeC Ang II PAR2-KO vs Controls. [c]$p < 0.001$, Ca^{2+}-release sites/cell, RR saline PAR2-KO vs Controls; [b]$p < 0.01$, Ca^{2+}-release sites/cell, RR saline PAR2-WT vs Controls. [c]$p < 0.001$, Ca2+-release sites/cell, RR + XeC saline PAR2-WT and PAR2-KO vs Controls.

Treatment / Genotype	Ca^{2+}-Event Type	Agonist	Inhibitor	n	Amplitude[ab c] (F/F_o)	FWHM[b c] (%)	t_{rise}[c] (ms)	$t_{1/2}$ (ms)	Frequency[c] (Hz)
Saline PAR2-WT	Peripheral	Baseline	Control	4	1.79 ± 0.09	23 ± 2	82 ± 4	205 ± 4	N/A
			XeC	0	N/A	N/A	N/A	N/A	N/A
			RR	4	1.63 ± 0.06	18 ± 3	75 ± 2	202 ± 4	N/A
			RR + XeC	1	1.49 ± 0	9 ± 0	112 ± 0	205 ± 0	N/A
		2fly	Control	230	1.77 ± 0.01	20 ± 1	81 ± 1	205 ± 1	N/A
			XeC	10	1.52 ± 0.09[c]	9 ± 1[c]	118 ± 3[c]	207 ± 3	N/A
			RR	132	1.62 ± 0.02	16 ± 1[b]	81 ± 1	206 ± 1	N/A
			RR + XeC	5	1.48 ± 0.07[b]	10 ± 1[c]	116 ± 4[c]	200 ± 2	N/A
		ACh	Control	92	1.80 ± 0.02	20 ± 1	81 ± 1	205 ± 1	N/A
			XeC	7	1.50 ± 0.04[b]	10 ± 1[c]	116 ± 2[c]	205 ± 3	N/A
			RR	55	1.60 ± 0.04	15 ± 1[b]	81 ± 1	205 ± 1	N/A
			RR + XeC	4	1.46 ± 0.10[a]	8 ± 2[c]	120 ± 2[c]	208 ± 4	N/A
	Central	Baseline	Control	1	3.03 ± 0	32 ± 0	96 ± 0	122 ± 0	0.01 ± 0
			XeC	1	1.93 ± 0	11 ± 0	137 ± 0	121 ± 0	0.01 ± 0
			RR	1	2.46 ± 0	34 ± 0	93 ± 0	123 ± 0	0.01 ± 0
			RR + XeC	1	1.91 ± 0	10 ± 0	133 ± 0	111 ± 0	0.01 ± 0
		2fly	Control	36	3.14 ± 0.02	32 ± 1	99 ± 2	114 ± 1	0.40 ± 0.05
			XeC	3	1.90 ± 0.10[c]	11 ± 1[c]	130 ± 5[c]	115 ± 3	0.03 ± 0.02[c]
			RR	17	2.46 ± 0.04[c]	33 ± 1	98 ± 2	117 ± 2	0.17 ± 0.02[c]
			RR + XeC	1	1.89 ± 0	9 ± 0	135 ± 0	119 ± 0	0.01 ± 0
		ACh	Control	33	3.16 ± 0.08	32 ± 1	100 ± 2	115 ± 2	0.34 ± 0.03
			XeC	2	1.96 ± 0.10	11 ± 1	132 ± 4	114 ± 5	0.02 ± 0.01
			RR	17	2.45 ± 0.03[c]	33 ± 1	100 ± 2	116 ± 2	0.18 ± 0.03[c]
			RR + XeC	1	1.95 ± 0	12 ± 0	134 ± 0	112 ± 0	0.01 ± 0

Table S14. Effect of IP3R and TRP channel inhibitors on characteristics of peripheral and central Ca^{2+}-transient characteristics from saline-infused PAR2-WT. Values are means ± S.E.M., n = number of Ca^{2+}-events from 10 cells, 5 animals per group. S.E.M. = 0 indicates only 1 cell from 10 observed had Ca^{2+}-events, or that all cells observed had the same number of Ca^{2+}-release sites or rate. S.E.M. calculated from number of cells with Ca^{2+}-transients present. 2fly, 2-furoyl-LIGRLO-amide (30 nM); ACh, acetylcholine (30 μM); Baseline, no agonist added; FWHM, full width at half-maximum Ca^{2+}-event amplitude (% maximum cell length). Values were obtained by line scan analysis of Ca^{2+}-events in freshly isolated PAR2-WT and PAR2-KO mesenteric endothelial cells. Data were analyzed by 2 way ANOVA (Ca^{2+}-event type x genotype/treatment group) followed by Bonfferoni post-hoc testing. Where S.E.M. = 0, unweighted 2 way ANOVA was used. $^{c}p < 0.001$, Amplitude, peripheral XeC 2fly vs Controls; central XeC, RR 2fly vs Controls; central RR ACh vs Controls.. $^{b}p < 0.01$, Amplitude, peripheral RR + XeC 2fly vs Controls; peripheral XeC ACh vs Controls. $^{a}p < 0.05$, Amplitude, peripheral RR + XeC ACh vs Controls. $^{c}p < 0.001$, FWHM, peripheral XeC and RR + XeC 2fly and ACh vs Controls; central XeC 2fly vs Controls. $^{b}p < 0.01$, FWHM, peripheral RR 2fly and ACh vs Controls. $^{c}p < 0.001$, t_{rise}, peripheral XeC and RR + XeC 2fly and ACh vs Controls; central XeC 2fly vs Controls. $^{c}p < 0.001$, Frequency, central XeC, RR 2fly vs Controls; central RR ACh vs Controls .

Treatment / Genotype	Ca^{2+}-Event Type	Agonist	Inhibitor	n	Amplitude[b] [c] (F/F_o)	FWHM[a] [c] (%)	t_{rise} [c] (ms)	$t_{1/2}$ (ms)	Frequency[c] (Hz)
Ang II PAR2-WT	Peripheral	Baseline	Control	5	1.79 ± 0.10	22 ± 2	83 ± 3	205 ± 3	N/A
			XeC	1	1.47 ± 0	12 ± 0	119 ± 0	210 ± 0	N/A
			RR	4	1.63 ± 0.10	16 ± 2	80 ± 3	204 ± 3	N/A
			RR + XeC	4	1.5 ± 0.06[b]	9 ± 2[c]	114 ± 3[c]	205 ± 4	N/A
		2fly	Control	239	1.76 ± 0.01	20 ± 1	81 ± 1	205 ± 1	N/A
			XeC	10	1.50 ± 0.04[b]	8 ± 1[c]	114 ± 2[c]	206 ± 2	N/A
			RR	138	1.62 ± 0.01	15 ± 1[a]	80 ± 1	205 ± 1	N/A
			RR + XeC	3	1.49 ± 0.05[b]	8 ± 2[c]	117 ± 5[c]	214 ± 2	N/A
		ACh	Control	53	1.77 ± 0.03	20 ± 1	78 ± 1	206 ± 1	N/A
			XeC	5	1.51 ± 0.08[b]	8 ± 1[c]	114 ± 3[c]	202 ± 3	N/A
			RR	34	1.61 ± 0.04	15 ± 1[a]	80 ± 1	204 ± 2	N/A
			RR + XeC	1	1.5 ± 0	11 ± 0	125 ± 0	202 ± 0	N/A
	Central	Baseline	Control	2	3.13 ± 0.07	34 ± 1	94 ± 3	118 ± 2	0.02 ± 0.01
			XeC	2	1.93 ± 0.04	11 ± 1	126 ± 5	117 ± 5	0.02 ± 0.01
			RR	2	2.44 ± 0.06	32 ± 1	100 ± 3	123 ± 1	0.02 ± 0.01
			RR + XeC	0	N/A	N/A	N/A	N/A	N/A
		2fly	Control	37	3.17 ± 0.02	32 ± 1	101 ± 1	115 ± 1	0.38 ± 0.03
			XeC	3	1.93 ± 0.03[c]	9 ± 2[c]	127 ± 5[c]	122 ± 2	0.03 ± 0.02[c]
			RR	18	2.44 ± 0.04[c]	34 ± 1	100 ± 2	116 ± 2	0.18 ± 0.03[c]
			RR + XeC	0	N/A	N/A	N/A	N/A	N/A
		ACh	Control	15	3.21 ± 0.04	33 ± 1	99 ± 2	116 ± 2	0.15 ± 0.03
			XeC	0	N/A	N/A	N/A	N/A	N/A
			RR	13	2.44 ± 0.05[c]	32 ± 1	100 ± 2	114 ± 2	0.13 ± 0.03
			RR + XeC	1	1.92 ± 0	12 ± 0	132 ± 0	115 ± 0	0.01 ± 0

Table S15. Effect of IP3R and TRP channel inhibitors on characteristics of peripheral and central Ca^{2+}-transient characteristics from Ang II-infused PAR2-WT. Values are means ± S.E.M., n = number of Ca^{2+}-events from 10 cells, 5 animals per group. S.E.M. = 0 indicates only 1 cell from 10 observed had Ca^{2+}-events, or that all cells observed had the same number of Ca^{2+}-release sites or rate. S.E.M. calculated from number of cells with Ca^{2+}-transients present. 2fly, 2-furoyl-LIGRLO-amide (30 nM); ACh, acetylcholine (30 μM); Baseline, no agonist added; FWHM, full width at half-maximum Ca^{2+}-event amplitude (% maximum cell length). Values were obtained by line scan analysis of Ca^{2+}-events in freshly isolated PAR2-WT and PAR2-KO mesenteric endothelial cells. Data were analyzed by 2 way ANOVA (Ca^{2+}-event type x genotype/treatment group) followed by Bonfferoni post-hoc testing. Where S.E.M. = 0, unweighted 2 way ANOVA was used. [c]$p < 0.001$, Amplitude, central XeC 2fly vs Controls; central RR 2fly and ACh vs Controls. [b]$p < 0.01$, Amplitude, peripheral XeC 2fly and ACh vs Controls; peripheral RR + XeC Baseline and 2fly vs Controls. [c]$p < 0.001$, FWHM, peripheral XeC and RR + XeC 2fly vs Controls; peripheral XeC ACh vs Controls; peripheral RR + XeC Baseline vs Controls; central XeC 2fly vs Controls. [a]$p < 0.05$, FWHM, peripheral RR 2fly and ACh vs Controls. [c]$p < 0.001$, t_{rise}, peripheral XeC and RR + XeC 2fly vs Controls; peripheral XeC ACh vs Controls; peripheral RR + XeC Baseline vs Controls; central XeC 2fly vs Controls. [c]$p < 0.001$, Frequency, central XeC and RR 2fly vs Controls.

Treatment / Genotype	Ca^{2+}-Event Type	Agonist	Inhibitor	n	Amplitude[ab][c] (F/F_o)	FWHM[b][c] (%)	t_{rise}[c] (ms)	$t_{1/2}$ (ms)	Frequency[c] (Hz)
Saline PAR2-KO	Peripheral	Baseline	Control	5	1.78 ± 0.04	20 ± 2	75 ± 2	205 ± 3	N/A
			XeC	6	1.47 ± 0.07[b]	12 ± 1[b]	115 ± 3[c]	204 ± 3	N/A
			RR	3	1.61 ± 0.05	16 ± 3	78 ± 5	198 ± 2	N/A
			RR + XeC	2	1.48 ± 0.07	10 ± 1	124 ± 1	202 ± 2	N/A
		2fly	Control	5	1.76 ± 0.08	19 ± 2	84 ± 3	202 ± 3	N/A
			XeC	6	1.48 ± 0.09[a]	7 ± 1[c]	116 ± 3[c]	203 ± 3	N/A
			RR	4	1.59 ± 0.08	17 ± 2	81 ± 4	206 ± 4	N/A
			RR + XeC	4	1.49 ± 0.05[a]	10 ± 2[b]	116 ± 5[c]	201 ± 3	N/A
		ACh	Control	93	1.81 ± 0.02	20 ± 1	79 ± 1	204 ± 1	N/A
			XeC	8	1.53 ± 0.06[b]	9 ± 1[c]	119 ± 2[c]	204 ± 3	N/A
			RR	54	1.62 ± 0.02	15 ± 1	81 ± 1	205 ± 1	N/A
			RR + XeC	3	1.48 ± 0.10[b]	9 ± 3[c]	116 ± 4[c]	205 ± 5	N/A
	Central	Baseline	Control	0	N/A	N/A	N/A	N/A	N/A
			XeC	0	N/A	N/A	N/A	N/A	N/A
			RR	1	2.50 ± 0	33 ± 0	106 ± 0	124 ± 0	0.01 ± 0
			RR + XeC	0	N/A	N/A	N/A	N/A	N/A
		2fly	Control	1	3.15 ± 0	31 ± 0	101 ± 0	121 ± 0	0.01 ± 0
			XeC	0	N/A	N/A	N/A	N/A	N/A
			RR	1	2.42 ± 0	30 ± 0	107 ± 0	123 ± 0	0.01 ± 0
			RR + XeC	2	1.92 ± 0.10	11 ± 2	123 ± 2	115 ± 6	0.02 ± 0.01
		ACh	Control	33	3.16 ± 0.03	32 ± 1	100 ± 2	116 ± 1	0.33 ± 0.02
			XeC	2	1.92 ± 0.09	10 ± 1	127 ± 7	115 ± 1	0.02 ± 0.01
			RR	14	2.44 ± 0.04[c]	33 ± 1	98 ± 2	115 ± 2	0.14 ± 0.03[c]
			RR + XeC	2	1.94 ± 0.08	8 ± 1	124 ± 6	111 ± 2	0.02 ± 0.01

Table S16. Effect of IP3R and TRP channel inhibitors on characteristics of peripheral and central Ca^{2+}-transient characteristics from saline-infused PAR2-KO. Values are means ± S.E.M., n = number of Ca^{2+}-events from 10 cells, 5 animals per group. S.E.M. = 0 indicates only 1 cell from 10 observed had Ca^{2+}-events, or that all cells observed had the same number of Ca^{2+}-release sites or rate. S.E.M. calculated from number of cells with Ca^{2+}-transients present. 2fly, 2-furoyl-LIGRLO-amide (30 nM); ACh, acetylcholine (30 μM); Baseline, no agonist added; FWHM, full width at half-maximum Ca^{2+}-event amplitude (% maximum cell length). Values were obtained by line scan analysis of Ca^{2+}-events in freshly isolated PAR2-WT and PAR2-KO mesenteric endothelial cells. Data were analyzed by 2 way ANOVA (Ca^{2+}-event type x genotype/treatment group) followed by Bonfferoni post-hoc testing. Where S.E.M. = 0, unweighted 2 way ANOVA was used. [c]$p < 0.001$, Amplitude, central RR ACh vs Controls. [b]$p < 0.01$, Amplitude, peripheral XeC and RR + XeC ACh vs Controls; peripheral XeC Baseline vs Controls. [a]$p < 0.05$, Amplitude, peripheral XeC and RR + XeC 2fly vs Controls. [c]$p < 0.001$, FWHM, peripheral XeC 2fly and ACh vs Controls; peripheral RR + XeC ACh vs Controls. [b]$p < 0.01$, FWHM, peripheral XeC Baseline vs Controls; peripheral RR + XeC 2fly vs Controls. [c]$p < 0.001$, t_{rise}, peripheral XeC and RR + XeC 2fly and ACh vs Controls; peripheral XeC Baseline vs Controls. [c]$p < 0.001$, Frequency, central RR ACh vs Controls.

Treatment/ Genotype	Ca^{2+}-Event Type	Agonist	Inhibitor	n	Amplitude[c] (F/F_o)	FWHM[bc] (%)	t_{rise}[c](ms)	$t_{1/2}$ (ms)	Frequency[c] (Hz)
Ang II PAR2-KO	Peripheral	Baseline	Control	4	1.78 ± 0.05	19 ± 2	82 ± 4	203 ± 4	N/A
			XeC	1	1.48 ± 0	8 ± 0	110 ± 0	208 ± 0	N/A
			RR	4	1.61 ± 0.06	18 ± 1	81 ± 4	206 ± 4	N/A
			RR + XeC	4	1.47 ± 0.09[c]	10 ± 2[c]	113 ± 5[c]	205 ± 3	N/A
		2fly	Control	4	1.79 ± 0.04	18 ± 2	82 ± 2	200 ± 3	N/A
			XeC	4	1.49 ± 0.06[c]	10 ± 1[b]	116 ± 4[c]	202 ± 2	N/A
			RR	5	1.64 ± 0.03	17 ± 2	78 ± 2	201 ± 3	N/A
			RR + XeC	2	1.49 ± 0.08	9 ± 3	117 ± 5	210 ± 5	N/A
		ACh	Control	55	1.80 ± 0.02	21 ± 1	80 ± 1	204 ± 1	N/A
			XeC	5	1.50 ± 0.03[c]	11 ± 2[c]	116 ± 3[c]	205 ± 4	N/A
			RR	47	1.63 ± 0.01	16 ± 1	80 ± 1	205 ± 1	N/A
			RR + XeC	6	1.51 ± 0.08[c]	9 ± 1[c]	118 ± 3[c]	205 ± 3	N/A
	Central	Baseline	Control	0	N/A	N/A	N/A	N/A	N/A
			XeC	1	1.91 ± 0	11 ± 0	120 ± 0	107 ± 0	0.01 ± 0
			RR	1	2.42 ± 0	35 ± 0	106 ± 0	124 ± 0	0.01 ± 0
			RR + XeC	0	N/A	N/A	N/A	N/A	N/A
		2fly	Control	0	N/A	N/A	N/A	N/A	N/A
			XeC	0	N/A	N/A	N/A	N/A	N/A
			RR	1	2.46 ± 0	33 ± 0	99 ± 0	116 ± 0	0.01 ± 0
			RR + XeC	0	N/A	N/A	N/A	N/A	N/A
		ACh	Control	16	3.15 ± 0.06	33 ± 1	102 ± 2	114 ± 2	0.17 ± 0.04
			XeC	3	1.91 ± 0.08[c]	10 ± 2[c]	128 ± 5[c]	118 ± 7	0.03 ± 0.02[c]
			RR	12	2.46 ± 0.04[c]	34 ± 1	97 ± 2	115 ± 3	0.12 ± 0.03
			RR + XeC	0	N/A	N/A	N/A	N/A	N/A

Table S17. Effect of IP3R and TRP channel inhibitors on characteristics of peripheral and central Ca^{2+}-transient characteristics from Ang II-infused PAR2-KO. Values are means ± S.E.M., n = number of Ca^{2+}-events from 10 cells, 5 animals per group. S.E.M. = 0 indicates only 1 cell from 10 observed had Ca^{2+}-events, or that all cells observed had the same number of Ca^{2+}-release sites or rate. S.E.M. calculated from number of cells with Ca^{2+}-transients present. 2fly, 2-furoyl-LIGRLO-amide (30 nM); ACh, acetylcholine (30 μM); Baseline, no agonist added; FWHM, full width at half-maximum Ca^{2+}-event amplitude (% maximum cell length). Values were obtained by line scan analysis of Ca^{2+}-events in freshly isolated PAR2-WT and PAR2-KO mesenteric endothelial cells. Data were analyzed by 2 way ANOVA (Ca^{2+}-event type x genotype/treatment group) followed by Bonfferoni post-hoc testing. Where S.E.M. = 0, unweighted 2 way ANOVA was used. [c]$p < 0.001$, Amplitude, peripheral XeC and RR + XeC ACh vs Controls; peripheral XeC 2fly vs Controls; peripheral RR + XeC Baseline vs Controls; central XeC and RR ACh vs Controls. [c]$p < 0.001$, FWHM, peripheral XeC ACh vs Controls; peripheral RR + XeC Baseline and ACh vs Controls; central XeC ACh vs Controls. [b]$p < 0.01$, FWHM, peripheral XeC 2fly vs Controls. [c]$p < 0.001$, t_{rise}, peripheral XeC and RR + XeC ACh vs Controls; peripheral XeC 2fly vs Controls; peripheral RR + XeC Baseline vs Controls; central XeC ACh vs Controls. [c]$p < 0.001$, Frequency, central XeC ACh vs Controls.

Reference List

1. Absi, M., Burnham, M. P., Weston, A. H., Harno, E., Rogers, M., & Edwards, G. (2007). Effects of methyl beta-cyclodextrin on EDHF responses in pig and rat arteries; association between SK(Ca) channels and caveolin-rich domains. *Br.J.Pharmacol., 151,* 332-340.

2. Adams, M. N., Pagel, C. N., Mackie, E. J., & Hooper, J. D. (2012). Evaluation of antibodies directed against human protease-activated receptor-2. *Naunyn Schmiedebergs Arch.Pharmacol., 385,* 861-873.

3. Adams, M. N., Ramachandran, R., Yau, M. K., Suen, J. Y., Fairlie, D. P., Hollenberg, M. D. et al. (2011). Structure, function and pathophysiology of protease activated receptors. *Pharmacol.Ther., 130,* 248-282.

4. Adeagbo, A. S. & Triggle, C. R. (1993). Varying extracellular [K+]: a functional approach to separating EDHF- and EDNO-related mechanisms in perfused rat mesenteric arterial bed. *J Cardiovasc.Pharmacol., 21,* 423-429.

5. Al-Ani, B. & Hollenberg, M. D. (2003). Selective tryptic cleavage at the tethered ligand site of the amino terminal domain of proteinase-activated receptor-2 in intact cells. *J Pharmacol.Exp.Ther., 304,* 1120-1128.

6. Al-Ani, B., Saifeddine, M., Kawabata, A., & Hollenberg, M. D. (1999a). Proteinase activated receptor 2: Role of extracellular loop 2 for ligand-mediated activation. *Br.J Pharmacol., 128,* 1105-1113.

7. Al-Ani, B., Saifeddine, M., Kawabata, A., Renaux, B., Mokashi, S., & Hollenberg, M. D. (1999b). Proteinase-activated receptor 2 (PAR(2)): development of a ligand-binding assay correlating with activation of PAR(2) by PAR(1)- and PAR(2)-derived peptide ligands. *J Pharmacol.Exp.Ther., 290,* 753-760.

8. Amadesi, S., Cottrell, G. S., Divino, L., Chapman, K., Grady, E. F., Bautista, F. et al. (2006). Protease-activated receptor 2 sensitizes TRPV1 by protein kinase Cepsilon- and A-dependent mechanisms in rats and mice. *J.Physiol, 575,* 555-571.

9. Ansurudeen, I., Pietzsch, J., Graessler, J., Ehrhart-Bornstein, M., Saha, S., Bornstein, S. R. et al. (2010). Modulation of adrenal aldosterone release by oxidative modification of low-density lipoprotein. *Am J Hypertens., 23,* 1061-1068.

10. Aromolaran, A. S., Zima, A. V., & Blatter, L. A. (2007). Role of glycolytically generated ATP for CaMKII-mediated regulation of intracellular Ca2+ signaling in bovine vascular endothelial cells. *Am.J.Physiol Cell Physiol, 293,* C106-C118.

11. Aroor, A. R., Demarco, V. G., Jia, G., Sun, Z., Nistala, R., Meininger, G. A. et al. (2013). The Role of Tissue Renin-Angiotensin-Aldosterone System in the Development of Endothelial Dysfunction and Arterial Stiffness. *Front Endocrinol.(Lausanne), 4,* 161.

12. Arun, K. H., Kaul, C. L., & Ramarao, P. (2005). AT1 receptors and L-type calcium channels: functional coupling in supersensitivity to angiotensin II in diabetic rats. *Cardiovasc.Res., 65,* 374-386.

13. Aure, M. H., Roed, A., & Galtung, H. K. (2010). Intracellular Ca2+ responses and cell volume regulation upon cholinergic and purinergic stimulation in an immortalized salivary cell line. *Eur.J Oral Sci., 118,* 237-244.

14. Avendano, M. S., Lucas, E., Jurado-Pueyo, M., Martinez-Revelles, S., Vila-Bedmar, R., Mayor, F., Jr. et al. (2013). Increased Nitric Oxide Bioavailability in Adult GRK2 Hemizygous Mice Protects Against Angiotensin II-Induced Hypertension. *Hypertension*.

15. Awasthi, V., Mandal, S. K., Papanna, V., Rao, L. V., & Pendurthi, U. R. (2007). Modulation of tissue factor-factor VIIa signaling by lipid rafts and caveolae. *Arterioscler.Thromb.Vasc.Biol., 27,* 1447-1455.

16. Ayajiki, K., Fujioka, H., & Okamura, T. (2000). Mechanisms underlying endothelium-dependent, nitric oxide/prostacyclin-independent, acetylcholine-induced relaxation in canine corpus cavernosum. *Naunyn Schmiedebergs Arch.Pharmacol., 362,* 448-451.

17. Bagher, P., Beleznai, T., Kansui, Y., Mitchell, R., Garland, C. J., & Dora, K. A. (2012). Low intravascular pressure activates endothelial cell TRPV4 channels, local Ca2+ events, and IKCa channels, reducing arteriolar tone. *Proc.Natl.Acad.Sci.U.S.A, 109,* 18174-18179.

18. Banquet, S., Delannoy, E., Agouni, A., Dessy, C., Lacomme, S., Hubert, F. et al. (2011). Role of G(i/o)-Src kinase-PI3K/Akt pathway and caveolin-1 in beta(2)-adrenoceptor coupling to endothelial NO synthase in mouse pulmonary artery. *Cell Signal., 23,* 1136-1143.

19. Barry, G. D., Suen, J. Y., Le, G. T., Cotterell, A., Reid, R. C., & Fairlie, D. P. (2010). Novel agonists and antagonists for human protease activated receptor 2. *J Med.Chem., 53,* 7428-7440.

20. Behringer, E. J. & Segal, S. S. (2012). Spreading the signal for vasodilatation: implications for skeletal muscle blood flow control and the effects of ageing. *J.Physiol, 590,* 6277-6284.

21. Beleznai, T., Takano, H., Hamill, C., Yarova, P., Douglas, G., Channon, K. et al. (2011). Enhanced K(+)-channel-mediated endothelium-dependent local and conducted dilation of small mesenteric arteries from ApoE(-/-) mice. *Cardiovasc.Res., 92,* 199-208.

22. Berstein, G., Blank, J. L., Smrcka, A. V., Higashijima, T., Sternweis, P. C., Exton, J. H. et al. (1992). Reconstitution of agonist-stimulated phosphatidylinositol 4,5-bisphosphate hydrolysis using purified m1 muscarinic receptor, Gq/11, and phospholipase C-beta 1. *J Biol.Chem., 267,* 8081-8088.

23. Bevers, L. M., Braam, B., Post, J. A., van Zonneveld, A. J., Rabelink, T. J., Koomans, H. A. et al. (2006). Tetrahydrobiopterin, but not L-arginine, decreases NO synthase uncoupling in cells expressing high levels of endothelial NO synthase. *Hypertension, 47,* 87-94.

24. Bintig, W., Begandt, D., Schlingmann, B., Gerhard, L., Pangalos, M., Dreyer, L. et al. (2012). Purine receptors and Ca(2+) signalling in the human blood-brain barrier endothelial cell line hCMEC/D3. *Purinergic.Signal., 8,* 71-80.

25. Bishara, N. B., Murphy, T. V., & Hill, M. A. (2002). Capacitative Ca(2+) entry in vascular endothelial cells is mediated via pathways sensitive to 2 aminoethoxydiphenyl borate and xestospongin C. *Br.J.Pharmacol., 135,* 119-128.

26. Bkaily, G., Sleiman, S., Stephan, J., Asselin, C., Choufani, S., Kamal, M. et al. (2003). Angiotensin II AT1 receptor internalization, translocation and de novo synthesis modulate cytosolic and nuclear calcium in human vascular smooth muscle cells. *Can.J Physiol Pharmacol., 81,* 274-287.

27. Bohm, S. K., Khitin, L. M., Grady, E. F., Aponte, G., Payan, D. G., & Bunnett, N. W. (1996). Mechanisms of desensitization and resensitization of proteinase-activated receptor-2. *J.Biol.Chem., 271,* 22003-22016.

28. Boitano, S., Flynn, A. N., Schulz, S. M., Hoffman, J., Price, T. J., & Vagner, J. (2011). Potent agonists of the protease activated receptor 2 (PAR2). *J.Med.Chem., 54,* 1308-1313.

29. Bolton, T. B., Lang, R. J., & Takewaki, T. (1984). Mechanisms of action of noradrenaline and carbachol on smooth muscle of guinea-pig anterior mesenteric artery. *J.Physiol, 351,* 549-572.

30. Brass, L. F. & Molino, M. (1997). Protease-activated G protein-coupled receptors on human platelets and endothelial cells. *Thromb.Haemost., 78,* 234-241.

31. Bretschneider, E., Spanbroek, R., Lotzer, K., Habenicht, A. J., & Schror, K. (2003). Evidence for functionally active protease-activated receptor-3 (PAR-3) in human vascular smooth muscle cells. *Thromb.Haemost., 90,* 704-709.

32. Browning, K. N. (2010). Protease-activated receptors: novel central role in modulation of gastric functions. *Neurogastroenterol.Motil., 22,* 361-365.

33. Brunt, V. E. & Minson, C. T. (2012). KCa channels and epoxyeicosatrienoic acids: major contributors to thermal hyperaemia in human skin. *J.Physiol, 590,* 3523-3534.

34. Budel, S., Schuster, A., Stergiopoulos, N., Meister, J. J., & Beny, J. L. (2001). Role of smooth muscle cells on endothelial cell cytosolic free calcium in porcine coronary arteries. *Am.J.Physiol Heart Circ.Physiol, 281,* H1156-H1162.

35. Burdyga, T., Shmygol, A., Eisner, D. A., & Wray, S. (2003). A new technique for simultaneous and in situ measurements of Ca2+ signals in arteriolar smooth muscle and endothelial cells. *Cell Calcium, 34,* 27-33.

36. Caliman, I. F., Lamas, A. Z., Dalpiaz, P. L., Medeiros, A. R., Abreu, G. R., Figueiredo, S. G. et al. (2013). Endothelial relaxation mechanisms and oxidative stress are restored by atorvastatin therapy in ovariectomized rats. *PLoS.One., 8,* e80892.

37. Canto, I., Soh, U. J., & Trejo, J. (2012). Allosteric modulation of protease-activated receptor signaling. *Mini.Rev.Med.Chem., 12,* 804-811.

38. Carey, R. M. (2013). Newly discovered components and actions of the renin-angiotensin system. *Hypertension, 62,* 818-822.

39. Carr, M. J., Schechter, N. M., & Undem, B. J. (2000). Trypsin-induced, neurokinin-mediated contraction of guinea pig bronchus. *Am.J.Respir.Crit Care Med., 162,* 1662-1667.

40. Cheang, W. S., Wong, W. T., Shen, B., Lau, C. W., Tian, X. Y., Tsang, S. Y. et al. (2010). 4-aminopyridine-sensitive K+ channels contributes to NaHS-induced membrane hyperpolarization and relaxation in the rat coronary artery. *Vascul.Pharmacol., 53,* 94-98.

41. Chen, G., Suzuki, H., & Weston, A. H. (1988). Acetylcholine releases endothelium-derived hyperpolarizing factor and EDRF from rat blood vessels. *Br.J.Pharmacol., 95,* 1165-1174.

42. Chen, K., Fu, C., Chen, C., Liu, L., Ren, H., Han, Y. et al. (2013). Role of GRK4 in the Regulation of Arterial AT1 Receptor in Hypertension. *Hypertension*.

43. Chen, X., Li, Y., Hollenberg, M., Triggle, C. R., & Ding, H. (2012). The contribution of d-tubocurarine-sensitive and apamin-sensitive K-channels to EDHF-mediated relaxation of mesenteric arteries from eNOS-/- mice. *J.Cardiovasc.Pharmacol., 59,* 413-425.

44. Chen, Y., Yang, C., & Wang, Z. J. (2011). Proteinase-activated receptor 2 sensitizes transient receptor potential vanilloid 1, transient receptor potential vanilloid 4, and transient receptor potential ankyrin 1 in paclitaxel-induced neuropathic pain. *Neuroscience, 193*, 440-451.

45. Cheng, H. & Lederer, W. J. (2008). Calcium sparks. *Physiol Rev, 88*, 1491-1545.

46. Chia, E., Kagota, S., Wijekoon, E. P., & McGuire, J. J. (2011). Protection of protease-activated receptor 2 mediated vasodilatation against angiotensin II-induced vascular dysfunction in mice. *BMC.Pharmacol., 11*, 10.

47. Cleator, J. H., Zhu, W. Q., Vaughan, D. E., & Hamm, H. E. (2006). Differential regulation of endothelial exocytosis of P-selectin and von Willebrand factor by protease-activated receptors and cAMP. *Blood, 107*, 2736-2744.

48. Climent, B., Schubert, R., Stankevicius, E., Garcia-Sacristan, A., Simonsen, U., & Rivera, L. (2012). Large conductance Ca2+-activated K+ channels modulate endothelial cell outward currents and nitric oxide release in the intact rat superior mesenteric artery. *Biochem.Biophys.Res.Commun., 417*, 1007-1013.

49. Cottrell, G. S., Amadesi, S., Grady, E. F., & Bunnett, N. W. (2004). Trypsin IV, a novel agonist of protease-activated receptors 2 and 4. *J.Biol.Chem., 279*, 13532-13539.

50. Craig, J. & Martin, W. (2012). Dominance of flow-mediated constriction over flow-mediated dilatation in the rat carotid artery. *Br.J.Pharmacol., 167*, 527-536.

51. Crane, G. J., Gallagher, N., Dora, K. A., & Garland, C. J. (2003). Small- and intermediate-conductance calcium-activated K+ channels provide different facets of endothelium-dependent hyperpolarization in rat mesenteric artery. *J.Physiol, 553*, 183-189.

52. Csanyi, G., Bauer, M., Dietl, W., Lomnicka, M., Stepuro, T., Podesser, B. K. et al. (2006). Functional alterations in NO, PGI2 and EDHF pathways in the aortic endothelium after myocardial infarction in rats. *Eur.J.Heart Fail., 8*, 769-776.

53. D'Andrea, M. R., Derian, C. K., Leturcq, D., Baker, S. M., Brunmark, A., Ling, P. et al. (1998). Characterization of protease-activated receptor-2 immunoreactivity in normal human tissues. *J.Histochem.Cytochem., 46*, 157-164.

54. Dauphin, F. & Hamel, E. (1990). Muscarinic receptor subtype mediating vasodilation feline middle cerebral artery exhibits M3 pharmacology. *Eur.J.Pharmacol., 178*, 203-213.

55. Dawson, K., Wu, C. T., Qi, X. Y., & Nattel, S. (2012). Congestive heart failure effects on atrial fibroblast phenotype: differences between freshly-isolated and cultured cells. *PLoS.One., 7*, e52032.

56. Deanfield, J. E., Halcox, J. P., & Rabelink, T. J. (2007). Endothelial function and dysfunction: testing and clinical relevance. *Circulation, 115,* 1285-1295.

57. Defea, K., Schmidlin, F., Dery, O., Grady, E. F., & Bunnett, N. W. (2000). Mechanisms of initiation and termination of signalling by neuropeptide receptors: a comparison with the proteinase-activated receptors. *Biochem.Soc.Trans., 28,* 419-426.

58. Dery, O., Thoma, M. S., Wong, H., Grady, E. F., & Bunnett, N. W. (1999). Trafficking of proteinase-activated receptor-2 and beta-arrestin-1 tagged with green fluorescent protein. beta-Arrestin-dependent endocytosis of a proteinase receptor. *J.Biol.Chem., 274,* 18524-18535.

59. Desai, K. M., Gopalakrishnan, V., Hiebert, L. M., McNeill, J. R., & Wilson, T. W. (2006). EDHF-mediated rapid restoration of hypotensive response to acetylcholine after chronic, but not acute, nitric oxide synthase inhibition in rats. *Eur.J.Pharmacol., 546,* 120-126.

60. Dong, Y., Watabe, H., Cui, J., Abe, S., Sato, N., Ishikawa, H. et al. (2010). Reduced effects of endothelium-derived hyperpolarizing factor in ocular ciliary arteries from spontaneous hypertensive rats. *Exp.Eye Res., 90,* 324-329.

61. Dora, K. A. (2010). Coordination of vasomotor responses by the endothelium. *Circ.J., 74,* 226-232.

62. Dora, K. A., Gallagher, N. T., McNeish, A., & Garland, C. J. (2008). Modulation of endothelial cell KCa3.1 channels during endothelium-derived hyperpolarizing factor signaling in mesenteric resistance arteries. *Circ.Res., 102,* 1247-1255.

63. Edwards, D. H., Chaytor, A. T., Bakker, L. M., & Griffith, T. M. (2007). Modulation of gap-junction-dependent arterial relaxation by ascorbic acid. *J.Vasc.Res., 44,* 410-422.

64. Edwards, F. R. & Hirst, G. D. (1988). Inward rectification in submucosal arterioles of guinea-pig ileum. *J.Physiol, 404,* 437-454.

65. Edwards, G., Dora, K. A., Gardener, M. J., Garland, C. J., & Weston, A. H. (1998). K+ is an endothelium-derived hyperpolarizing factor in rat arteries. *Nature, 396,* 269-272.

66. Edwards, G. & Weston, A. H. (2004). Potassium and potassium clouds in endothelium-dependent hyperpolarizations. *Pharmacol.Res., 49,* 535-541.

67. Endemann, D. H. & Schiffrin, E. L. (2004). Endothelial dysfunction. *J Am Soc.Nephrol., 15,* 1983-1992.

68. Favaloro, J. L. & Kemp-Harper, B. K. (2009). Redox variants of NO (NO{middle dot} and HNO) elicit vasorelaxation of resistance arteries via distinct mechanisms. *Am.J.Physiol Heart Circ.Physiol, 296,* H1274-H1280.

69. Feletou, M., Kohler, R., & Vanhoutte, P. M. (2012). Nitric oxide: orchestrator of endothelium-dependent responses. *Ann.Med., 44,* 694-716.

70. Feletou, M. & Vanhoutte, P. M. (2006). Endothelium-derived hyperpolarizing factor: where are we now? *Arterioscler.Thromb.Vasc.Biol., 26,* 1215-1225.

71. Fernandez-Alfonso, M. S., Gil-Ortega, M., Garcia-Prieto, C. F., Aranguez, I., Ruiz-Gayo, M., & Somoza, B. (2013). Mechanisms of Perivascular Adipose Tissue Dysfunction in Obesity. *Int.J Endocrinol., 2013,* 402053.

72. Ferrell, W. R., Lockhart, J. C., Kelso, E. B., Dunning, L., Plevin, R., Meek, S. E. et al. (2003). Essential role for proteinase-activated receptor-2 in arthritis. *J.Clin.Invest, 111,* 35-41.

73. Fletcher, P. A., Scriven, D. R., Schulson, M. N., & Moore, E. D. (2010). Multi-image colocalization and its statistical significance. *Biophys.J, 99,* 1996-2005.

74. Foskett, J. K., White, C., Cheung, K. H., & Mak, D. O. (2007). Inositol trisphosphate receptor Ca2+ release channels. *Physiol Rev., 87,* 593-658.

75. Furchgott, R. F. & Zawadzki, J. V. (1980). The obligatory role of endothelial cells in the relaxation of arterial smooth muscle by acetylcholine. *Nature, 288,* 373-376.

76. Gafni, J., Munsch, J. A., Lam, T. H., Catlin, M. C., Costa, L. G., Molinski, T. F. et al. (1997). Xestospongins: potent membrane permeable blockers of the inositol 1,4,5-trisphosphate receptor. *Neuron, 19,* 723-733.

77. Gangopadhyay, J. P. & Ikemoto, N. (2010). Intracellular translocation of calmodulin and Ca2+/calmodulin-dependent protein kinase II during the development of hypertrophy in neonatal cardiomyocytes. *Biochem.Biophys.Res.Commun., 396,* 515-521.

78. Gao, P., Xu, T. T., Lu, J., Li, L., Xu, J., Hao, D. L. et al. (2013). Overexpression of SIRT1 in vascular smooth muscle cells attenuates angiotensin II-induced vascular remodeling and hypertension in mice. *J Mol.Med (Berl).*

79. Gao, Y. J., Hirota, S., Zhang, D. W., Janssen, L. J., & Lee, R. M. (2003). Mechanisms of hydrogen-peroxide-induced biphasic response in rat mesenteric artery. *Br.J.Pharmacol., 138,* 1085-1092.

80. Gao, Y. J., Lu, C., Su, L. Y., Sharma, A. M., & Lee, R. M. (2007). Modulation of vascular function by perivascular adipose tissue: the role of endothelium and hydrogen peroxide. *Br.J.Pharmacol., 151,* 323-331.

81. Gardell, L. R., Ma, J. N., Seitzberg, J. G., Knapp, A. E., Schiffer, H. H., Tabatabaei, A. et al. (2008). Identification and characterization of novel small-molecule protease-activated receptor 2 agonists. *J.Pharmacol.Exp.Ther., 327,* 799-808.

82. Garland, C. J., Hiley, C. R., & Dora, K. A. (2011). EDHF: spreading the influence of the endothelium. *Br.J.Pharmacol., 164,* 839-852.

83. Garland, J. G. & McPherson, G. A. (1992). Evidence that nitric oxide does not mediate the hyperpolarization and relaxation to acetylcholine in the rat small mesenteric artery. *Br.J.Pharmacol., 105,* 429-435.

84. Gauthier, K. M., Liu, C., Popovic, A., Albarwani, S., & Rusch, N. J. (2002). Freshly isolated bovine coronary endothelial cells do not express the BK Ca channel gene. *J.Physiol, 545,* 829-836.

85. Giles, T. D., Sander, G. E., Nossaman, B. D., & Kadowitz, P. J. (2012). Impaired vasodilation in the pathogenesis of hypertension: focus on nitric oxide, endothelial-derived hyperpolarizing factors, and prostaglandins. *J.Clin.Hypertens.(Greenwich.), 14,* 198-205.

86. Gluais, P., Edwards, G., Weston, A. H., Falck, J. R., Vanhoutte, P. M., & Feletou, M. (2005). Role of SK(Ca) and IK(Ca) in endothelium-dependent hyperpolarizations of the guinea-pig isolated carotid artery. *Br.J.Pharmacol., 144,* 477-485.

87. Grayson, T. H., Haddock, R. E., Murray, T. P., Wojcikiewicz, R. J., & Hill, C. E. (2004). Inositol 1,4,5-trisphosphate receptor subtypes are differentially distributed between smooth muscle and endothelial layers of rat arteries. *Cell Calcium, 36,* 447-458.

88. Gu, Q. & Lee, L. Y. (2009). Effect of protease-activated receptor 2 activation on single TRPV1 channel activities in rat vagal pulmonary sensory neurons. *Exp.Physiol, 94,* 928-936.

89. Hamilton, C. A., Brosnan, M. J., Al-Benna, S., Berg, G., & Dominiczak, A. F. (2002). NAD(P)H oxidase inhibition improves endothelial function in rat and human blood vessels. *Hypertension, 40,* 755-762.

90. Hamilton, J. R., Frauman, A. G., & Cocks, T. M. (2001). Increased expression of protease-activated receptor-2 (PAR2) and PAR4 in human coronary artery by inflammatory stimuli unveils endothelium-dependent relaxations to PAR2 and PAR4 agonists. *Circ.Res., 89,* 92-98.

91. Hansen, K. K., Oikonomopoulou, K., Li, Y., & Hollenberg, M. D. (2008). Proteinases, proteinase-activated receptors (PARs) and the pathophysiology of cancer and diseases of the cardiovascular, musculoskeletal, nervous and gastrointestinal systems. *Naunyn Schmiedebergs Arch.Pharmacol., 377,* 377-392.

92. Haq, K. T., Daniels, R. E., Miller, L. S., Miura, M., ter Keurs, H. E., Bungay, S. D. et al. (2013). Evoked centripetal Ca(2+) mobilization in cardiac Purkinje cells: insight from a model of three Ca(2+) release regions. *J Physiol, 591,* 4301-4319.

93. Hasdemir, B., Murphy, J. E., Cottrell, G. S., & Bunnett, N. W. (2009). Endosomal deubiquitinating enzymes control ubiquitination and down-regulation of protease-activated receptor 2. *J.Biol.Chem., 284,* 28453-28466.

94. Hennessey, J. C. & McGuire, J. J. (2013). Attenuated vasodilator effectiveness of protease-activated receptor 2 agonist in heterozygous par2 knockout mice. *PLoS.One., 8,* e55965.

95. Herichova, I. & Szantoova, K. (2013). Renin-angiotensin system: upgrade of recent knowledge and perspectives. *Endocr.Regul., 47,* 39-52.

96. Higashi, Y., Kihara, Y., & Noma, K. (2012). Endothelial dysfunction and hypertension in aging. *Hypertens.Res., 35,* 1039-1047.

97. Hollenberg, M. D. (2003). Proteinase-mediated signaling: proteinase-activated receptors (PARs) and much more. *Life Sci., 74,* 237-246.

98. Hollenberg, M. D. & Compton, S. J. (2002). International Union of Pharmacology. XXVIII. Proteinase-activated receptors. *Pharmacol.Rev., 54,* 203-217.

99. Hollenberg, M. D., Saifeddine, M., & Al-Ani, B. (1996). Proteinase-activated receptor-2 in rat aorta: structural requirements for agonist activity of receptor-activating peptides. *Mol.Pharmacol., 49,* 229-233.

100. Hollenberg, M. D., Saifeddine, M., Al-Ani, B., & Kawabata, A. (1997). Proteinase-activated receptors: structural requirements for activity, receptor cross-reactivity, and receptor selectivity of receptor-activating peptides. *Can.J.Physiol Pharmacol., 75,* 832-841.

101. Hughes, K. H., Wijekoon, E. P., Valcour, J. E., Chia, E. W., & McGuire, J. J. (2013). Effects of chronic in-vivo treatments with protease-activated receptor 2 agonist on endothelium function and blood pressures in mice. *Can.J.Physiol Pharmacol., 91,* 295-305.

102. Huser, J. & Blatter, L. A. (1997). Elementary events of agonist-induced Ca2+ release in vascular endothelial cells. *Am.J.Physiol, 273,* C1775-C1782.

103. Isshiki, M., Mutoh, A., & Fujita, T. (2004). Subcortical Ca2+ waves sneaking under the plasma membrane in endothelial cells. *Circ.Res., 95,* e11-e21.

104. Jornot, L., Maechler, P., Wollheim, C. B., & Junod, A. F. (1999). Reactive oxygen metabolites increase mitochondrial calcium in endothelial cells: implication of the Ca2+/Na+ exchanger. *J.Cell Sci., 112 (Pt 7),* 1013-1022.

105. Joshi, S., Nelson, M. T., & Werner, M. E. (2012). Amplified NO/cGMP-mediated relaxation and ryanodine receptor-to-BKCa channel signalling in corpus cavernosum smooth muscle from phospholamban knockout mice. *Br.J.Pharmacol., 165,* 455-466.

106. Kagota, S., Chia, E., & McGuire, J. J. (2011). Preserved arterial vasodilatation via endothelial protease-activated receptor-2 in obese type 2 diabetic mice. *Br.J Pharmacol., 164,* 358-371.

107. Kahn, M. L., Zheng, Y. W., Huang, W., Bigornia, V., Zeng, D., Moff, S. et al. (1998). A dual thrombin receptor system for platelet activation. *Nature, 394,* 690-694.

108. Kameritsch, P., Pogoda, K., Ritter, A., Munzing, S., & Pohl, U. (2012). Gap junctional communication controls the overall endothelial calcium response to vasoactive agonists. *Cardiovasc.Res., 93,* 508-515.

109. Kanikarla-Marie, P. & Jain, S. K. (2014). L-Cysteine supplementation reduces high-glucose and ketone-induced adhesion of monocytes to endothelial cells by inhibiting ROS. *Mol.Cell Biochem.*.

110. Kanke, T., Kabeya, M., Kubo, S., Kondo, S., Yasuoka, K., Tagashira, J. et al. (2009). Novel antagonists for proteinase-activated receptor 2: inhibition of cellular and vascular responses in vitro and in vivo. *Br.J.Pharmacol., 158,* 361-371.

111. Karashima, T. & Kuriyama, H. (1981). Electrical properties of smooth muscle cell membrane and neuromuscular transmission in the guinea-pig basilar artery. *Br.J.Pharmacol., 74,* 495-504.

112. Kassmann, M., Harteneck, C., Zhu, Z., Nurnberg, B., Tepel, M., & Gollasch, M. (2013). Transient receptor potential vanilloid 1 (TRPV1), TRPV4, and the kidney. *Acta Physiol (Oxf), 207,* 546-564.

113. Kawabata, A., Kanke, T., Yonezawa, D., Ishiki, T., Saka, M., Kabeya, M. et al. (2004a). Potent and metabolically stable agonists for protease-activated receptor-2: evaluation of activity in multiple assay systems in vitro and in vivo. *J.Pharmacol.Exp.Ther., 309,* 1098-1107.

114. Kawabata, A., Nakaya, Y., Ishiki, T., Kubo, S., Kuroda, R., Sekiguchi, F. et al. (2004b). Receptor-activating peptides for PAR-1 and PAR-2 relax rat gastric artery via multiple mechanisms. *Life Sci., 75,* 2689-2702.

115. Kawao, N., Hiramatsu, K., Inoi, N., Kuroda, R., Nishikawa, H., Sekiguchi, F. et al. (2003). The PAR-1-activating peptide facilitates pepsinogen secretion in rats. *Peptides, 24,* 1449-1451.

116. Kelso, E. B., Lockhart, J. C., Hembrough, T., Dunning, L., Plevin, R., Hollenberg, M. D. et al. (2006). Therapeutic promise of proteinase-activated receptor-2 antagonism in joint inflammation. *J.Pharmacol.Exp.Ther., 316,* 1017-1024.

117. Kerr, P. M., Tam, R., Ondrusova, K., Mittal, R., Narang, D., Tran, C. H. et al. (2012). Endothelial feedback and the myoendothelial projection. *Microcirculation., 19,* 416-422.

118. Khambata, R. S., Panayiotou, C. M., & Hobbs, A. J. (2011). Natriuretic peptide receptor-3 underpins the disparate regulation of endothelial and vascular smooth muscle cell proliferation by C-type natriuretic peptide. *Br.J.Pharmacol., 164,* 584-597.

119. Khan, I., Sandhu, V., Misquitta, C. M., & Grover, A. K. (2000). SERCA pump isoform expression in endothelium of veins and arteries: every endothelium is not the same. *Mol.Cell Biochem., 203,* 11-15.

120. Knot, H. J., Zimmermann, P. A., & Nelson, M. T. (1996). Extracellular K(+)-induced hyperpolarizations and dilatations of rat coronary and cerebral arteries involve inward rectifier K(+) channels. *J.Physiol, 492 (Pt 2),* 419-430.

121. Lassegue, B., Alexander, R. W., Nickenig, G., Clark, M., Murphy, T. J., & Griendling, K. K. (1995). Angiotensin II down-regulates the vascular smooth muscle AT1 receptor by transcriptional and post-transcriptional mechanisms: evidence for homologous and heterologous regulation. *Mol.Pharmacol., 48,* 601-609.

122. Ledoux, J., Taylor, M. S., Bonev, A. D., Hannah, R. M., Solodushko, V., Shui, B. et al. (2008). Functional architecture of inositol 1,4,5-trisphosphate signaling in restricted spaces of myoendothelial projections. *Proc.Natl.Acad.Sci.U.S.A, 105,* 9627-9632.

123. Lee, H. & Hamilton, J. R. (2012a). Physiology, pharmacology, and therapeutic potential of protease-activated receptors in vascular disease. *Pharmacol.Ther., 134,* 246-259.

124. Lee, H. J., Yang, Y. M., Kim, K., Shin, D. M., Yoon, J. H., Cho, H. J. et al. (2012b). Protease-activated receptor 2 mediates mucus secretion in the airway submucosal gland. *PLoS.One., 7,* e43188.

125. Leung, H. S., Leung, F. P., Yao, X., Ko, W. H., Chen, Z. Y., Vanhoutte, P. M. et al. (2006). Endothelial mediators of the acetylcholine-induced relaxation of the rat femoral artery. *Vascul.Pharmacol., 44,* 299-308.

126. Li, C., Li, Q. Y., Liao, S. P., Jiang, R. J., Kong, H., Lai, J. C. et al. (2010). [Vasodilatory effects of CNP on aortic arteries of rabbits]. *Sichuan.Da.Xue.Xue.Bao.Yi.Xue.Ban., 41,* 767-770.

127. Liang, G. H., Xi, Q., Leffler, C. W., & Jaggar, J. H. (2012). Hydrogen sulfide activates Ca(2)(+) sparks to induce cerebral arteriole dilatation. *J.Physiol, 590,* 2709-2720.

128. Liu, Y., Bubolz, A. H., Mendoza, S., Zhang, D. X., & Gutterman, D. D. (2011). H2O2 is the transferrable factor mediating flow-induced dilation in human coronary arterioles. *Circ.Res., 108,* 566-573.

129. Lohman, R. J., Cotterell, A. J., Suen, J., Liu, L., Do, A. T., Vesey, D. A. et al. (2012). Antagonism of protease-activated receptor 2 protects against experimental colitis. *J.Pharmacol.Exp.Ther., 340,* 256-265.

130. Lopez-Miranda, V., Dannert, M. T., Herradon, E., Alsasua, A., & Martin, M. I. (2010). Cytochrome P450 pathway contributes to methanandamide-induced vasorelaxation in rat aorta. *Cardiovasc.Drugs Ther., 24,* 379-389.

131. Ma, X., Cao, J., Luo, J., Nilius, B., Huang, Y., Ambudkar, I. S. et al. (2010). Depletion of intracellular Ca2+ stores stimulates the translocation of vanilloid transient receptor potential 4-c1 heteromeric channels to the plasma membrane. *Arterioscler.Thromb.Vasc.Biol., 30,* 2249-2255.

132. Macfarlane, S. R., Seatter, M. J., Kanke, T., Hunter, G. D., & Plevin, R. (2001). Proteinase-activated receptors. *Pharmacol.Rev., 53,* 245-282.

133. Marchesi, C., Rehman, A., Rautureau, Y., Kasal, D. A., Briet, M., Leibowitz, A. et al. (2013). Protective role of vascular smooth muscle cell PPARgamma in angiotensin II-induced vascular disease. *Cardiovasc.Res., 97,* 562-570.

134. Marie, I. & Beny, J. L. (2002). Calcium imaging of murine thoracic aorta endothelium by confocal microscopy reveals inhomogeneous distribution of endothelial cells responding to vasodilator agents. *J.Vasc.Res., 39,* 260-267.

135. Mather, S., Dora, K. A., Sandow, S. L., Winter, P., & Garland, C. J. (2005). Rapid endothelial cell-selective loading of connexin 40 antibody blocks endothelium-derived hyperpolarizing factor dilation in rat small mesenteric arteries. *Circ.Res., 97,* 399-407.

136. McGuire JJ, Gui Y, Wang X, Loutzenhiser RD, Triggle CR, & Hollenberg MD (2002). Proteinase-activated receptor-2 (PAR2): release of an endothelium-derived hyperpolarizing factor distinct from that released by acetylcholine. In Vanhoutte PM (Ed.), *EDHF* (pp. 47-54). London: Taylor & Francis.

137. McGuire, J. J. (2004). Proteinase-activated Receptor 2 (PAR2): a challenging new target for treatment of vascular diseases. *Curr.Pharm.Des, 10,* 2769-2778.

138. McGuire, J. J., Hollenberg, M. D., Bennett, B. M., & Triggle, C. R. (2004a). Hyperpolarization of murine small caliber mesenteric arteries by activation of

endothelial proteinase-activated receptor 2. *Can.J.Physiol Pharmacol., 82,* 1103-1112.

139. McGuire, J. J., Hollenberg, M. D., ndrade-Gordon, P., & Triggle, C. R. (2002). Multiple mechanisms of vascular smooth muscle relaxation by the activation of proteinase-activated receptor 2 in mouse mesenteric arterioles. *Br.J.Pharmacol., 135,* 155-169.

140. McGuire, J. J., Saifeddine, M., Triggle, C. R., Sun, K., & Hollenberg, M. D. (2004b). 2-furoyl-LIGRLO-amide: a potent and selective proteinase-activated receptor 2 agonist. *J.Pharmacol.Exp.Ther., 309,* 1124-1131.

141. McGuire, J. J., Van Vliet, B. N., Gimenez, J., King, J. C., & Halfyard, S. J. (2007). Persistence of PAR-2 vasodilation despite endothelial dysfunction in BPH/2 hypertensive mice. *Pflugers Arch., 454,* 535-543.

142. McGuire, J. J., Van Vliet, B. N., & Halfyard, S. J. (2008). Blood pressures, heart rate and locomotor activity during salt loading and angiotensin II infusion in protease-activated receptor 2 (PAR2) knockout mice. *BMC.Physiol, 8,* 20.

143. McLean, P. G., Aston, D., Sarkar, D., & Ahluwalia, A. (2002). Protease-activated receptor-2 activation causes EDHF-like coronary vasodilation: selective preservation in ischemia/reperfusion injury: involvement of lipoxygenase products, VR1 receptors, and C-fibers. *Circ.Res., 90,* 465-472.

144. McNeish, A. J., Dora, K. A., & Garland, C. J. (2005). Possible role for K+ in endothelium-derived hyperpolarizing factor-linked dilatation in rat middle cerebral artery. *Stroke, 36,* 1526-1532.

145. Mendoza, S. A., Fang, J., Gutterman, D. D., Wilcox, D. A., Bubolz, A. H., Li, R. et al. (2010). TRPV4-mediated endothelial Ca2+ influx and vasodilation in response to shear stress. *Am.J.Physiol Heart Circ.Physiol, 298,* H466-H476.

146. Misaki, T., Satoh, Y., Saino, T., & Ogawa, A. (2006). The role of protease-activated receptors on the intracellular calcium ion dynamics of vascular smooth muscles, with special reference to cerebral arterioles. *Arch.Histol.Cytol., 69,* 49-60.

147. Mollnau, H., Wendt, M., Szocs, K., Lassegue, B., Schulz, E., Oelze, M. et al. (2002). Effects of angiotensin II infusion on the expression and function of NAD(P)H oxidase and components of nitric oxide/cGMP signaling. *Circ.Res., 90,* E58-E65.

148. Mountian, I., Manolopoulos, V. G., De, S. H., Parys, J. B., Missiaen, L., & Wuytack, F. (1999). Expression patterns of sarco/endoplasmic reticulum Ca(2+)-ATPase and inositol 1,4,5-trisphosphate receptor isoforms in vascular endothelial cells. *Cell Calcium, 25,* 371-380.

149. Mukohda, M., Morita, T., Okada, M., Hara, Y., & Yamawaki, H. (2013). Long-term methylglyoxal treatment causes endothelial dysfunction of rat isolated mesenteric artery. *J Vet.Med Sci., 75,* 151-157.

150. Mumtaz, S., Burdyga, G., Borisova, L., Wray, S., & Burdyga, T. (2011). The mechanism of agonist induced Ca2+ signalling in intact endothelial cells studied confocally in in situ arteries. *Cell Calcium, 49,* 66-77.

151. Murad, F., Waldman, S., Molina, C., Bennett, B., & Leitman, D. (1987). Regulation and role of guanylate cyclase-cyclic GMP in vascular relaxation. *Prog.Clin.Biol.Res., 249,* 65-76.

152. Mustafa, A. K., Sikka, G., Gazi, S. K., Steppan, J., Jung, S. M., Bhunia, A. K. et al. (2011). Hydrogen sulfide as endothelium-derived hyperpolarizing factor sulfhydrates potassium channels. *Circ.Res., 109,* 1259-1268.

153. Mutoh, A., Isshiki, M., & Fujita, T. (2008). Aldosterone enhances ligand-stimulated nitric oxide production in endothelial cells. *Hypertens.Res., 31,* 1811-1820.

154. Nakayama, T., Hirano, K., Nishimura, J., Takahashi, S., & Kanaide, H. (2001). Mechanism of trypsin-induced endothelium-dependent vasorelaxation in the porcine coronary artery. *Br.J.Pharmacol., 134,* 815-826.

155. Naser, N., Januszewski, A. S., Brown, B. E., Jenkins, A. J., Hill, M. A., & Murphy, T. V. (2013). Advanced glycation end products acutely impair ca(2+) signaling in bovine aortic endothelial cells. *Front Physiol, 4,* 38.

156. Nausch, L. W., Bonev, A. D., Heppner, T. J., Tallini, Y., Kotlikoff, M. I., & Nelson, M. T. (2012). Sympathetic nerve stimulation induces local endothelial Ca2+ signals to oppose vasoconstriction of mouse mesenteric arteries. *Am J Physiol Heart Circ.Physiol, 302,* H594-H602.

157. Nistri, S., Di Cesare, M. L., Mazzetti, L., Feil, R., Bani, D., & Failli, P. (2012). Restoring nitric oxide cytosolic calcium regulation by cyclic guanosine monophosphate protein kinase I alpha transfection in coronary endothelial cells of spontaneously hypertensive rats. *J.Vasc.Res., 49,* 221-230.

158. Nystedt, S., Emilsson, K., Larsson, A. K., Strombeck, B., & Sundelin, J. (1995). Molecular cloning and functional expression of the gene encoding the human proteinase-activated receptor 2. *Eur.J.Biochem., 232,* 84-89.

159. Nystedt, S., Emilsson, K., Wahlestedt, C., & Sundelin, J. (1994). Molecular cloning of a potential proteinase activated receptor. *Proc.Natl.Acad.Sci.U.S.A, 91,* 9208-9212.

160. Ohashi, M., Faraci, F., & Heistad, D. (2005). Peroxynitrite hyperpolarizes smooth muscle and relaxes internal carotid artery in rabbit via ATP-sensitive K+ channels. *Am.J.Physiol Heart Circ.Physiol, 289,* H2244-H2250.

161. Ohata, H., Yamada, H., Niioka, T., Yamamoto, M., & Momose, K. (2003). Optical bioimaging: from living tissue to a single molecule: calcium imaging in blood vessel in situ employing two-photon excitation fluorescence microscopy. *J.Pharmacol.Sci., 93,* 242-247.

162. Oishi, H., Budel, S., Schuster, A., Stergiopulos, N., Meister, J. J., & Beny, J. L. (2001). Cytosolic-free calcium in smooth-muscle and endothelial cells in an intact arterial wall from rat mesenteric artery in vitro. *Cell Calcium, 30,* 261-267.

163. Parisi, V. M. & Rankin, J. H. (1985). The effect of prostacyclin on angiotensin II-induced placental vasoconstriction. *Am J Obstet.Gynecol., 151,* 444-449.

164. Patel, B. M. & Mehta, A. A. (2012). Aldosterone and angiotensin: Role in diabetes and cardiovascular diseases. *Eur.J Pharmacol., 697,* 1-12.

165. Perez, G. J., Bonev, A. D., Patlak, J. B., & Nelson, M. T. (1999). Functional coupling of ryanodine receptors to KCa channels in smooth muscle cells from rat cerebral arteries. *J.Gen.Physiol, 113,* 229-238.

166. Phan, M. N., Leddy, H. A., Votta, B. J., Kumar, S., Levy, D. S., Lipshutz, D. B. et al. (2009). Functional characterization of TRPV4 as an osmotically sensitive ion channel in porcine articular chondrocytes. *Arthritis Rheum., 60,* 3028-3037.

167. Plane, F. & Garland, C. J. (1993). Differential effects of acetylcholine, nitric oxide and levcromakalim on smooth muscle membrane potential and tone in the rabbit basilar artery. *Br.J.Pharmacol., 110,* 651-656.

168. Poole, D. P., Amadesi, S., Veldhuis, N. A., Abogadie, F. C., Lieu, T., Darby, W. et al. (2013). Protease-activated Receptor 2 (PAR2) Protein and Transient Receptor Potential Vanilloid 4 (TRPV4) Protein Coupling Is Required for Sustained Inflammatory Signaling. *J.Biol.Chem., 288,* 5790-5802.

169. Pueyo, M. E., Arnal, J. F., Rami, J., & Michel, J. B. (1998). Angiotensin II stimulates the production of NO and peroxynitrite in endothelial cells. *Am J Physiol, 274,* C214-C220.

170. Rajagopalan, S., Kurz, S., Munzel, T., Tarpey, M., Freeman, B. A., Griendling, K. K. et al. (1996). Angiotensin II-mediated hypertension in the rat increases vascular superoxide production via membrane NADH/NADPH oxidase activation. Contribution to alterations of vasomotor tone. *J Clin.Invest, 97,* 1916-1923.

171. Ramachandran, R., Eissa, A., Mihara, K., Oikonomopoulou, K., Saifeddine, M., Renaux, B. et al. (2012a). Proteinase-activated receptors (PARs): differential

signalling by kallikrein-related peptidases KLK8 and KLK14. *Biol.Chem., 393,* 421-427.

172. Ramachandran, R., Mihara, K., Chung, H., Renaux, B., Lau, C. S., Muruve, D. A. et al. (2011). Neutrophil elastase acts as a biased agonist for proteinase-activated receptor-2 (PAR2). *J.Biol.Chem., 286,* 24638-24648.

173. Ramachandran, R., Noorbakhsh, F., Defea, K., & Hollenberg, M. D. (2012b). Targeting proteinase-activated receptors: therapeutic potential and challenges. *Nat.Rev.Drug Discov., 11,* 69-86.

174. Rhee, S. G. (2006). Cell signaling. H2O2, a necessary evil for cell signaling. *Science, 312,* 1882-1883.

175. Ricks, T. K. & Trejo, J. (2009). Phosphorylation of protease-activated receptor-2 differentially regulates desensitization and internalization. *J.Biol.Chem., 284,* 34444-34457.

176. Roosterman, D., Schmidlin, F., & Bunnett, N. W. (2003). Rab5a and rab11a mediate agonist-induced trafficking of protease-activated receptor 2. *Am.J.Physiol Cell Physiol, 284,* C1319-C1329.

177. Saliez, J., Bouzin, C., Rath, G., Ghisdal, P., Desjardins, F., Rezzani, R. et al. (2008). Role of caveolar compartmentation in endothelium-derived hyperpolarizing factor-mediated relaxation: Ca2+ signals and gap junction function are regulated by caveolin in endothelial cells. *Circulation, 117,* 1065-1074.

178. Sandow, S. L., Goto, K., Rummery, N. M., & Hill, C. E. (2004). Developmental changes in myoendothelial gap junction mediated vasodilator activity in the rat saphenous artery. *J.Physiol, 556,* 875-886.

179. Sandow, S. L., Gzik, D. J., & Lee, R. M. (2009). Arterial internal elastic lamina holes: relationship to function? *J.Anat., 214,* 258-266.

180. Sandow, S. L., Neylon, C. B., Chen, M. X., & Garland, C. J. (2006). Spatial separation of endothelial small- and intermediate-conductance calcium-activated potassium channels (K(Ca)) and connexins: possible relationship to vasodilator function? *J.Anat., 209,* 689-698.

181. Schiessl, I. M. & Castrop, H. (2013). Angiotensin II AT2 receptor activation attenuates AT1 receptor-induced increases in the glomerular filtration of albumin: a multiphoton microscopy study. *Am J Physiol Renal Physiol, 305,* F1189-F1200.

182. Schroder, K., Zhang, M., Benkhoff, S., Mieth, A., Pliquett, R., Kosowski, J. et al. (2012). Nox4 is a protective reactive oxygen species generating vascular NADPH oxidase. *Circ.Res., 110,* 1217-1225.

183. Scriven, D. R., Klimek, A., Asghari, P., Bellve, K., & Moore, E. D. (2005). Caveolin-3 is adjacent to a group of extradyadic ryanodine receptors. *Biophys.J, 89,* 1893-1901.

184. Scriven, D. R., Lynch, R. M., & Moore, E. D. (2008). Image acquisition for colocalization using optical microscopy. *Am J Physiol Cell Physiol, 294,* C1119-C1122.

185. Seatter, M. J., Drummond, R., Kanke, T., Macfarlane, S. R., Hollenberg, M. D., & Plevin, R. (2004). The role of the C-terminal tail in protease-activated receptor-2-mediated Ca2+ signalling, proline-rich tyrosine kinase-2 activation, and mitogen-activated protein kinase activity. *Cell Signal., 16,* 21-29.

186. Sevigny, L. M., Zhang, P., Bohm, A., Lazarides, K., Perides, G., Covic, L. et al. (2011). Interdicting protease-activated receptor-2-driven inflammation with cell-penetrating pepducins. *Proc.Natl.Acad.Sci.U.S.A, 108,* 8491-8496.

187. Shimokawa, H., Yasutake, H., Fujii, K., Owada, M. K., Nakaike, R., Fukumoto, Y. et al. (1996). The importance of the hyperpolarizing mechanism increases as the vessel size decreases in endothelium-dependent relaxations in rat mesenteric circulation. *J.Cardiovasc.Pharmacol., 28,* 703-711.

188. Silva, B. R., Pernomian, L., & Bendhack, L. M. (2012). Contribution of oxidative stress to endothelial dysfunction in hypertension. *Front Physiol, 3,* 441.

189. Skovgaard, N., Gouliaev, A., Aalling, M., & Simonsen, U. (2011). The role of endogenous H2S in cardiovascular physiology. *Curr.Pharm.Biotechnol., 12,* 1385-1393.

190. Smeda, J. S., McGuire, J. J., & Daneshtalab, N. (2010). Protease-activated receptor 2 and bradykinin-mediated vasodilation in the cerebral arteries of stroke-prone rats. *Peptides, 31,* 227-237.

191. Socha, M. J., Domeier, T. L., Behringer, E. J., & Segal, S. S. (2012). Coordination of intercellular Ca(2+) signaling in endothelial cell tubes of mouse resistance arteries. *Microcirculation., 19,* 757-770.

192. Sonkusare, S. K., Bonev, A. D., Ledoux, J., Liedtke, W., Kotlikoff, M. I., Heppner, T. J. et al. (2012). Elementary Ca2+ signals through endothelial TRPV4 channels regulate vascular function. *Science, 336,* 597-601.

193. Spitzer, A. (1982). The role of the kidney in sodium homeostasis during maturation. *Kidney Int., 21,* 539-545.

194. Stankevicius, E., Dalsgaard, T., Kroigaard, C., Beck, L., Boedtkjer, E., Misfeldt, M. W. et al. (2011). Opening of small and intermediate calcium-activated potassium channels induces relaxation mainly mediated by nitric-oxide release in

large arteries and endothelium-derived hyperpolarizing factor in small arteries from rat. *J.Pharmacol.Exp.Ther., 339*, 842-850.

195. Statistics Canada (2009). Mortality, Summary List of Causes. Statistics Canada [On-line]. Available: http://www.statcan.gc.ca/pub/84f0209x/84f0209x2009000-eng.htm

196. Statistics Canada (2013). Health Trends - High blood pressure. Statistics Canada [On-line]. Available: http://www12.statcan.gc.ca/health-sante/82-213/Op2.cfm?Lang=ENG&TABID=0&IND=R&SX=TOTAL&HEADER_ID=10000&LINE_ID=2305&S=2&O=D

197. Straub, A. C., Billaud, M., Johnstone, S. R., Best, A. K., Yemen, S., Dwyer, S. T. et al. (2011). Compartmentalized connexin 43 s-nitrosylation/denitrosylation regulates heterocellular communication in the vessel wall. *Arterioscler.Thromb.Vasc.Biol., 31*, 399-407.

198. Stuyvers, B. D., Dun, W., Matkovich, S., Sorrentino, V., Boyden, P. A., & ter Keurs, H. E. (2005). Ca2+ sparks and waves in canine purkinje cells: a triple layered system of Ca2+ activation. *Circ.Res., 97*, 35-43.

199. Sullivan, M. N. & Earley, S. (2013). TRP channel Ca2+ sparklets: fundamental signals underlying endothelium-dependent hyperpolarization. *Am J Physiol Cell Physiol, 305*, C999-C1008.

200. Sullivan, M. N., Francis, M., Pitts, N. L., Taylor, M. S., & Earley, S. (2012). Optical recording reveals novel properties of GSK1016790A-induced vanilloid transient receptor potential channel TRPV4 activity in primary human endothelial cells. *Mol.Pharmacol., 82*, 464-472.

201. Sun, X. P., Callamaras, N., Marchant, J. S., & Parker, I. (1998). A continuum of InsP3-mediated elementary Ca2+ signalling events in Xenopus oocytes. *J Physiol, 509 (Pt 1)*, 67-80.

202. Tae, J., Han, S. W., Yoo, J. Y., Kim, J. A., Kang, O. H., Baek, O. S. et al. (2003). Anti-inflammatory effect of Lonicera japonica in proteinase-activated receptor 2-mediated paw edema. *Clin.Chim.Acta, 330*, 165-171.

203. Takahashi, A., Camacho, P., Lechleiter, J. D., & Herman, B. (1999). Measurement of intracellular calcium. *Physiol Rev., 79*, 1089-1125.

204. Takaki, A., Morikawa, K., Tsutsui, M., Murayama, Y., Tekes, E., Yamagishi, H. et al. (2008). Crucial role of nitric oxide synthases system in endothelium-dependent hyperpolarization in mice. *J.Exp.Med., 205*, 2053-2063.

205. Takeuchi, T., Harris, J. L., Huang, W., Yan, K. W., Coughlin, S. R., & Craik, C. S. (2000). Cellular localization of membrane-type serine protease 1 and

identification of protease-activated receptor-2 and single-chain urokinase-type plasminogen activator as substrates. *J.Biol.Chem., 275,* 26333-26342.

206. Tang, E. H., Leung, F. P., Huang, Y., Feletou, M., So, K. F., Man, R. Y. et al. (2007). Calcium and reactive oxygen species increase in endothelial cells in response to releasers of endothelium-derived contracting factor. *Br.J.Pharmacol., 151,* 15-23.

207. Taylor, S. G. & Weston, A. H. (1988). Endothelium-derived hyperpolarizing factor: a new endogenous inhibitor from the vascular endothelium. *Trends Pharmacol.Sci., 9,* 272-274.

208. Teshima, K., Kim, S. H., & Allen, C. N. (2003). Characterization of an apamin-sensitive potassium current in suprachiasmatic nucleus neurons. *Neuroscience, 120,* 65-73.

209. The Nobel Foundation. (1998). The Nobel Prize in Physiology or Medicine 1998. nobelprize.org.
Ref Type: Generic

210. Thomas, D., Lipp, P., Tovey, S. C., Berridge, M. J., Li, W., Tsien, R. Y. et al. (2000). Microscopic properties of elementary Ca2+ release sites in non-excitable cells. *Curr.Biol., 10,* 8-15.

211. Thorsen, J., Lilleeng, E., Valen, E. C., & Krogdahl, A. (2008). Proteinase-activated receptor-2: two potential inflammatory mediators of the gastrointestinal tract in Atlantic salmon. *J Inflamm.(Lond), 5,* 18.

212. Tran, C. H., Taylor, M. S., Plane, F., Nagaraja, S., Tsoukias, N. M., Solodushko, V. et al. (2012). Endothelial Ca2+ wavelets and the induction of myoendothelial feedback. *Am.J.Physiol Cell Physiol, 302,* C1226-C1242.

213. Triggle, C. R., Samuel, S. M., Ravishankar, S., Marei, I., Arunachalam, G., & Ding, H. (2012). The endothelium: influencing vascular smooth muscle in many ways. *Can.J.Physiol Pharmacol., 90,* 713-738.

214. Uhrenholt, T. R., Domeier, T. L., & Segal, S. S. (2007). Propagation of calcium waves along endothelium of hamster feed arteries. *Am.J.Physiol Heart Circ.Physiol, 292,* H1634-H1640.

215. Vang, A., Mazer, J., Casserly, B., & Choudhary, G. (2010). Activation of endothelial BKCa channels causes pulmonary vasodilation. *Vascul.Pharmacol., 53,* 122-129.

216. Vu, T. K., Hung, D. T., Wheaton, V. I., & Coughlin, S. R. (1991). Molecular cloning of a functional thrombin receptor reveals a novel proteolytic mechanism of receptor activation. *Cell, 64,* 1057-1068.

217. Wachtfogel, Y. T., Kucich, U., James, H. L., Scott, C. F., Schapira, M., Zimmerman, M. et al. (1983). Human plasma kallikrein releases neutrophil elastase during blood coagulation. *J.Clin.Invest, 72,* 1672-1677.

218. Wakui, H., Dejima, T., Tamura, K., Uneda, K., Azuma, K., Maeda, A. et al. (2013). Activation of angiotensin II type 1 receptor-associated protein exerts an inhibitory effect on vascular hypertrophy and oxidative stress in angiotensin II-mediated hypertension. *Cardiovasc.Res., 100,* 511-519.

219. Wang, Q., Zhang, M., Ding, Y., Wang, Q., Zhang, W., Song, P. et al. (2013). Activation of NAD(P)H Oxidase by Tryptophan-Derived 3-Hydroxykynurenine Accelerates Endothelial Apoptosis and Dysfunction In Vivo. *Circ.Res.*.

220. Weston, A. H., Absi, M., Harno, E., Geraghty, A. R., Ward, D. T., Ruat, M. et al. (2008). The expression and function of Ca(2+)-sensing receptors in rat mesenteric artery; comparative studies using a model of type II diabetes. *Br.J.Pharmacol., 154,* 652-662.

221. Weston, A. H., Feletou, M., Vanhoutte, P. M., Falck, J. R., Campbell, W. B., & Edwards, G. (2005). Bradykinin-induced, endothelium-dependent responses in porcine coronary arteries: involvement of potassium channel activation and epoxyeicosatrienoic acids. *Br.J.Pharmacol., 145,* 775-784.

222. Weston, A. H., Richards, G. R., Burnham, M. P., Feletou, M., Vanhoutte, P. M., & Edwards, G. (2002). K+-induced hyperpolarization in rat mesenteric artery: identification, localization and role of Na+/K+-ATPases. *Br.J.Pharmacol., 136,* 918-926.

223. White, R. & Hiley, C. R. (1997). A comparison of EDHF-mediated and anandamide-induced relaxations in the rat isolated mesenteric artery. *Br.J.Pharmacol., 122,* 1573-1584.

224. Wolfe, B. L., Marchese, A., & Trejo, J. (2007). Ubiquitination differentially regulates clathrin-dependent internalization of protease-activated receptor-1. *J.Cell Biol., 177,* 905-916.

225. Yamauchi, K., Stone, A. J., Stocker, S. D., & Kaufman, M. P. (2012). Blockade of ATP-sensitive potassium channels prevents the attenuation of the exercise pressor reflex by tempol in rats with ligated femoral arteries. *Am.J.Physiol Heart Circ.Physiol, 303,* H332-H340.

226. Yang, G., Wu, L., Jiang, B., Yang, W., Qi, J., Cao, K. et al. (2008). H2S as a physiologic vasorelaxant: hypertension in mice with deletion of cystathionine gamma-lyase. *Science, 322,* 587-590.

227. Yang, Y. M., Huang, A., Kaley, G., & Sun, D. (2009). eNOS uncoupling and endothelial dysfunction in aged vessels. *Am J Physiol Heart Circ.Physiol, 297,* H1829-H1836.

228. Yao, Y., Choi, J., & Parker, I. (1995). Quantal puffs of intracellular Ca2+ evoked by inositol trisphosphate in Xenopus oocytes. *J Physiol, 482 (Pt 3),* 533-553.

229. Yi, X. Y., Gauthier, K. M., Cui, L., Nithipatikom, K., Falck, J. R., & Campbell, W. B. (2007). Metabolism of adrenic acid to vasodilatory 1alpha,1beta-dihomo-epoxyeicosatrienoic acids by bovine coronary arteries. *Am.J.Physiol Heart Circ.Physiol, 292,* H2265-H2274.

230. Yip, K. P. & Marsh, D. J. (1996). [Ca2+]i in rat afferent arteriole during constriction measured with confocal fluorescence microscopy. *Am.J.Physiol, 271,* F1004-F1011.

231. Yoon, M. J., Lee, A. R., Jeong, S. A., Kim, Y. S., Kim, J. Y., Kwon, Y. J. et al. (2014). Release of Ca2+ from the endoplasmic reticulum and its subsequent influx into mitochondria trigger celastrol-induced paraptosis in cancer cells. *Oncotarget., 5,* 6816-6831.

232. Zhang, D. M., Lin, S. M., Lau, C. W., Yiu, A., Wang, J., Li, Y. et al. (2010). Anemoside A3-induced relaxation in rat renal arteries: role of endothelium and Ca2+ channel inhibition. *Planta Med., 76,* 1814-1819.

233. Zhang, D. X., Mendoza, S. A., Bubolz, A. H., Mizuno, A., Ge, Z. D., Li, R. et al. (2009). Transient receptor potential vanilloid type 4-deficient mice exhibit impaired endothelium-dependent relaxation induced by acetylcholine in vitro and in vivo. *Hypertension, 53,* 532-538.

234. Zhu, T., Sennlaub, F., Beauchamp, M. H., Fan, L., Joyal, J. S., Checchin, D. et al. (2006). Proangiogenic effects of protease-activated receptor 2 are tumor necrosis factor-alpha and consecutively Tie2 dependent. *Arterioscler.Thromb.Vasc.Biol., 26,* 744-750.